



**UNIVERSITY OF TWENTE.**



**Assessing the Efficiency of Mitigation Measures  
for Saltwater Intrusion in Man-Made Canals:  
A Comprehensive Modelling Study of the Ghent-Terneuzen Canal**

**Tijl C. Wijnants**

**M.Sc. Thesis Civil Engineering and Management**

**July 2023**

**Version: Final**



---

**Chair Graduation Committee:**

dr. ir. B.W. Borsje

**Supervisors:**

ir. R.W.A. Siemes

ir. R.J. Daggenvoorde

Faculty of Engineering & Technology,  
Department of Civil Engineering & Management  
Group Water Engineering Management  
Master River and Coastal Engineering  
University of Twente  
P.O. Box 217  
7500 AE Enschede  
The Netherlands

---

# Preface

In presenting this document, I bring to a close my journey through the master's program in Civil Engineering and Management with a specialization in "River and Coastal Engineering" at the University of Twente. This thesis represents the culmination of my external graduation project, carried out in collaboration with HKV from February 2023 to July 2023.

The focus of this research revolves around assessing potential mitigation measures for reducing saltwater intrusion in man-made canals with specific emphasis on the Ghent-Terneuzen canal. I am pleased with the final outcome of this study, but more importantly, I reflect upon my student career with joy and optimism, witnessing personal growth both within and beyond the academic realm.

I would like to express my appreciation for the assistance and contribution throughout the execution of my master's thesis at HKV. Firstly, I want to extend my thanks to Bas Borsje for the thorough preparations during the Advanced Research Skills course, which played a crucial role in laying the foundation for my thesis. Secondly, I sincerely appreciate Rutger Siemes for his valuable input and guidance, both prior to and during the thesis. His insights have been immensely valuable. I would also like to acknowledge the guidance and support provided by Roy Daggenvoorde from HKV, who provided daily assistance and helped me navigate within the organization. Lastly, I would like to express my gratitude to the staff at HKV for the invaluable learning experience they provided.

I sincerely hope you will enjoy reading this master thesis!

*Tijl Wijnants*

*'s-Hertogenbosch, July 2023*

# abstract

This thesis aims to assess the efficiency of mitigation measures for reducing saltwater intrusion in the Ghent-Terneuzen canal, a man-made waterway vulnerable to saltwater intrusion. By employing a comprehensive 3D modelling approach, the study investigates various physical and management measures to identify effective strategies for mitigating the saltwater intrusion. The primary objective is to evaluate and quantify the effectiveness of these measures using the Delft 3D model. The methodology involves setting up the Delft 3D model specifically for the Ghent-Terneuzen canal. Eight mitigation measures are tested, including four physical measures (saltwater trap, elevated threshold, canal constriction and selective withdrawal) and four management measures related to upstream discharge (summer discharge spreading, summer pulses, winter flushing, and a rainfall pulse). The model is used to simulate and analyze the impact of these measures on saltwater intrusion dynamics.

The research contributes to the current understanding of saltwater intrusion in closed systems, providing valuable insights into the efficiency of mitigation measures in the context of the Ghent-Terneuzen canal. The study highlights the need for further adjustments to the model calibration and validation to achieve improved accuracy, as the model did not perfectly fit the observed values. While the model proves reliable for testing measures, it cannot predict future scenarios for saltwater intrusion examination.

As the New Lock Terneuzen is currently being build, the saltwater intrusion is expected to become more pronound if no action is taken, illustrating the need for mitigation measures. This research's findings lead to the conclusion that the canal's salinity levels will escalate as a direct consequence of the construction of the New Lock Terneuzen, necessitating the implementation of appropriate measures. The study emphasizes the importance of physical structures in achieving significant reductions in saltwater intrusion. particularly the saltwater trap and elevated threshold show promising effectiveness in reducing saltwater intrusion. The continuous discharge through culverts is believed to contribute to their success. Consequently, the management measures regarding upstream discharge exhibit limited potential and high uncertainty in water availability, indicating their inadequate strength in mitigating saltwater intrusion.

# Contents

<b>Preface</b>	<b>2</b>
<b>abstract</b>	<b>3</b>
<b>1 Introduction</b>	<b>9</b>
1.1 Background	9
1.2 Problem analysis	10
1.3 Research objective	11
1.4 Report structure	11
<b>2 Study area</b>	<b>12</b>
2.1 Westerscheldt estuary and Ghent-Terneuzen canal	12
2.2 Lock complex Terneuzen	14
2.3 Changes due to lock modifications (New Lock Terneuzen)	15
2.4 Data availability for the Ghent-Terneuzen canal	17
2.5 Data sources	17
<b>3 Method</b>	<b>18</b>
3.1 Delft3D	18
3.2 Model schematization	19
3.3 Boundary conditions	22
3.4 Initial conditions	27
3.5 Physical/numerical and additional parameters	28
3.6 Implementation of mitigation measures	31
3.7 Result analysis	37
<b>4 Calibration and Validation</b>	<b>38</b>
4.1 Hydrodynamics and salinity	38
4.2 Initial model results	39
4.3 Statistical performance of a model	40
4.4 Sensitivity analysis	41
4.5 Calibration	46
4.6 Validation	49
4.7 Understanding model discrepancies	51
<b>5 Results of mitigation measures New Lock Terneuzen</b>	<b>54</b>
5.1 Changed schematized domain	54
5.2 General overview of the effectiveness of implemented mitigation measures	56
5.3 Mitigation measure 1; Submerged threshold with additional discharge	57
5.4 Mitigation measure 2; Elevated threshold with additional discharge	58
5.5 Mitigation measure 3; Canal constriction	60
5.6 Mitigation measure 4; Selective withdrawal	62
5.7 Mitigation measure 5; Summer discharge spreading	63
5.8 Mitigation measure 6; Freshwater pulse	65
5.9 Mitigation measure 7; Winter Flushing	67
5.10 Mitigation measure 8; Rainfall pulse	68

<b>6</b>	<b>Discussion</b>	<b>70</b>
6.1	Model set up . . . . .	70
6.2	Depth dependent Calibration and validation on a stratified system . . . . .	71
6.3	Interpretation of the effectiveness of implemented measures to reduce saltwater intrusion . . . . .	73
6.4	Assumptions and simplifications throughout the research . . . . .	74
6.5	Trustworthiness of the model and its applicability . . . . .	75
6.6	Research’s implication on management of the Ghent-Terneuzen canal . . . . .	76
<b>7</b>	<b>Conclusion</b>	<b>77</b>
<b>A</b>	<b>Management practices and additional information for the Ghent-Terneuzen canal</b>	<b>83</b>
A.1	Management and Development Plan of National Waters . . . . .	83
A.2	Upstream discharge . . . . .	85
A.3	Water level management . . . . .	85
<b>B</b>	<b>Sensitivity analysis</b>	<b>87</b>

# List of Figures

2.1	Geographical location Lock Complex Terneuzen (Google earth, n.d.) . . . . .	13
2.2	3D schematization of new design Lock Complex Terneuzen (Ministerie van Infrastructuur en Waterstaat, 2021) . . . . .	13
2.3	Ghent-Terneuzen Canal. Showing two Monitoring Locations (Skikuil brug and Sas van Ghent) and all upstream discharge (Evergrem, Tolhuis weir, Moervaart, Zuidelde). (Vuik & Lambrechts, 2023) . . . . .	14
2.4	Overview new design (coloured part) in comparison to old design (transparent part) (iv-groep, n.d.) . . . . .	16
2.5	Schematic representation of New Lock Terneuzen and salt threshold (source: nieuwewelusterneuzen.eu) . . . . .	16
3.1	The developed computational grid; representing the model of the Gent-Terneuzen channel (a). Details are showed in (b), (c) and (d) . . . . .	20
3.2	Implemented bathymetry representing the GTC . . . . .	21
3.3	Schematic representation of sigma (left) and Z-layers (right) . . . . .	22
3.4	Cumulative distribution function (CDF) of gate opening durations (blue) and salt exchange durations (orange) for the <b>West Lock</b> (Vuik & Lambrechts, 2023). . . . .	26
3.5	Cumulative distribution function (CDF) of gate opening durations (blue) and salt exchange durations (orange) for the <b>Middle Lock</b> (Vuik & Lambrechts, 2023). . . . .	27
3.6	Cumulative distribution function (CDF) of gate opening durations (blue) and salt exchange durations (orange) for the <b>East Lock</b> (Vuik & Lambrechts, 2023). . . . .	27
3.7	Average observed water temperature GTC 2018-2019 . . . . .	30
3.8	Wind speed and Direction observed at Vlissingen . . . . .	31
3.9	Physical measures. (a) Elevated threshold, (b) Submerged threshold, (c) Canal constriction, (d) selective withdrawal . . . . .	32
3.10	Management-related measures. (a) Summer discharge spreading, (b) Freshwater pulse, (c) Winter flushing, (d) Rainfall pulse . . . . .	33
3.11	Measure 1, Submerged threshold with additional discharge for New Lock Terneuzen . . . . .	34
3.12	Measure 2, Schematic representation of the current design and the inclusion of the threshold . . . . .	35
3.13	Measure 3, Canal constriction of 170m and 400m . . . . .	36
4.1	Salinity values (waterinfo.nl) for location Skikuil brug and Sas van Gent on left axis (blue). Discharges values (waterinfo.be) covering upstream discharge for the GTC. Period 2014 - 2023 . . . . .	39
4.2	Initial results for salinity values across vertical layers at location Skikuil brug . . . . .	40
4.3	Initial results for salinity values across vertical layers at location Skikuil brug . . . . .	40
4.4	Calibration run at locatoin Skikuil brug (RMSE:1095, NRMSE:0.28, BIAS:-294) . . . . .	48
4.5	Calibration run at locatoin Sas van Gent (RMSE:985, NRMSE:0.26, BIAS:206) . . . . .	48
4.6	Validation run at locatoin Skikuil brug (RMSE:766, NRMSE:0.19, BIAS:-380) . . . . .	49
4.7	Validation run at locatoin Sas van Gent (RMSE:552, NRMSE:0.0.15, BIAS:199) . . . . .	49
4.8	Relationship between percentage difference upstream discharge (green line) to salinity concentrations in the canal (red line) in 2020 . . . . .	51
4.9	Relationship between percentage difference upstream discharge (green line) to salinity concentrations in the canal (red line) in 2020 . . . . .	52
4.10	Effect of abrupt percentage change in upstream discharge to salinity concentrations 2018 (left) and 2020 (right) . . . . .	53

5.1	Visual comparison grid schematization new design Lock Terneuzen . . . . .	55
5.2	Visual comparison bathymetry new design Lock Terneuzen . . . . .	55
5.3	Comparison of New Lock Terneuzen (black) to old situation (red) and to old situation with new salt exchange volumes and door open times (green) . . . . .	56
5.4	Results mitigation measure 1; Submerged threshold with additional discharge. Top figure: Comparison of reference scenario to mitigation measure 1a and 1b. Middle figure: Difference measure 1a compared to reference scenario. Lower figure: Difference measure 1b compared to reference scenario. . . . .	58
5.5	Results mitigation measure 2; Elevated threshold with additional discharge. Top figure: Comparison of reference scenario to mitigation measure 2a and 2b. Middle figure: Difference measure 2a compared to reference scenario. Lower figure: Difference measure 2b compared to reference scenario. . . . .	59
5.6	Results mitigation measure 3; Canal constriction. Top figure: Comparison of reference scenario to mitigation measure 3a and 3b. Middle figure: Difference measure 3a compared to reference scenario. Lower figure: Difference measure 3b compared to reference scenario. . . . .	61
5.7	Bar plot showing the chainage (distance along the canal) of the salinity levels for Measure 3 and the reference scenario, providing a spatial representation of the salinity distribution along the canal for both scenarios. . . . .	61
5.8	Results mitigation measure 4; Selective withdrawal. Top figure: Comparison of reference scenario to mitigation measure 4. Lower figure: Difference measure 4 compared to reference scenario. . . . .	63
5.9	Results mitigation measure 5; Summer discharge spreading. Top figure: Comparison of reference scenario to mitigation measure 5. Lower figure: Difference measure 5 compared to reference scenario. . . . .	65
5.10	Results mitigation measure 6; Summer pulses. Top figure: Comparison of reference scenario to mitigation measure 6a and 6b. Middle figure: Difference measure 6a compared to reference scenario. Lower figure: Difference measure 6b compared to reference scenario. . . . .	66
5.11	Results mitigation measure 7; Winter flushing. Top figure: Comparison of reference scenario to mitigation measure 7. Lower figure: Difference measure 7 compared to reference scenario. . . . .	68
5.12	Results mitigation measure 8; Rainfall pulse. Top figure: Comparison of reference scenario to mitigation measure 8. Lower figure: Difference measure 8 compared to reference scenario. . . . .	69
6.1	Stratification observed +0.25mNAP and -5mNAP and modelled, layer 8 and 12 at location Sas van Gent . . . . .	71
6.2	Difference in salt concentration per layer . . . . .	72
A.1	The cross-sectional area of the salt trap at the Westsluis (Waterloopkundig Laboratorium, 1988). . . . .	84
A.2	Interior view of the West Lock with the entrance of the bypass sewer (Waterloopkundig Laboratorium, 1988). . . . .	85
A.3	Water distribution around Ghent (Rijkswaterstaat, 2020) . . . . .	86
B.1	Horizontal Eddy Diffusivity bottom layer . . . . .	87
B.2	Horizontal Eddy Diffusivity surface layer . . . . .	88
B.3	Horizontal Eddy Viscosity bottom layer . . . . .	89
B.4	Horizontal Eddy Viscosity surface layer . . . . .	90
B.5	Vertical Eddy Diffusivity bottom layer . . . . .	91
B.6	Vertical Eddy Diffusivity surface layer . . . . .	92
B.7	Vertical Eddy Viscosity bottom layer . . . . .	93
B.8	Vertical layer offset (kmx); 10 . . . . .	94
B.9	Vertical layer offset (kmx); 15 . . . . .	95
B.10	Vertical layer offset (kmx); 20 . . . . .	96

# List of Tables

2.1	Dimensions of the locks (Source: vaarweginfo.nl and nieuwesluisterneuzen.nl). Depths are referenced with respect to the canal level. . . . .	15
2.2	The average number of lockage operations per day per lock chamber for different years is presented (source: registration of passages and empty lockage operations by Rijkswaterstaat). The last row represents the average number of lock cycles per day, which is half of the number of lockage operations. . . . .	15
2.3	Detailed overview of the data sources utilized for the Ghent-Terneuzen canal. Location GTC refers to the locations Skikuil brug and Sas van Gent . . . . .	17
3.1	Estimation of lock exchange flows per lock (FINEL3D) performed by (Svasek, 2015) . . . . .	25
3.2	Saltwater exchange and average door opening times per lock (MER Deelrapport Water)	26
3.3	Overview value, unit and source physical/numerical and additional parameters . . . . .	28
4.1	Parameter value range for calibration indicated by lower end to higher end values . . . . .	43
4.2	Overview of statistical performance indicators for the sensitivity analysis (19 runs). Green indicates the best performance indicator, while red indicates the worst performance indicator. . . . .	45
4.3	Overview of statistical performance indicators for the 4 calibration runs. Green indicates the best performance indicator, while red indicates the worst performance indicator. . . . .	47
4.4	Results of first calibration procedure . . . . .	47
4.5	Second calibration procedure; changing the assumption of constant upstream discharge at Tolhuis weir at the inner city of Ghent . . . . .	47
4.6	Statistical performance for calibration and validation period . . . . .	50
5.1	Overview of the effectiveness of physical structure measures to reduce saltwater intrusion	57
5.2	Overview of the effectiveness of management-oriented measures to reduce saltwater intrusion . . . . .	57

# Chapter 1

## Introduction

### 1.1 Background

Saltwater intrusion poses a significant threat to coastal regions, impacting freshwater supplies, agriculture, and ecology. Saltwater intrusion can occur in open systems, such as estuaries and deltas, or in closed systems where locks or barriers separate saltwater bodies from freshwater bodies. In the case of closed systems, locks are designed to regulate water level differences between the sea and inland waterways, but they can also influence the intrusion of saltwater. It is crucial to understand the mechanisms and impacts of saltwater intrusion through locks in order to effectively manage water resources and preserve freshwater resources. The consequences of saltwater intrusion can have far-reaching effects, emphasizing the importance of exploring effective mitigation measures to manage this problem. Moreover, with the ongoing climate change, saltwater intrusion is expected to become an increasingly significant problem in the future (Friocourt et al., 2014; de la Reguera et al., 2020; Costa et al., 2023). Factors such as reduced river discharge during dry summers, rising sea levels, and increasing freshwater demand contribute to the increased trend of saltwater intrusion (Friocourt et al., 2014). In this study the focus will be specifically on man-made canals that separate the open sea by locks, with a particular emphasis on the Ghent-Terneuzen canal situated in The Netherlands and Belgium.

There are still significant gaps in our understanding of the mechanisms and behavior of saltwater intrusion in closed systems with locks, despite the existing knowledge about saltwater intrusion in natural estuaries. Connecting these knowledge gaps is vital for developing effective strategies to manage and mitigate saltwater intrusion. Several important differences distinguish closed systems with locks from open systems. In closed systems, locks obstruct tidal movements and restrict the entry of salt into the channel. Moreover, man-made canals, which are typically narrower and deeper, differ in width-depth ratio from the wide and shallow natural estuaries (Friedrichs & Aubrey, 1994). Additionally, the discharge in man-made canals is often smaller and subject to human control. Consequently, knowledge regarding saltwater intrusion in open systems cannot be directly applied to closed systems.

Saltwater intrusion occurs when saltwater shifts landward into areas that have not previously experienced or adapted to saline water (Tully et al., 2019; Liu et al., 2019). The process is caused by the spatial density differences between the two types of water, with saline water weighing on average 2 - 3% more than fresh water (Friocourt et al., 2014). The salt concentration gradually decreases in the upstream direction due to the counter-pressure of the fresh water discharge (Friocourt et al., 2014; Chen et al., 2015). The extent of saltwater intrusion can depend on a variety of factors, including tidal amplitude, upstream river discharge, wind, river geometry, and bathymetry (Vanderkemp et al., 2012; Veerpagea et al., 2019; Ralston et al., 2012).

To minimize the effects of saltwater intrusion, a combination of engineering and management measures could be employed. Engineering measures include changes to the physical features of the environment, such as modifying the geometry or bathymetry of water bodies, installing bell screens, spillway pipes, or physical barriers like dikes or levees to prevent the movement of saltwater. These measures can help to control the amount and extent of saltwater intrusion. Management practices can also help to mitigate the effects of saltwater intrusion. For example, a minimum freshwater feed can be maintained to prevent excessive saltwater intrusion and maintain freshwater resources, while a maximum number of lock passages per day can help to regulate the amount of saltwater entering freshwater systems through locks and other channels. However, the most effective strategy for mitigating the effects of saltwater intrusion will depend on the specific and environmental context, as well as the available resources and technologies.

## 1.2 Problem analysis

The construction of the New Lock Terneuzen, which is anticipated to be one of the largest sea locks globally (Vanoutrive, 2020), will introduce a larger volume of water exchange, leading to increased saltwater intrusion (Vuik & Lambrechts, 2023). However, there is a limited understanding of the potential impacts of saltwater intrusion specifically at Lock Complex Terneuzen, and currently, no 3D model exists to assess and evaluate potential mitigation measures for reducing saltwater intrusion. The development of accurate models that simulate real-life scenarios is of great importance for testing the effectiveness of specific measures to mitigate saltwater intrusion.

Several agreements have been established between Dutch and Belgian authorities to manage saltwater intrusion at the Terneuzen lock complex. These agreements ensure a minimum discharge capacity, lock accessibility, and salinity concentration in the Ghent-Terneuzen canal. The Netherlands has committed to limiting saltwater intrusion at Terneuzen (Rijkswaterstaat, 2020). Additionally, the European Framework Directive for water policy has set a salinity target of 3000 mg/l near the Dutch-Flemish border, measured approximately 1 m below the surface (Water Framework Directive, 2018). However, significant fluctuations in salinity concentrations have been observed in the canal, with peak values reaching up to 6000 mg/l (Rijkswaterstaat, n.d.). The expected increase in saltwater intrusion due to the construction of the New Lock Terneuzen poses a threat to fulfilling these agreements in the near future.

To address these challenges and ensure the effectiveness of mitigation measures, it is important to develop comprehensive models and strategies specifically to the Lock Complex Terneuzen. These models should accurately represent real-world conditions and enable the evaluation and assessment of potential measures to reduce saltwater intrusion. By implementing effective mitigation measures, it is possible to minimize the negative impacts of saltwater intrusion and ensure compliance with the established agreements and regulatory standards.

### 1.3 Research objective

The objective of this study is to identify and assess potential mitigating measures aimed at reducing saltwater intrusion in the Ghent-Terneuzen canal. The effectiveness of the identified measures will be quantified through the use of a 3D-model, providing a comprehensive understanding of the underlying mechanisms and associated dynamics. The main objective of this master thesis is defined as follows:

**”To identify and evaluate potential mitigating measures for reducing saltwater intrusion in the Ghent-Terneuzen canal and quantifying their effectiveness using a 3D model”**

To reach this objective, three research questions have been defined:

1. What mitigation measures can be identified to effectively reduce saltwater intrusion, and which among them appears to be the most promising in terms of mitigating saltwater intrusion, feasibility and practically?
2. Can a Delft3D model be established to accurately simulate observed salinity levels in the Ghent-Terneuzen canal?
3. What effect do the (identified) mitigation measures have on saltwater intrusion, as determined by in-depth analysis using Delft3D, and what are the additional insights for these measure(s)?

### 1.4 Report structure

The report is structured to provide a clear and organized overview of the research conducted on the lock complex Terneuzen and its implications for saltwater intrusion in the Ghent-Terneuzen canal. It is divided into several chapters, each focusing on a specific aspect of the study.

Chapter 1 serves as the introduction, setting the context for the research and presenting the problem analysis. It also outlines the research objective and provides a brief overview of the report structure. Chapter 2 delves into the study area, providing detailed information on the Westerscheldt estuary and the Ghent-Terneuzen canal. The lock complex Terneuzen, as a crucial component of the study area, is explored. Also, the data sources used in the research are shown. It explains the availability and origin of the data. This chapter establishes the foundation for the subsequent analysis. Chapter 3 outlines the methodology employed in the study. It introduces the Delft3D modeling software used. The model schematization, selection of boundary conditions, determination of initial conditions, and incorporation of mitigation measures are explained in detail. Chapter 4 covers the calibration and validation process of the model. It describes the steps taken to ensure accurate simulation of salinity levels. Sensitivity analysis, statistical performance evaluation, and validation for the new lock Terneuzen are discussed. Chapter 5 presents the results of the model simulations. It provides an analysis of the effects of various mitigation measures on saltwater intrusion. Chapter 6 is dedicated to the discussion of the findings. It offers an in-depth analysis and interpretation of the results, exploring the applicability of the Delft3D model and addressing uncertainties in the modeling approach. Chapter 7 summarizes the key findings and conclusions drawn from the research. It highlights their significance and implications for addressing the problem of saltwater intrusion in the lock complex Terneuzen. Appendix A contains supplementary information regarding water level management in the Ghent-Terneuzen canal. Appendix B visualizes the conducted sensitivity analysis. References to the appendix can be found throughout the document.

# Chapter 2

## Study area

The objective of this chapter is to offer a comprehensive depiction of the study area, namely the Lock Complex Terneuzen located in the Ghent-Terneuzen canal.

### 2.1 Westerscheldt estuary and Ghent-Terneuzen canal

Lock complex Terneuzen is located in the Netherlands, specifically in the province of Zeeland (figure 2.1). The lock is the barrier between the Western Scheldt estuary and the Ghent-Terneuzen canal (GTC), allowing ships to travel between the North Sea and the port of city Ghent, Belgium.

The Westerscheldt Estuary has important environmental and commercial qualities. It is the main shipping route to the Port of Antwerp in Belgium (Sisterman & Nieuwenhuis, 2003). The Western Scheldt estuary has an open connection to the North Sea. Tidal amplitudes, wind and water inlets enhance the mixing process in the Western Scheldt estuary, making it a well-mixed estuary (Van Den Bergh et al., 2021). These mixing processes subsequently influence the salt concentration in the estuary. The salinity levels in the Western Scheldt estuary vary over time, and this variation can significantly impact the amount of salt intrusion. The semi-diurnal tide in the Western Scheldt estuary varies in range, with an average of 3,8 meters at Vlissingen (located at the mouth of the estuary) and 5.2 meters at Antwerp (78 kilometers upstream) and has been approximately constant over the last century (Pieters, 2002; van Rijn, 2010). As a result, the majority of the estuary is considered to be meso-tidal. The current speeds in the main channels of the estuary can reach 1-2 meters per second during an average tide. Due to a combination of rising sea levels and changes in the estuary's morphology, the tidal wave is amplified, resulting in higher water levels (Sisterman & Nieuwenhuis, 2003).

In 2022, the tidal range at Lock Terneuzen, which is located on the south side of the Western Scheldt estuary, fluctuated on average between +3.7m and -2.5m on the estuarine side of the lock complex (Rijkswaterstaat, n.d.). On the river side of the lock complex, the GTC, the water levels fluctuated between +2.4m NAP and +1.9m NAP.

The GTC has a length of approximately 31km, with 17km located in Belgium and 14km located in the Netherlands (see figure 2.3). The canal facilitates multiple industrial companies and thus, commercial navigation must be accommodated. The cross-sectional area is rectangular with a depth of 13.5m and a varying width of 120-350m (Vanderkimpen et al., 2012). Currently, the lock is under construction, with a new lock chamber being built and scheduled to open in 2023 (Nieuwe Sluis Terneuzen, n.d.).



Figure 2.1: Geographical location Lock Complex Terneuzen (Google earth, n.d.)



Figure 2.2: 3D schematization of new design Lock Complex Terneuzen (Ministerie van Infrastructuur en Waterstaat, 2021)

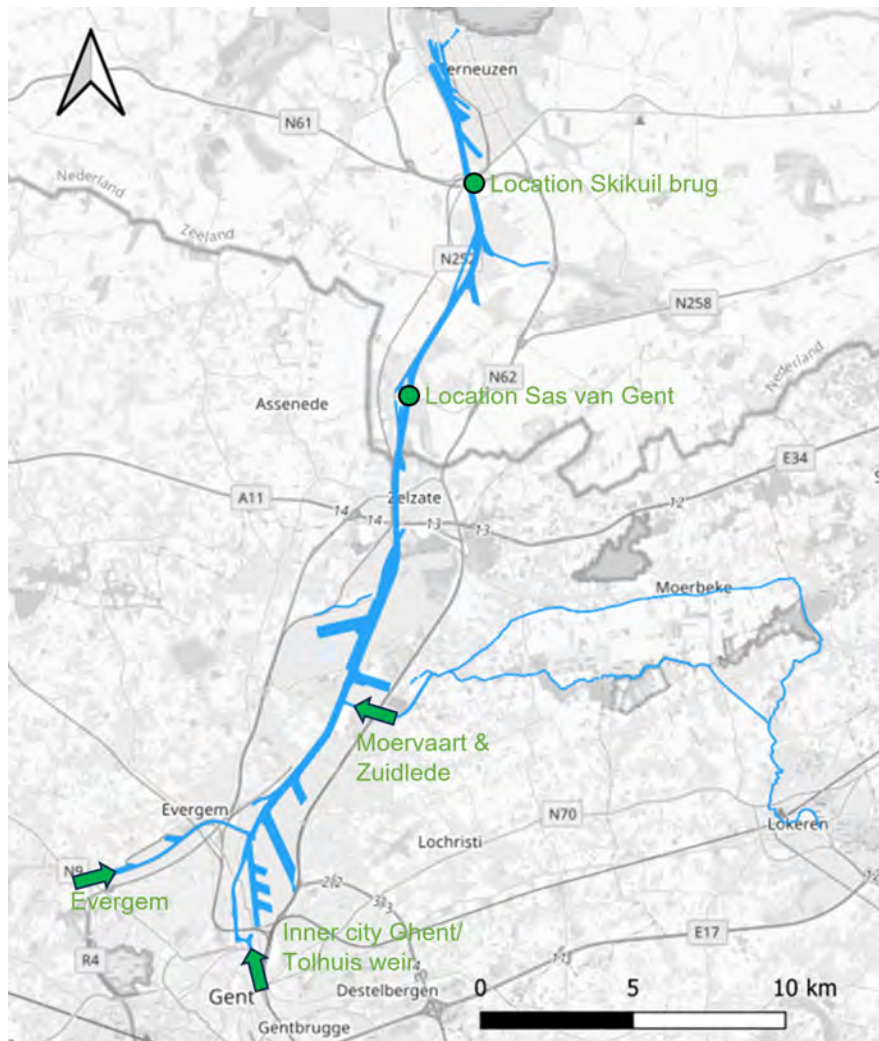


Figure 2.3: Ghent-Terneuzen Canal. Showing two Monitoring Locations (Skikuil brug and Sas van Ghent) and all upstream discharge (Evergem, Tolhuis weir, Moervaart, Zuidlede). (Vuik & Lambrechts, 2023)

## 2.2 Lock complex Terneuzen

The lock complex previously consisted of the West Lock, Middle Lock, and East Lock. However, since October 1st, 2021, the Middle Lock has been decommissioned and demolished. Construction of the New Terneuzen Lock, one of the largest sea locks worldwide is designed to replace the Middle Lock, began in 2017 and is (re)scheduled to become operational in 2024 (Figure 2.2). Table 2.1 provides an overview of the dimensions of the various lock chambers. Additional information for the Ghent-Terneuzen canal regarding management practices, upstream discharge and water level management are described in appendix A.

Table 2.2 provides an overview of the average number of lockage operations per day over the past six years for the three lock chambers. The number of passage cycles shown in the last row and is 50% of the average, as a passage cycle refers to an upward and downward directed lock passage. For water loss and salt intrusion, the number of complete lock cycles is more relevant than the number of individual passages. Therefore, in this report, numbers regarding lock chamber usage are expressed in terms of lock cycles.

In addition, in this report the terms of "lock passage" is used either to indicate a ship using the locks which go either upward in the canal direction or downward in the Scheldt direction. A passage cycle refers to the combination of both upward and downward passage.

Table 2.1: Dimensions of the locks (Source: vaarweginfo.nl and nieuwesluisterneuzen.nl). Depths are referenced with respect to the canal level.

<b>Lock:</b>	<b>unit</b>	<b>New Lock Terneuzen</b>	<b>East lock</b>	<b>Middle lock</b>	<b>West lock</b>
Width of lock	[m]	55	24	24	38
Length of lock	[m]	427	280	140	290
Surface area of lock	[m <sup>2</sup> ]	23.485	6.720	3.360	11.2
Depth of lock	[m]	-16,5	-7,5	-10,5	-13,5
Outer threshold depth	[m]	-15,8	-6,5	-7,6	-12,8
Inner threshold depth	[m]	-14,1	-6,6	-8,3	-13,5

Table 2.2: The average number of lockage operations per day per lock chamber for different years is presented (source: registration of passages and empty lockage operations by Rijkswaterstaat). The last row represents the average number of lock cycles per day, which is half of the number of lockage operations.

<b>Lock:</b>	<b>East lock</b>	<b>Middle lock</b>	<b>West lock</b>
Year:	[avg/open/day]	[avg/open/day]	[avg/open/day]
2016	32,9	21,2	24,1
2017	34,1	22,5	24,0
2018	33,6	21,4	24,3
2019	31,8	16,6	23,7
2020	31,1	15,5	23,3
2021	31,6	16,0	22,9
Average	32,5	18,9	23,7
Passage cycle	16,3	9,4	11,9

## 2.3 Changes due to lock modifications (New Lock Terneuzen)

The New Lock Terneuzen will replace the middle lock and form the New Lock Complex. The new lock will be longer, deeper, and wider, making it capable of accommodating the largest types of inland vessels (CEMT IV and Va categories). An estimation of the salt exchange has been conducted by Svasek (2015), indicating that saltwater exchange volumes will be more than twice as high as before.

Figure 2.4 below illustrates the modifications associated with the new design. The transparent sections represent the previous scenario with the Middle lock. The original/full depiction corresponds to the new scenario, wherein New Lock Terneuzen is introduced alongside the existing western lock.



Figure 2.4: Overview new design (coloured part) in comparison to old design (transparent part) (iv-groep, n.d.).

As of October 1st, 2021, the Middle Lock is no longer in use as a lock. According to the current (Rijkswaterstaat, 2023) plan, the New Lock Terneuzen will be operational in the course of 2024. The Middle Lock will still be available for discharge until mid-2022. The discharge option via the Middle Lock will only be removed when the culverts of the new lock are completed, which will happen before the use actual use of the new lock.

The final design of the New lock Terneuzen has the following characteristics (see figure 2.5 (VNSC, 2015)):

- Dimensions of  $427 \times 55 \times 16.44$  m;
- Additional discharge through the culverts of the New Lock, therefore no additional discharge facility;
- Water level control of the GTC through closures;
- No fresh-saltwater separation, only elevated threshold for a possible future bubble screen;
- A salt threshold on the canal side from NAP-16.5 to -14.1 m;
- A foundation for a possible future additional threshold up to NAP-11.8 m.

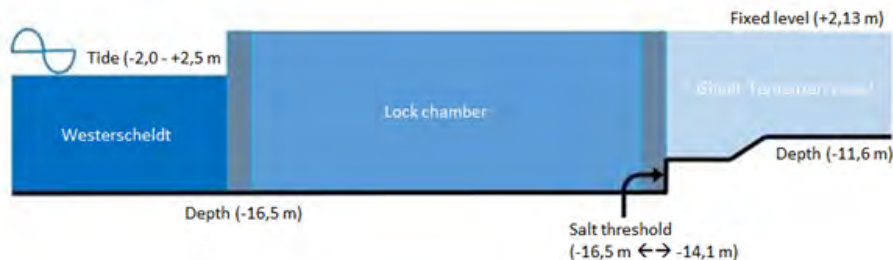


Figure 2.5: Schematic representation of New Lock Terneuzen and salt threshold (source: nieuwesluis-terneuzen.eu)

During periods of water excess, the New Lock provides sufficient additional overflow capacity to compensate for the loss of the Middle lock. Previously, the order of operation was: first the Middle Lock, then the East Lock, and then the West Lock. In the new design, the order of interruption is: West lock, East Lock, New Lock. The full overflow capacity of a lock is utilized before the next lock is interrupted. In times of water shortage, the order of interruption is: New Lock, East Lock, West Lock. In this situation as well, the capacity of the first lock is fully utilized before the second lock is interrupted (VNSC, 2015).

## 2.4 Data availability for the Ghent-Terneuzen canal

The reliability and quality of data are crucial for accurate simulations. In simulating saltwater intrusion in the Ghent-Terneuzen canal, hydrodynamics and salinity values are essential inputs for the Delft3D software package. The specific data required includes up-and downstream discharge, chloride concentrations, and the water level, as these have the most significant impact on accurate model output. However, reliable and high-quality data does not guarantee the desired output. This chapter gives an clear overview of all used data.

## 2.5 Data sources

Table 2.3 provides information about the parameters that have been used and the sources that they have been retrieved from. The way in which these have been utilized will be explained in the next chapters of this thesis.

Table 2.3: Detailed overview of the data sources utilized for the Ghent-Terneuzen canal. Location GTC refers to the locations Skikuil brug and Sas van Gent

Parameter	Variable	Location	Unit	Interval	Source
hydrodynamics	Discharge	Evergem/Ringvaart	m <sup>3</sup> /s	10-min	Waterinfo.be
		Mendonk/Moervaart	m <sup>3</sup> /s	10-min	Waterinfo.be
	Water level	GTC	mNAP	10-min	Waterinfo.nl
		Westerscheldt	mNAP	10-min	Waterinfo.nl
	Chloride concentrations +0.25mNAP & -5mNAP	GTC	mg/l	10-min	Waterinfo.nl
		Westerscheldt	mg/l	10-min	Waterinfo.nl
	Water temperature	GTC	°C	10-min	Waterinfo.nl
GTC		°C	hourly-averaged	KNMI.nl	
Bathymetry	Bed level	Dutch part GTC		16-06-2021	maps.rijkswaterstaat.nl
		Belgian part GTC		27-02-2023	bathy.agentschapmdk.be
Meteorological	Wind	Vlissingen	m/s	hourly-averaged	KNMI.nl
	Humidity	Vlissingen	%	hourly-averaged	KNMI.nl
	Air temperature	Vlissingen	°C	hourly-averaged	KNMI.nl
	Cloud coverage	Vlissingen	%	hourly-averaged	KNMI.nl

# Chapter 3

## Method

This section will provide a detailed explanation of the used methodology to schematize the GTC. The present chapter will formulate the establishment of the actual model, incorporating the grid generation process, bathymetry, boundary conditions, initial conditions, and additional parameters. Furthermore, the implementation and analysis of possible mitigation measures to reduce saltwater intrusion in the GTC will be presented.

### 3.1 Delft3D

The used software in this thesis is Delft3D-FM by (Deltares, 2023b). The key component of Delft3D-FM is the so called ‘‘D-Flow Flexible Mesh engine’’ which is designed for hydrodynamics simulations on unstructured grids in 1D-2D-3D. The Delft3D-FM model can simulate the hydrodynamics and water quality of coastal and estuarine systems. It is widely used to study the impacts of various human activities on these systems, including the impacts of saltwater intrusion in closed systems (Deltares, 2023b; de la Reguera et al., 2020).

#### 3.1.1 Model equations

Delft3D-FM is a powerful tool designed to simulate the flow of water by solving the unsteady shallow water equations in two or three dimensions. These equations, derived from the three-dimensional Navier-Stokes equations for incompressible flow, provide a comprehensive understanding of water movement and changes in water levels within a specified area. These equations capture the fundamental principles governing the flow of water.

Delft3D-FM incorporates the Boussinesq assumptions, which consider density differences through the pressure term, leading to a simplification of the Navier-Stokes equations.

Since saltwater intrusion is a form of transport of matter, advection, diffusion and dispersion explain the salinity distribution in space and time. Advection ensures horizontal movement of water, where diffusion occurs due to density differences between layers in the water column. Diffusion occurs relatively slow, and has therefore a larger timescale. Dispersion cause the saltwater to spread out and mix with the freshwater, leading to a gradual increase or decrease in salinity throughout the basin.

To accurately model turbulent flow conditions, Delft3D uses the so called k-epsilon ( $k$ - $\varepsilon$ ) model which is a widely used turbulence closure model employed to simulate mean flow characteristics under turbulent flow conditions. As an eddy viscosity model, it belongs to a class of turbulence models utilized for calculating the Reynolds stresses. In this model, two transport equations (partial differential equations) are solved in addition to the conservation equations. The two variables being transported are the turbulent kinetic energy ( $k$ ), which quantifies the energy within turbulence, and the turbulent dissipation rate ( $\varepsilon$ ), which governs the rate of dissipation of turbulent kinetic energy. By incorporating these equations, the k-epsilon model allows for more accurate predictions of turbulent flow behavior in a wide range of applications.

## 3.2 Model schematization

### 3.2.1 Schematized domain

Numerical models commonly utilize grids to represent the physical domain, and Delft3D is no exception. By discretizing the domain into smaller elements or cells, which are then used to solve the unsteady shallow water equations, grids enable accurate simulation of fluid behavior. Each computational grid cell is composed of net nodes (corners of a cell), net links (edges of a cell that connect net nodes), flow nodes (the cell circumcentre), and flow links (line segments connecting two flow nodes). However, as the computational grid has a significant impact on both the accuracy of the model output and the runtime, it is a crucial aspect that requires careful consideration. A tradeoff between accuracy and computational time will therefore always have to be made (Deltares 2023).

In the development of a computational grid, orthogonality and smoothness are vital properties to ensure accuracy and reliability. Orthogonality is determined by the cosine of the angle between a flowlink and a netlink, where ideally, the angle  $\phi$  should be 90 degrees, resulting in a cosine value of 0. Smoothness, on the other hand, is the ratio of the areas of two adjacent cells, and ideally, the ratio should be 1, indicating that the areas of the cells are equal to each other. A grid with high orthogonality and smoothness ensures a better representation of the physical domain and improves the accuracy of numerical models.

The computational grid for the GTC canal was generated entirely using RGFGRID, a built-in tool in Delft3D. As there was no pre-existing basis available, the entire GTC domain had to be constructed from scratch. The resulting computational grid encompasses an area of 1.14 km<sup>2</sup> and comprises 4101 grid cells.

The accuracy (i.e., orthogonality and smoothness) of the domain varies along the GTC canal, with the main channel having the highest importance for computations and therefore having the highest accuracy. As suggested by Deltares (2023) for keeping the orthogonality as low as possible, the orthogonality of the main channel is approximately 1%. However, achieving an orthogonality of under 1% for the harbor connections and side branches such as Moervaart or Evergem was not feasible. These areas have an orthogonality ranging from 1% to 5%. It is noteworthy that the individual computational grids with such relatively high orthogonality are never located within the main channel and therefore have minimal impact on the computations in the main channel. The side branches are crucial to meet the actual storage volume of the GTC.

The width-length ratio of the grid cells also varies throughout the GTC canal. The computational grid consists of six grid cells spanning the width of the canals. In the Dutch section, the width of the canals ranges from 120 to 200 meters, while in Belgium, it extends up to 350 meters. To achieve greater accuracy, the width-length ratio is reduced at harbor connections and side branches. Furthermore, the use of unstructured grids is avoided due to the shape of the canal and side branches, and instead, curvilinear grids with flexible structured connections are utilized.

The computational grid is shown below in Figure 3.1.

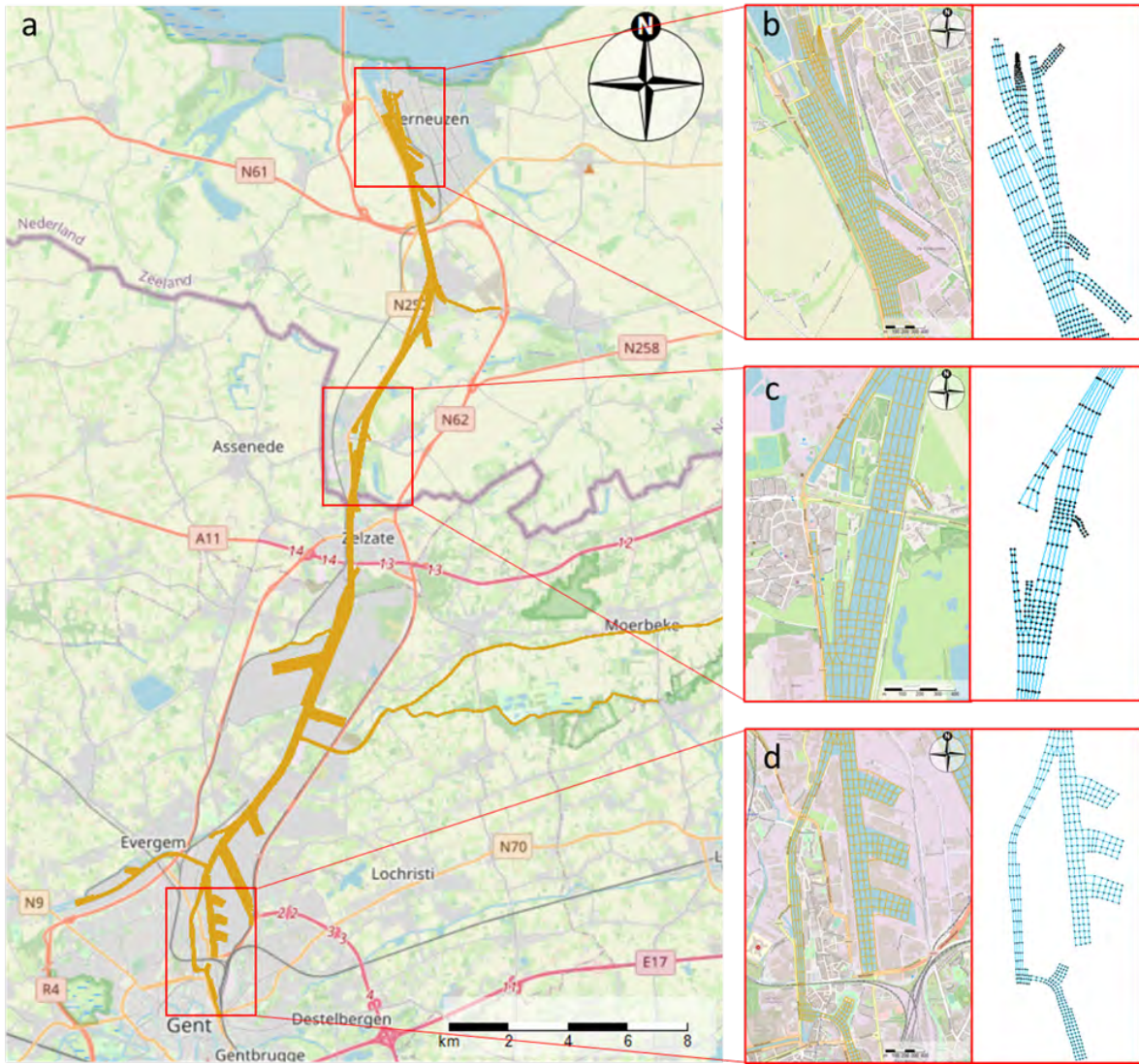


Figure 3.1: The developed computational grid; representing the model of the Gent-Terneuzen channel (a). Details are showed in (b), (c) and (d)

### 3.2.2 Bathymetry

To ensure a reliable representation of the subsurface, the most recent measurements were used. The utilized measurements/datasets were obtained from two sources, one for the Dutch section and one for the Belgian section.

The Dutch part of the dataset was obtained from the Data register of Rijkswaterstaat (n.d.) and consists of a sub-grid of the Bathymetry Netherlands - inland waters dataset. This is a 5-meter grid resolution interpolated land-cover grid of depth measurements obtained by hydrographic survey vessels stored in the National Storage System for Soundings. This dataset provides a snapshot of the bottom elevation of the inland waters from the German border to the baseline of the Dutch coast and connects to the Bathymetry of the North Sea. The measurements were taken on June 16, 2021.

The Belgian data was obtained from the Bathymetric database managed by the Agency for Maritime Services and Coast (Bathymetrische databank, n.d.). The data set has a resolution of 5 meters with interpolated values. The measurements in the Belgian section were taken on February 27, 2023.

The resolution of the bathymetric data is finer than the grid size that can be used in Delft3D, which

means that the data points cannot be directly used to generate the computational grid. In order to use the bathymetric data to create the computational grid, interpolation is necessary. The interpolation is performed using the Delaunay triangulation method, which is a mathematical technique for connecting data points to create a continuous surface (Deltares, 2023).

Moervaart, Zuidlede, Evergem and the branch to Gent were not included in the bathymetry measurements. For this reason, these side branches were assigned a fixed value. The fixed value corresponds to the local water depth at the respective point.

The final bathymetric map of the GTC is shown in Figure 3.2.

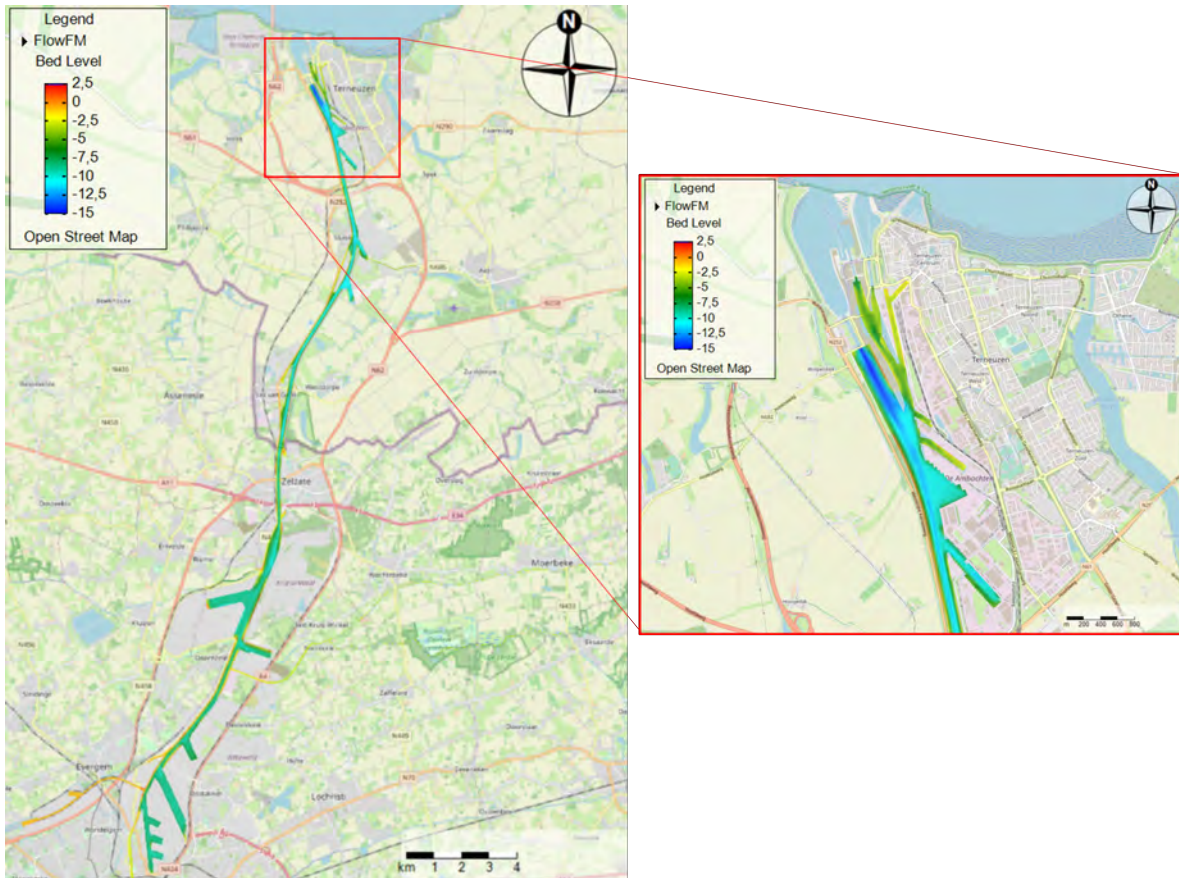


Figure 3.2: Implemented bathymetry representing the GTC

### 3.2.3 Model layers

Delft3D employs two different vertical layer types: the  $\sigma$ -coordinate system ( $\sigma$ -model) and the Cartesian  $z$ -coordinate system ( $Z$ -model). The  $Z$ -model uses layers that are bounded by two  $\sigma$ -planes that follow the bed topography and the free surface, resulting in a smooth representation of the topography. These layers are not uniformly thick but rather vary in thickness to provide a higher resolution in areas of interest such as the near-surface and near-bed zones. The number of layers remains constant throughout the computational area, regardless of the local water depth (Deltares, 2023).

To provide a better resolution around the pycnocline (the layer where the density gradient is greatest), the  $Z$ -model was introduced for 3D simulations of weakly forced stratified water systems. In contrast to the  $\sigma$ -model, the  $Z$ -model has horizontal coordinate lines that are nearly parallel with density interfaces in regions with steep bed slopes, thus reducing the artificial mixing of scalar properties such as salinity and temperature. However, the  $Z$ -model is not boundary-fitted in the vertical direction, and the bed and free surface are represented as a staircase (Deltares, 2023).

In the final model, the Z-layer approach is employed to capture the vertical mixing gradient more accurately. While the determination of the vertical resolution could be based on the largest vertical salinity gradient observed across the spatial domain, in this thesis, the number of layers is determined through a sensitivity analysis. This approach allows for a systematic exploration of different layer configurations and their impact on the model results. A schematic representation of the  $\sigma$ -model and Z-model is shown in Figure 3.3.

Although the largest vertical salinity gradient in the GTC is relatively small, suggesting that relatively a small number of layers would be sufficient. It has been decided to utilize 10 layers as a minimum to obtain more detailed and nuanced results. To ensure the robustness and reliability of the model, additional simulations have been conducted to assess the effectiveness of using both 15 and 20 Z-layers. The section Sensitivity Analysis describes the final chosen number of Z-layers (15).

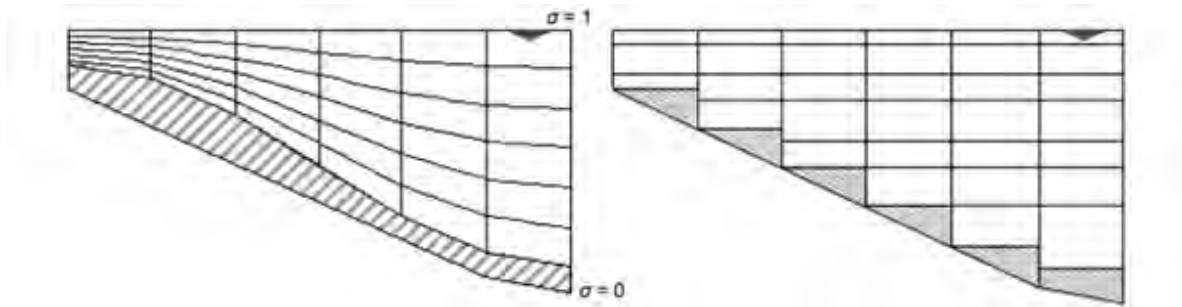


Figure 3.3: Schematic representation of sigma (left) and Z-layers (right)

### 3.3 Boundary conditions

This section will elaborate on the imposed (up-and downstream) boundary conditions. Various methods can be employed to establish boundary conditions within a Delft3D model. In this study, multiple upstream and downstream boundary conditions are necessary. Regarding the upstream boundary conditions, the approach of utilizing sources and sinks is adopted as the general method for imposing these conditions. On the other hand, careful deliberation was involved in determining the downstream boundary conditions, and their explanation will be provided in the subsequent subchapter. An overview of all factors which are a part of the up-and downstream boundary conditions are:

- Upstream boundary conditions:
  - Moervaart and Zuidlede;
  - Evergem;
  - Tolhuis weir.
- Downstream boundary conditions:
  - Consideration for different imposing methods;
  - Lock exchange flow and outflow estimation;
  - Saltwater influx and stratification;
  - Addressing Data Limitations for Lock Operation Modeling;
  - Effect door open time on saltwater exchange.

### 3.3.1 Upstream boundary conditions

As discussed in appendix A, the upstream discharge of water into the GTC, and the various channels that are responsible for this supply have been previously described. These channels include the Moervaart, Zuidlede, Evergem, and the tolhuis weir located in the inner harbor of Ghent. To accurately model these discharges in the top layer of the vertical offset, point sources were employed as per the recommendation of Deltares (2023). For modeling purposes, the upstream discharge was considered to be constant on a daily basis with a consistent salt load. Further subchapters provide a brief overview of each upstream channel. It is important to note that all inflows were assumed to have a constant salt load of 0.5 ppt (+/- 250 mg/l).

#### Moervaart and Zuidlede

To model the discharge from the Moervaart and Zuidlede channels, the total flow rate data from waterinfo.be was utilized, with measurements taken at Mendonk. This data reflects the combined flow rate of both channels. While there is also a measuring location at Sinaai on the Moervaart, the values recorded there are generally lower than those at Mendonk due to the discharge of various pumping stations along the Moervaart between these two locations. Unfortunately, no information is available on these pumping stations. Additionally, no discharge data is available for the Zuidlede channel, so a constant discharge value of  $1 \text{ m}^3/\text{s}$  was assumed. As a result, the total flow rate from the Moervaart and Zuidlede channels will be calculated using only the flow rate measurement at Mendonk on the Moervaart in combination with the constant discharge value for the Zuidlede.

#### Evergem

For the Evergem, there is both a weir and a lock present. The time series data used for this location was obtained from waterinfo.be and is called "location Evergem/Ringvaart". However, the data showed occasional negative values during times of low flow, which is physically impossible for water to flow from the lower downstream to the higher upstream section. A boundary condition has been implemented to prevent the flow from reaching negative values, where all occurrences of such instances have been set to a value of  $0 \text{ m}^3/\text{s}$ .

#### Tolhuis weir

Water flows from the city center of Ghent to the GTC through various structures, including both intentional spillage and leakage. There are no measurements available for these discharges. As a starting point, a constant value of  $2 \text{ m}^3/\text{s}$  has been assumed.

### 3.3.2 Downstream boundary conditions

#### Consideration for different imposing methods

The first considered way to impose the downstream boundary conditions is through 3D-boundary conditions. With this method, you can specify 3-dimensional boundary conditions for various quantities such as velocity, salinity, temperature, and tracer concentration. Here, you can choose between vertically uniform or varying boundary conditions, where the latter are defined as a percentage from the bed. This percentage from the bed in particular is important for modelling saltwater intrusion as saltwater intrusion usually occurs under stratified conditions. However, it's important to note that this tool is still a beta-functionality, meaning it is currently being tested and constantly improved.

The second way of imposing the boundary conditions is through so-called Sources and Sinks, which represent a point sources which can be used to introduce or remove water, heat, salt, or other constituents at specific points or areas in the model domain. These sources and sinks can be used to add or extract a discharge to or from the model, redistribute water and constituents within the model, model inflows or outflows from rivers or estuaries, or simulate the effects of pumping or discharging of water. Quantities such as velocity, salinity, temperature, and tracer concentration can be defined for a timeseries. The location, flow rate or concentration, and duration of the input or output have to be specified when using this tool. Sources and sinks can also be distributed over an area or along a line

in addition to being represented as point sources. Point sources can also be implemented in a depth dependent way when specifying the vertical grid cell.

After evaluating the different options for imposing boundary conditions in the model, the decision was made to use point sources. Point sources were chosen due to their ability to be implemented in a depth dependent manner, similar to 3D boundary conditions. However, when testing the model with 3D boundary conditions, errors were encountered. The model would either fill up continually or drain itself completely within a few days, leading to inaccurate results. Using point sources, water, heat, salt and other constituents can be introduced or removed at specific points or areas in the model domain, providing a more precise control of boundary conditions.

Point sources can also better represent the initial mixing process, depending on which vertical grid layer they are placed in. This is because they can be located at specific points or areas in the model domain and therefore, can be used to model the initial mixing process more accurately. When testing the same specified depths for salinity intrusion using 3D boundary conditions (which are defined as a percentage from the bed), it is found that the differences were much smaller. Therefore, using point sources provides a better control of the boundary conditions in which the point source can help to improve the accuracy of the model results. Overall, it is believed that using point sources is the best option for the model and will result in more accurate and reliable outcomes.

Defining the downstream boundary conditions proved to be a relatively difficult process. Actual measured information on the inflow and outflow per lock, number of lock cycles per day, door opening times, and salt exchange volumes are not available. Therefore, necessary assumptions have to be made for determining the downstream boundary conditions. The assumptions and underlying principles will be described separately in this chapter.

### Lock exchange flow and outflow estimation

Locks are the primary structures that allow the exchange of water between the GTC and the Westerscheldt. During each lock operation, salt-brackish water flows from the GTC into the Westerscheldt, and saltwater enters the canal. However, there is a net water displacement from the canal to the Westerscheldt. The amount of water that can be exchanged per lock operation depends on the lock chamber's surface area and the water level difference between the canal and the Westerscheldt. The formulas below indicate this water displacement.  $Q_{\text{loss/passage}}$  represents the amount of water,  $N_{\text{passage}}$  the amount of passages per day,  $A_{\text{lock}}$  the area of a lock, and  $\Delta h$  the water level difference between the canal and Westerscheldt.

$$Q_{\text{loss/passage}} = A_{\text{lock}} \cdot \Delta h$$

$$Q_{\text{loss/day}} = \sum N_{\text{passage}} \cdot A_{\text{lock}} \cdot \Delta h$$

To estimate the lock exchange flows, the results of Svašek Hydraulics (Svasek, 2015) were used, which estimated the exchange volumes for the existing Terneuzen lock complex and the new sea lock scenario. The exchange volumes were converted into lock exchange flows by distributing the total exchange volumes based on the number of lock operations per day and the accompanying simulated door-open times. Table 3.1 shows the results used in the model setup.

Table 3.1: Estimation of lock exchange flows per lock (FINEL3D) performed by (Svasek, 2015)

	<b>Width</b>	<b>Length</b>	<b>MSL</b>	<b>Bottom</b>	<b>Fresh-saline</b>	<b>Calibration</b>	<b>Exchange</b>
	[m]	[m]	[m]	<b>sluice</b>	<b>exchange</b>	[-]	<b>volume</b>
				[m]	FINEL3D		[m <sup>3</sup> ]
East Lock	24	260	0.43	-7	0.33	0.21	3213
Middle Lock	24.5	140	0.43	-7.5	0.83	0.21	4741
West Lock	40	290	0	-13	0.94	0	30,340
New Lock	55	427	0.43	-17	0.68	0.21	58,454

However, accurately modeling the saltwater influx near the locks is challenging due to mixing processes that cannot be resolved by open discharge boundaries. To overcome this limitation, depth dependent sources and sinks are implemented halfway the lock door, resulting in a single distinct discharge flux per lock. Depth dependent sources and sinks are utilized to discharge saltwater into the GTC and fresh/brackish water towards the Scheldt at the surface layer. Although the actual water exchange distribution per lock is complex and may vary, a uniform distribution is adopted for simplicity across all locks, by using a single point source halfway the depth of the lock door. The outflow represents the daily average outflow required to maintain the target water level of the GTC, accounting for actual levelling losses and drained volumes needed for water level control. From a grid schematization standpoint, the outflow for all locks is derived from a single cell in the upper layer.

### Saltwater influx and stratification

By using source and sinks, the imposed time series of inflow and outflow can be linked to a temporal variable salinity concentration. These two aspects together form the basis for saltwater intrusion per lock. The imposed salt concentrations at the inflow correspond to the salt concentrations of the Western Scheldt at the same time. These values fluctuate between 14 and 17 ppt (8000 and 15000 mg chloride/l). As described above, the salt flux into the canal is depth dependent.

Deltares (2023) state that if the mixing process cannot be resolved in the model, for instance if a river is modelled as a point discharge adjacent to a closed boundary, make sure that the whole river is discharged into the top layer or in the top layers, depending on the estimated thickness of the fresh water plume at the discharge cell.

Several tests have shown that when the salt flux is discharged into the top layer, the least amount of salt enters the canal with also the least stratification. This is likely due to the relatively high vertical velocity in the water column at this point, as mentioned by Deltares (2023). In contrast, when the saltwater is discharged at the bottom, there is a strong stratification and extremely high salt concentrations observed at the bottom. There is a remarkable effect of discharging saltwater at different depths to represent the locks.

Discharging in the middle of the water column showed negligible differences in terms of stratification and salt concentrations at the Skikuil bridge and Sas van Gent calibration points. However, there was a (relatively) small difference in salt concentrations near the locks, with discharges nearer to the bottom resulting in higher observed salt concentrations at the bottom.

### Addressing Data Limitations for Lock Operation Modeling

Although average yearly data is available, the exact timings of each lock’s operation are unknown. To address this, a cycle-averaging method has been employed for the current modeling approach. This decision was made due to the lack of data and uncertainty regarding the future lock operations and duration for the New Lock. Additionally, the scenarios outlined in the MER only provide average daily lock frequencies, with no information regarding the potential sequencing of short and long door

opening times (Lieveense CSO, 2015).

### Effect door open time on saltwater exchange

The door open time refers to the duration of time for which the lock doors remain open during a lock operation. The door opening times of the locks are also unknown, but they are crucial in determining the salt exchange between the lock chamber and the canal. To address this, a uniform approach has been taken in implementing door opening times for the locks. The primary goal is to ensure that the simulation accurately represents the amount of saltwater intrusion to achieve the desired concentrations in the canal.

However, there are estimates available for the door open times for all locks of the lock complex. One of these estimates was made by Svašek Hydraulics (Svasek, 2015), which they used for their calculations. Table 3.2 below shows the door opening times, and it is clear that the doors remain open significantly longer than the salt exchange (factor 2-3). So it can be assumed that all saltwater enters the GTC, no matter the simulated door opening time and theoretically, no reduction factor should be applied during the calibration phase.

Table 3.2: Saltwater exchange and average door opening times per lock (MER Deelrapport Water)

	Saltwater change [min]	ex-Average open time [min]	door Average door open time / exchange time [-]
East Lock	16	32	2
Middle Lock	8	26	3
West Lock	13	42	3
New Lock	20	60	3

In more detail, figure 3.4, 3.5 and 3.6 display the distribution of the maximum door opening time: the time that results when the doors remain open when no leveling, opening, or closing takes place (internal document HKV, Vuik & Lambrechts, 2023). This figure reveals that only the shortest door opening times in the vicinity of the salt exchange time are found in the West Lock and Middle Lock. In the majority of lock passages, the door opening time is so long that the salt has already been exchanged well before the doors close again. For the total salt intrusion, the West Lock is dominant. In 95% of the cases, the salt exchange time at this lock is shorter than 17 minutes, while the door opening time is longer than 21 minutes in 95% of cases. Thus, shortening the door opening time only has a sporadic effect on the salt exchange, as the time duration's are often too far apart. As a result, the calculated salt intrusion (and the actual situation) is relatively insensitive to details in the lock operation, such as faster or slower door closure or even the use of a bubble screen.

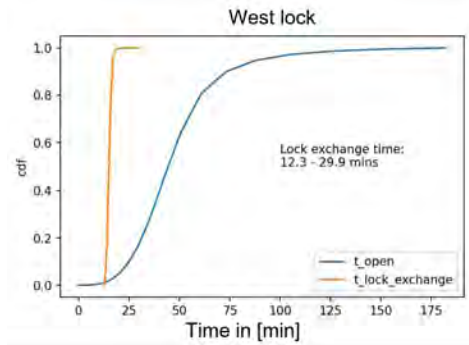


Figure 3.4: Cumulative distribution function (CDF) of gate opening durations (blue) and salt exchange durations (orange) for the **West Lock** (Vuik & Lambrechts, 2023).

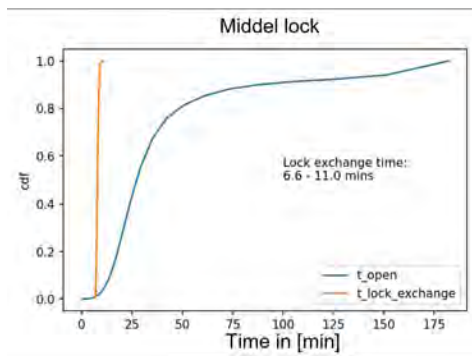


Figure 3.5: Cumulative distribution function (CDF) of gate opening durations (blue) and salt exchange durations (orange) for the **Middle Lock** (Vuik & Lambrechts, 2023).

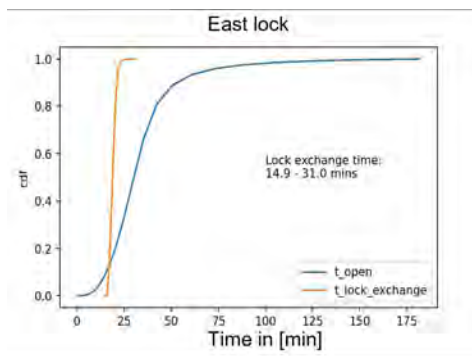


Figure 3.6: Cumulative distribution function (CDF) of gate opening durations (blue) and salt exchange durations (orange) for the **East Lock** (Vuik & Lambrechts, 2023).

Based on the information above, it can be concluded that the actual door open time during the simulations has little to no effect on the salt exchange. From figure 3.4, 3.5 and 3.6 it shows that the assumption can be assumed realistic. For simplicity, it has been chosen to set the door open times equal to a single time step of the input data, which is 10 minutes. Changing the door open times to 20 minutes for example will also have little effect since the total amount of salt intrusion remains exactly the same during the period.

## 3.4 Initial conditions

### 3.4.1 Water level

The defined initial conditions are rather straightforward. The initial water level is set at 2,13 meters, which is the target level of the GTC, and is held constant throughout the simulation time. In reality, the water level fluctuates, and there is a gradient of approximately 10 cm between upstream and downstream boundaries. However, accurately simulating the water level (fluctuation) is beyond the scope of this thesis and thus not considered. The fluctuations in the water level have minimal effect on the ultimate goal, which is to test measures to reduce the saltwater intrusion in the GTC.

### 3.4.2 Salinity

In the model, a uniform initial salinity value of 1.5 ppt (880 mg/l) is applied to the entire canal domain. Although the actual salt concentration exhibits spatial and vertical variations, Delft 3D can

only account for spatial variations in the horizontal plane. As a result, setting the initial salt concentration uniformly across the domain leads to a variable spatio-temporal distribution of salinity during the warm-up period. The selected initial salt concentration does not correspond precisely to either of the calibration points, Sluiskil brug and Sas van Gent, as it is intentionally set slightly below the lowest actual initial value. This approach requires a spin-up time to achieve a realistic salinity distribution.

### 3.4.3 Temperature

The initial temperature for both calibration points is similar, as they are both located in close proximity to each other and are subject to the same environmental conditions. The data used for the initial temperature comes from waterinfo.nl (Rijkswaterstaat, n.d.). The initial water temperature is set to correspond to the actual temperature at the beginning of the simulation. For 2018 this is 8 degree Celsius.

## 3.5 Physical/numerical and additional parameters

In this section, the parameters discussed for initial model setup encompass roughness, viscosity, temperature, and wind. Table 3.3 provides an overview of the utilized values for these parameters along with their respective sources of origin.

Table 3.3: Overview value, unit and source physical/numerical and additional parameters

Parameter	Value	Unit	source
Roughness	0.023	$m^{1/3}/s$	Deltares, 2023; Verbruggen & Van Der Baan, 2022; Buschman et al., 2015
Viscosity [HED\HEV]	0.1	$m^2/s$	Default value Deltares, 2023
Viscosity [VED\VEV]	1E-6	$m^2/s$	Default value Deltares, 2023
Temperature		$^{\circ}C$	Rijkswaterstaat, n.d.
Wind direction		$^{\circ}$	KNMI, n.d.
Wind speed		$m/s$	KNMI, n.d.

### 3.5.1 Roughness

When 3D models are run within Delft3D, a quadratic bed stress formulation is assumed at the bed slip boundary. This formulation is similar to depth-averaged computations, which are commonly used in hydraulic engineering and fluid dynamics. The quadratic bed stress formulation takes into account the interaction between the water and the bed, considering factors such as bed roughness, turbulence, and sediment transport, dependent on the initialized processes. By utilizing this formulation, Delft3D can accurately simulate complex hydrodynamic processes and provide valuable insights into the behavior of water systems.

However, due to the lack of clear information or data about the roughness of the GTC, approximations have to be made. The default roughness value, expressed as Manning’s coefficient, in Delft3D is set to  $0.023 m^{1/3}/s$ , according to (Deltares, 2023). This value is also used in similar literature sources (Verbruggen & Van Der Baan, 2022; Buschman et al., 2015). Furthermore, according to the geological composition of the GTC, which is primarily composed of clay and fine sands, a Manning’s coefficient of 0.023 corresponding to the fine materials (DINOloket, n.d.). Therefore, this value has been used as an approximation for the roughness of the GTC in the simulations.

### 3.5.2 Viscosity

In fluid flow simulations, both flow and turbulence parameters play a crucial role in determining the accuracy of the results. For the model setup, the default values of the Horizontal Eddy Viscosity and diffusivity are used,  $0.1 \text{ m}^2/\text{s}$ . Similarly, the default values of the Vertical Eddy Viscosity and diffusivity are set to  $1\text{e-}6 \text{ m}^2/\text{s}$ . These values serve as ambient values in the  $k\text{-}\varepsilon$  turbulence model, which calculates the mixing length based on these parameters. The Smagorinsky factor is also employed to estimate the eddy viscosity and diffusivity and can be adjusted to match the level of turbulence in the simulated flow. Overall, these parameters will be utilized for calibration in a later stage to obtain accurate model results. The calibration procedure for these values will involve a sensitivity analysis, which will be conducted in Section 4.4.

### 3.5.3 Temperature

The influence of temperature on saltwater intrusion is indirect and is mediated by its effect on water density. Temperature does not have a direct impact on the salt content of water. The water temperature data for the GTC was obtained from waterinfo.nl (Rijkswaterstaat, n.d.) with a 10-minute interval. Two depth dependent measurement stations are present in the GTC, Skikuil brug and Sas van Gent, at the bottom ( $-5\text{mNAP}$ ) and surface ( $+0.25\text{mNAP}$ ) levels. Due to negligible differences, the average temperature was used for the computations. Below, Figure 3.7 shows the water temperature for the computational time frame.

Incorporating temperature in the model can be done in different ways. The most complete heat flux model are the so called Composite heat flux model (i.e., the Ocean heat flux model) and the simplest model, the Excess temperature model.

The Composite heat flux model takes into account surface heat exchange mechanisms (combination of water temperature, air temperature, humidity and cloudiness). This model is able to catch the most dynamics. However, the computational time for this model is higher in comparison to the Excess model.

In the Excess model, the observed water temperature is used as model input. This means that the water in the GTC has the right temperature values but without complex computations. All model input contains the observed water temperature, by means of this, the warm up period of the model increases slightly.

After careful evaluation, the Composite heat flux model has been chosen as the preferred temperature model. Despite its high computational time compared to the Excess model, this model takes into account various surface heat exchange mechanisms, resulting in a more dynamic representation. While the Excess model provides accurate temperature values without complex computations, the Composite model's ability to calculate new water temperatures based on multiple factors allows for a more comprehensive understanding of real-life conditions, justifying the increased computational time.

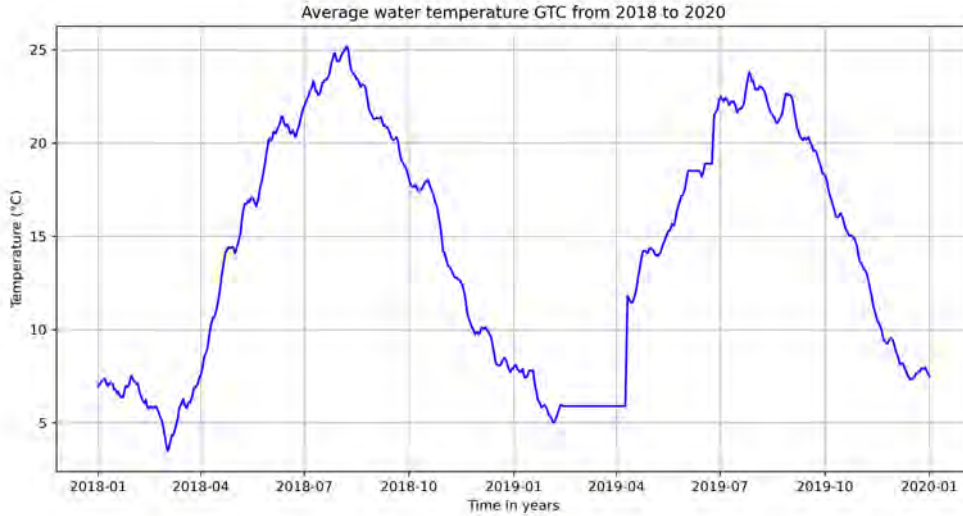


Figure 3.7: Average observed water temperature GTC 2018-2019

### 3.5.4 Wind

External factors, such as wind can have an impact on the flow field of fluids. Recent studies by Zhang et al., (2019) and Scroccaro et al., (2023) have emphasized the influence of wind on saltwater intrusion. It has been observed that wind blowing in either direction can either intensify or weaken the extent of saltwater intrusion. For example, wind can create an exchange flow that causes saltwater to flow against the wind direction near the bottom.

In the model, the local wind is included as a shear stress in the flow equations. Wind speeds (m/s) and wind direction (degrees) are obtained from the Dutch national weather service, KNMI (KNMI, n.d.), and are measured at Vlissingen with hourly averaged values at a height of 10 mNAP. Although these measurements may differ slightly from the actual wind conditions at GTC, they provide a more realistic representation than exclusion of the wind.

To incorporate the wind in the model, a Smith & Banks (2 break points) drag coefficient is used. This approach specifies a linearly varying dependency for one range of wind speeds. The default values provided by Deltares (2023) are used for this parameter.

Figure 3.8 illustrates the temporal variations in wind speed and direction throughout the computational time frame. The wind speed remains relatively constant, with a noticeable increase during the summer months around July. A distinct trend of (south)westward wind direction is evident, which is not expected to have a significant impact on the longitudinal extent of salinity intrusion in the canal. Conversely, wind directions from the north and south can exert a more pronounced influence on the salinity intrusion length (Zhang et al., 2019 & Scroccaro et al., 2023). However, these are observed less. The wind's influence on the extent of saltwater intrusion appears limited, except for higher daily variability.

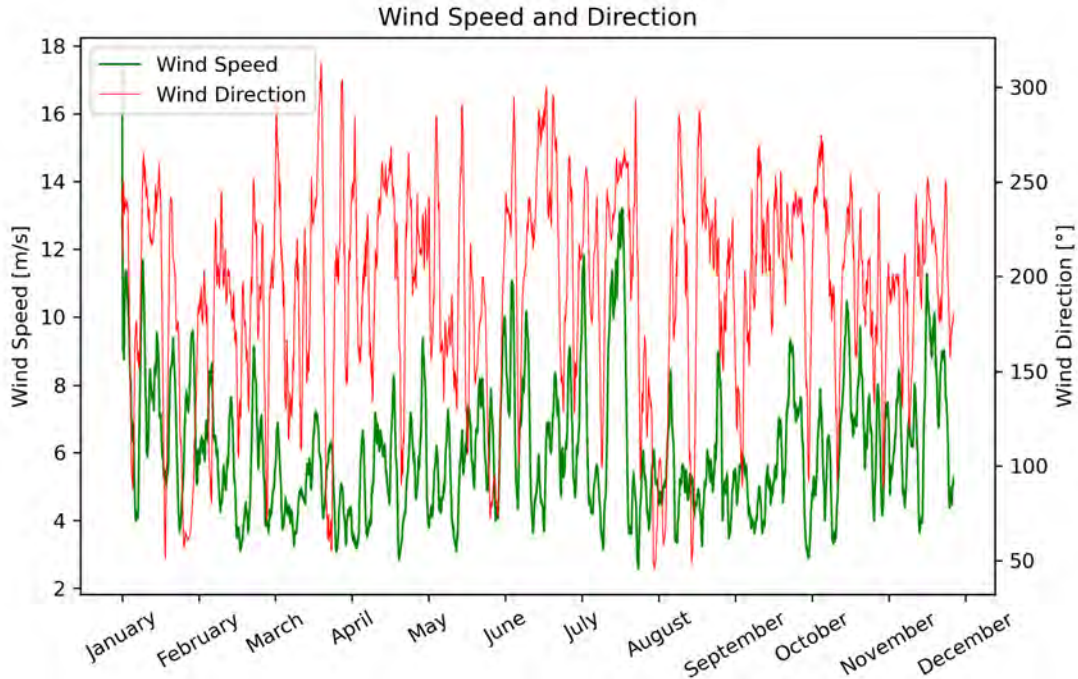


Figure 3.8: Wind speed and Direction observed at Vlissingen

## 3.6 Implementation of mitigation measures

In order to systematically address saltwater intrusion in the GTC, a total of eight measures will be evaluated using the calibrated and validated model. These measures encompass physical structures (referred to as measures 1 to 4) and management-related measures (referred to as measures 5 to 8). The following subchapters provide detailed descriptions of each measure to be analyzed.

### 3.6.1 Measures encompassing physical structures

For the physical structure measures, the focus will be on the New Lock, as it presents a significant opportunity for improvement in mitigating saltwater intrusion. The West lock already has existing measures in place, while the East lock primarily caters to recreational boating and contributes minimally to saltwater intrusion (only 5%). Due to its larger size and potential for higher saltwater intrusion, the New Lock is a prime target for implementing effective measures. The measures are shown below including a short description about how they work and why they are chosen. The measures are schematically visualized from figure 3.9a to 3.9d.

#### 1. Submerged threshold with additional discharge

The submerged threshold, or saltwater trap, capitalizes on the density difference between saltwater and freshwater to capture saltwater at the bottom. This measure relies on the principle that saltwater, being heavier, can be effectively trapped by a submerged threshold structure (see figure 3.9a). It is important to emphasize that the effectiveness of this measure is contingent upon the presence of additional discharge. The selection of this measure is based on its recognition as a potentially effective approach in (scientific) literature for mitigating saltwater intrusion.

## 2. Elevated threshold with additional discharge

The elevated threshold measure takes advantage of the density differences between saltwater and freshwater. By employing an elevated threshold, the saltwater can be effectively captured and confined at the bottom (see figure 3.9b). It is worth noting that this measure relies on the presence of additional discharge to yield any impact. The selection of this measure is based on its recognition as a potentially effective approach in (scientific) literature for mitigating saltwater intrusion.

## 3. Canal constriction

The narrowing of the canal can potentially reduce saltwater intrusion due to the alteration of hydrodynamic processes (see figure 3.9c). As the canal becomes narrower, localized flow acceleration can occur, leading to increased mixing and freshwater dominance, subsequently reducing saltwater intrusion. This measure is derived from knowledge gained in estuarine systems, where the effectiveness of this measure has been demonstrated.

## 4. Selective withdrawal

Selective withdrawal also utilizes the density differences between fresh and saltwater. In this measure, a freshwater barrier can be placed near the saltwater intrusion point at the surface layer, effectively preventing the intrusion of freshwater. Subsequently, the saltwater can flow underneath the barrier and be extracted (see figure 3.9d). This measure is derived from the successful implementation of selective withdrawal in the Nort Sea Canal (Amsterdam-Rijnkanaal). By strategically controlling the flow and selectively extracting saltwater, this measure contributes to the reduction of saltwater intrusion.

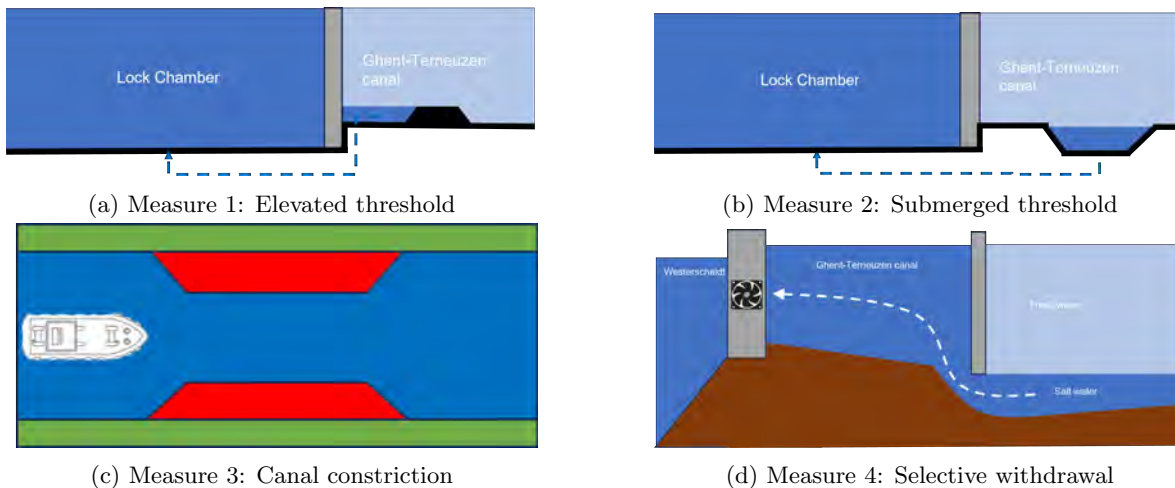


Figure 3.9: Physical measures. (a) Elevated threshold, (b) Submerged threshold, (c) Canal constriction, (d) selective withdrawal

### 3.6.2 Measures encompassing management practices

The management-related measures (measures 5 to 8) incorporate modifications in the upstream discharge, as it exerts the most significant influence on saltwater intrusion. The upstream discharge utilized in the scenarios is sourced from the Evergem lock and the Tolhuis weir near Ghent. The Moervaart and Zuidlede waterways were not considered due to their considerably downstream location, making it unrealistic to merge them in the analysis. The area of interest is how salt responds to discharge variations at different time scales. These measures are chosen as previous research by Vuik & Lambrechts (2023) investigated these exact measures using a 2DV model. It is expected that a 3D model could better represent this phenomenon. The measures are shown below including a short description about how they work. A schematic visualization is given in figure 3.10a to 3.10d.

## 5. Summer discharge spreading

Through the summer discharge spreading, where the average discharge remains constant, the salt load could effectively be controlled (see figure 3.10a). By distributing the averaged discharge over a longer duration, the concentration of saltwater intrusion could be mitigated.

## 6. Freshwater pulse

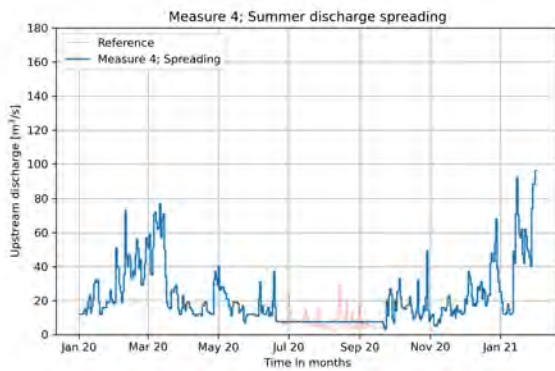
The freshwater pulses measure involves pulsing the summer discharge while maintaining the average discharge (see figure 3.10b). By periodically increasing the discharge for short durations, the saltwater intrusion can be pushed back.

## 7. Winter flushing

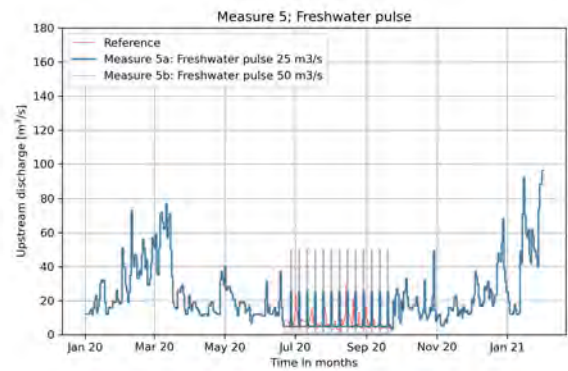
Increasing the winter discharge can effectively reduce saltwater intrusion and its impact throughout the year (see figure 3.10c). By increasing the discharge during the winter season, when the saltwater intrusion is less pronounced, the saltwater can be diluted and flushed downstream.

## 8. Rainfall pulse

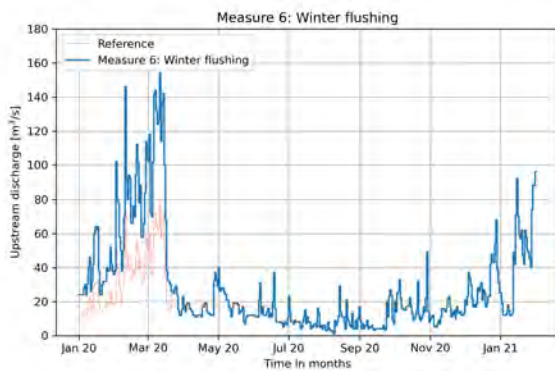
Simulating an intense summer rainfall event provides insights into its potential effectiveness in reducing salt concentration (see figure 3.10d). By simulating the conditions of a localized heavy rainfall event, the measure explores the extent to which such events can contribute to flushing the saltwater.



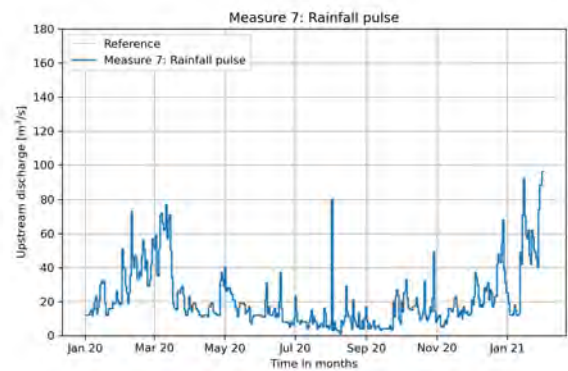
(a) Measure 4, Summer discharge spreading



(b) Measure 5, Freshwater pulse



(c) Measure 6, Winter flushing



(d) Measure 7, Rainfall pulse

Figure 3.10: Management-related measures. (a) Summer discharge spreading, (b) Freshwater pulse, (c) Winter flushing, (d) Rainfall pulse

### 3.6.3 Description of mitigation measure 1; Submerged threshold with additional discharge

Since there is currently no available data or knowledge regarding the bottom elevation of the New Lock, there is the possibility of implementing a submerged threshold with additional discharge, acting as a salt trap. As the West lock already has a similar design, the deepened position can be combined. In this case, the cross-section of the salt trap as shown in Figure A.1 from the West lock would be extended to the New Lock. The implementation of the modified bathymetry in Delft3D is illustrated in figure 3.11 below.

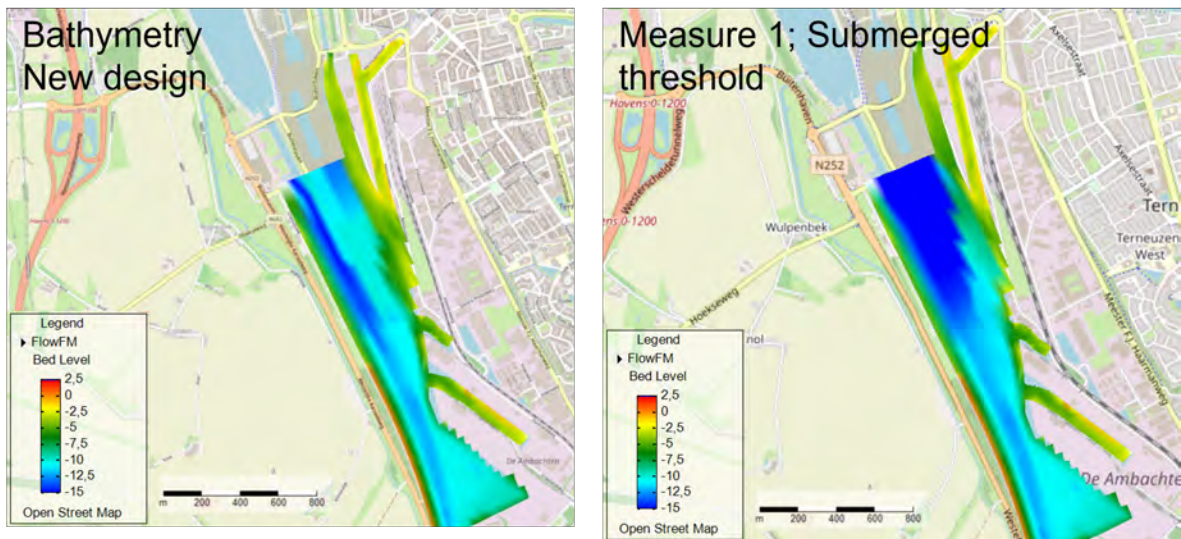


Figure 3.11: Measure 1, Submerged threshold with additional discharge for New Lock Terneuzen

Two scenarios will be analyzed regarding the additional threshold, namely a scenario with an additional discharge of  $10 \text{ m}^3/\text{s}$  and a scenario with an additional discharge of  $20 \text{ m}^3/\text{s}$  if sufficient upstream discharge is available. These values have been selected based on the capacity of  $10 \text{ m}^3/\text{s}$  for unobstructed exchange discharges according to VNSC (2015), whereas in the current study it is found to be  $22 \text{ m}^3/\text{s}$  due to the recent increase in the threshold for exchange discharges.

### 3.6.4 Description of mitigation measure 2; Elevated threshold with additional discharge

Section 2.3 “Changes due to lock modifications” described the design of the New Lock Terneuzen. Staying as close as possible to the actual design enhances the applicability of this research and the analysis of mitigation measures. Therefore, the following bullet points are provided below, highlighting the relevant aspects related to the new lock:

- No fresh-saltwater separation, only elevated threshold for a possible future bubble screen;
- A salt threshold on the canal side from  $-16.5$  to  $-14.1$  mNAP;
- A foundation for a possible future additional threshold up to  $-11.8$  mNAP;
- Additional discharge through the culverts of the New Lock, therefore no additional discharge facility.

The new design incorporates an elevated threshold for the potential implementation of a bubble screen, suggesting the possibility of testing such a measure. However, it should be noted that a bubble screen only serves to delay saltwater exchange. Considering that the New Lock exhibits a 3-fold increase in saltwater exchange and door opening times, it is expected that a bubble screen would indicate minimal benefits. Additionally, preliminary research conducted by Vuik & Lambrechts (2023)

indicates that a bubble screen at the West lock, which exhibits a 2-fold increase in saltwater exchange and door opening times, proves to be relatively ineffective.

The salt threshold on the canal side, ranging from -16.5 to -14.1 mNAP, is incorporated into the new design, but little adjustment can be done to it at present. However, a foundation for a possible future additional threshold up to -11.8 mNAP has been established. In the current design, the threshold itself is not yet implemented, only the foundation will be implemented. It is therefore worth investigating the extent to which this threshold can effectively reduce saltwater intrusion, in order to determine its feasibility. This threshold will not cause problems for accommodating the future inland vessel category of CEMT-VI and CEMT-Va, enough vertical space is available since these vessels have a submerged draught of 3 and 3,5 meter respectively (Standardization of inland waterways, 2020).

In addition, it is important to note that a salt threshold often functions in conjunction with culverts for additional discharge, which are already present in the current design. These culverts are implemented at the bottom, unlike the Middle lock where backflushing occurred from the surface water.

The additional salt threshold follows the same concept as the salt threshold on the canal side. The heavier saline water is located at or near the bottom of the canal. Therefore, a barrier or threshold at the bottom can potentially intercept or reduce the intrusion of this denser water. A schematic representation of the current design and the inclusion of the threshold is depicted in Figure 3.12 below.

Furthermore, the two scenarios with a constant additional discharge of 10 m<sup>3</sup>/s and 20 m<sup>3</sup>/s will be conducted based on the report by VNSC (2015).

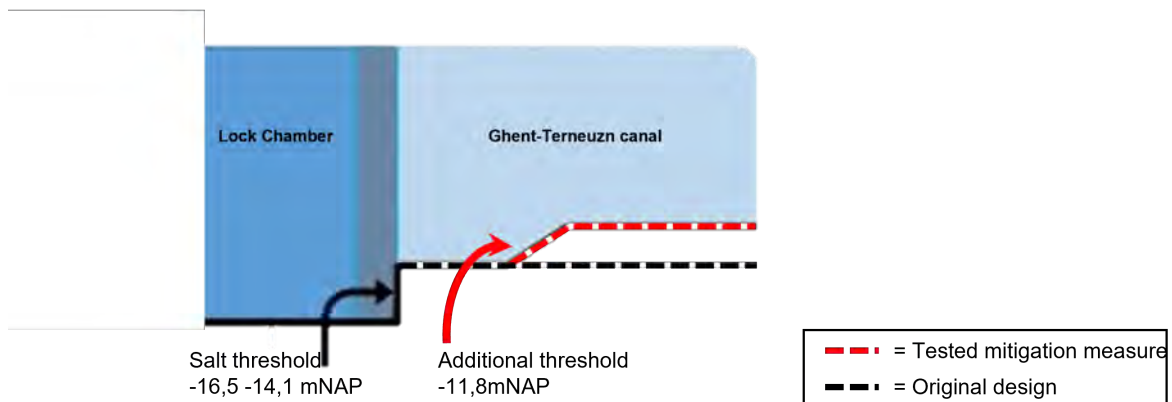


Figure 3.12: Measure 2, Schematic representation of the current design and the inclusion of the threshold

### 3.6.5 Description of mitigation measure 3; Canal constriction.

The Ghent-Terneuzen Canal varies in width between 120 and 200 meters. Potential modifications to this width can result in a reduction in the quantity or length of saltwater intrusion. According to Mendelsohn et al., 2000, constrictions play a role in controlling flow rates and salinity conditions in rivers (including canals). Therefore, the implementation of a narrowing section in the GTC has been carried out. At this location near Sluiskil, the canal has been narrowed from 160m to 110m, allowing normal vessels (vessels without hazardous substances, according to Rijkswaterstaat, 2017) to pass each other unhindered.

Two variants have been implemented, one with a narrowing length of 170 meters and another variant with a narrowing length of 400 meters. The implementation of these variants in Delft3D, including their locations, is illustrated in Figure 3.13 below.

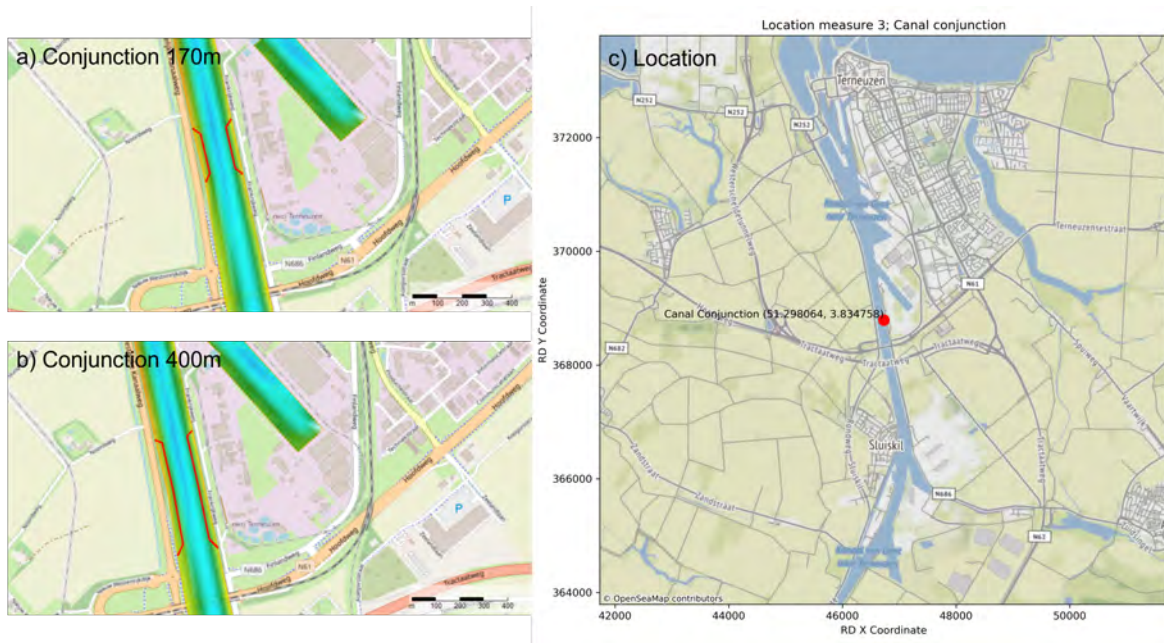


Figure 3.13: Measure 3, Canal constriction of 170m and 400m

### 3.6.6 Description of mitigation measure 4; Selective withdrawal

The selective withdrawal measure leverages the principle of density differences between saltwater and freshwater. By strategically placing a freshwater dam near the inflow of saltwater, the barrier prevents the upward movement of freshwater, allowing saltwater to flow underneath and be extracted. This process effectively removes the saltwater component from the system. It is important to note that the full implementation of this measure in Delft3D was not entirely feasible due to limitations in representing the freshwater dam as a 3D object. As a result, a thin dam was employed, and water extraction was performed at the bottom, an schematic representation of selective withdrawal is illustrated in Figure 3.9d.

### 3.6.7 Description of mitigation measure 5; Summer discharge spreading

In this scenario, the upstream discharge is smoothed over the period from the 21st of June to the 21st of September. The cumulative upstream discharge during this period remains the same as in the reference situation. The purpose is to investigate the effect of temporarily stored water evenly distributing water throughout the summer. It is noteworthy that a significant buffer volume is needed to be able to perform this scenario. Gradually spreading an average discharge of in this case  $7,5 \text{ m}^3/\text{s}$  results in a total buffer volume of 27 million  $\text{m}^3$ . The graph to represent this upstream discharge is plotted against the reference scenario in Figure 3.10a.

### 3.6.8 Description of mitigation measure 6; Freshwater pulse

Similar to measure 7, but with alternating 6 days of low upstream discharge followed by 1 day of high upstream discharge (freshwater pulses). This scenario aims to assess the impact of different pulses flows on saltwater intrusion. The graph to represent this upstream discharges is plotted against the reference scenario in Figure 3.10b.

### 3.6.9 Description of mitigation measure 7; Winter flushing

This scenario replicates the reference situation, but with doubled upstream discharge during the winter season. The objective is to investigate the influence of increased discharge during winter on salt intrusion. The graph to represent this upstream discharge is plotted against the reference scenario in Figure 3.10c.

### 3.6.10 Description of mitigation measure 8; Rainfall pulse

In this scenario, the reference situation is maintained, but an  $75 \text{ m}^3/\text{s}$  freshwater pulse is introduced on August 1st. This pulse represents a short-duration period of intense rainfall in a dry summer and is modelled by an increased discharge for 2 days. The graph to represent this upstream discharge is plotted against the reference scenario in Figure 3.10d.

## 3.7 Result analysis

To assess the effectiveness of the implemented measures in reducing salt intrusion, a systematic comparison will be conducted between the reference run and the evaluated interventions. This comparative analysis aims to determine the extent to which saltwater intrusion has been reduced by the applied measures in a consistent manner.

After the calibration and validation phases, a reference model will be established to represent the new situation of the Terneuzen Lock Complex, including the West lock, New lock, and East lock. Since the model has been validated, it is considered to be consistent and reliable, providing a solid foundation for the assessment of the implemented measures.

To analyze the reduction of saltwater intrusion, the comparison will focus on evaluating the quantity of incoming salt and the extent of saltwater intrusion. The two calibration points will remain central to the evaluation, as their accuracy has been validated. Furthermore, the salinity values near the locks will be examined, although the availability of data makes it challenging to ascertain their exact accuracy. However, the validated model incorporates essential physical aspects necessary for representing reality. It is important to note that there is a possibility of the validated model exhibiting slight deviations in salt concentration near the locks. Nevertheless, a relative comparison of the implemented measures against the reference run can still provide insights into achieving the desired outcomes.

In addition, a more objective comparison can be conducted by showing the difference between two graph lines. This will be done for location Skikuil brug (downstream), location Sas van Gent (halfway the canal) and location Evergem (upstream). This allows for a direct comparison between different scenarios, enabling the identification of potential hotspots, peaks, or troughs.

Any variations in salinity levels will be quantified such as percentages or chloride concentrations, indicating the extent of decrease or increase over a specific time period in relation to the reference run.

## Chapter 4

# Calibration and Validation

The calibration and validation of the model were performed using the data from 2018 and 2020, respectively. These years were selected as they exhibit high salinity peaks, which are of particular interest for this study area. Before calibrating the model, a sensitivity analysis was conducted to determine how sensitive the model's outputs are to changes in its input parameters. The result of this analysis is then used for the calibration process. During the calibration process, the model was optimized to obtain the best parameter set that could simulate the salinity dynamics in the GTC for the calibration year (2018). The validation year was then used to assess the ability of the model to accurately predict the salinity levels in the GTC for a period that was not used for calibration (2020). The performance of the model with the initial parameter settings will be presented first to provide an overview of the flow processes near the locks.

### 4.1 Hydrodynamics and salinity

The upstream discharge and salinity values are the key parameters for developing the model. The upstream discharge has the greatest influence on the amount and the length of saltwater intrusion in the GTC (Fricourt et al., 2014; Vanderkimpen et al., 2012; Tully et al., 2019). As shown in Table 2.3 data is sourced from waterinfo.be (discharge) and waterinfo.nl (salinity values). The data covers the period from 2014 to 2018, as depicted in Figure 4.1. In this figure, salt concentrations (plotted on the left y-axis in blue) are shown against the upstream discharge (plotted on the right y-axis in red).

A clear trend is observed throughout the entire period, wherein low discharge corresponds to high salt concentrations in the canal and vice versa. This trend is particularly prominent during the summer when the minimum discharge of  $13\text{m}^3/\text{s}$  is not achievable. These observations visually illustrate the problem described in the problem analysis and provide further support for the statements made by others (Fricourt et al., 2014; Vanderkimpen et al., 2012; Tully et al., 2019).

The salinity concentrations are measured at two locations in the canal, namely Skikuil brug and Sas van Gent (SVG). At these locations, measurements are taken at two depths (+0.25mNAP and -5mNAP). However, due to the small differences between these two measurements and the focus of this thesis on evaluating mitigation measures to reduce saltwater intrusion rather than conducting precise curve fitting, the average value of the depth-dependent measurements are used. The actual difference in depth-dependent chloride concentrations at Skikuil brug and Sas van Gent are below 5%.

In the years 2017 to 2020, clear peaks in salt concentration can be observed. One of these years will be suitable as the actual calibration year. The most comprehensive dataset available is from the year 2018, and therefore it has been selected as the calibration year.

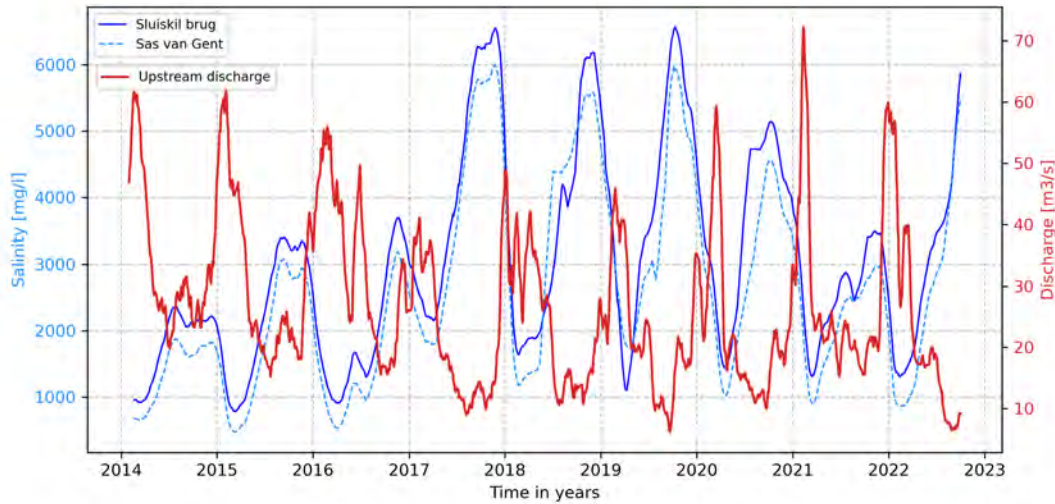


Figure 4.1: Salinity values (waterinfo.nl) for location Skikuil brug and Sas van Gent on left axis (blue). Discharges values (waterinfo.be) covering upstream discharge for the GTC. Period 2014 - 2023

## 4.2 Initial model results

The initial test runs from the established base model provide preliminary insights. Figure 4.2 and 4.3 illustrates the initial results for both calibration points. It is evident that the model reasonably captures the behavior during the first six months. However, during the summer period when the upstream discharge is low and a distinct peak is observed, the model struggles to accurately represent this peak. Therefore, the goal during the calibration process will be to improve the model's ability to simulate this peak event. Additionally, the stratification in the canal is clearly visible, with higher numbered layers containing lower salinity values, consistent with the real-world scenario where the surface layer exhibits the lowest salinity. In reality, the stratification in the canal is relatively mild. However, this thesis primarily focuses on capturing the main flow pattern rather than performing detailed curve fitting of depth-dependent salinity values.

The model evaluations in this chapter were conducted on a cluster comprising 10 servers, utilizing varying node configurations ranging from 10 to 24. This setup allowed for efficient parallel processing. The computations were distributed among 4 nodes per computation, allowing for greater flexibility in node allocation to accommodate the concurrent usage by other individuals. It is important to note that the servers exhibited inherent variability, leading to variable computational speeds. The computation time for the calculations varied between 4 and 18 days, which can be attributed to a combination of workload, server performance and possible queues. However, rigorous preliminary testing has demonstrated that these discrepancies in server performance do not introduce any differences in the resulting output.

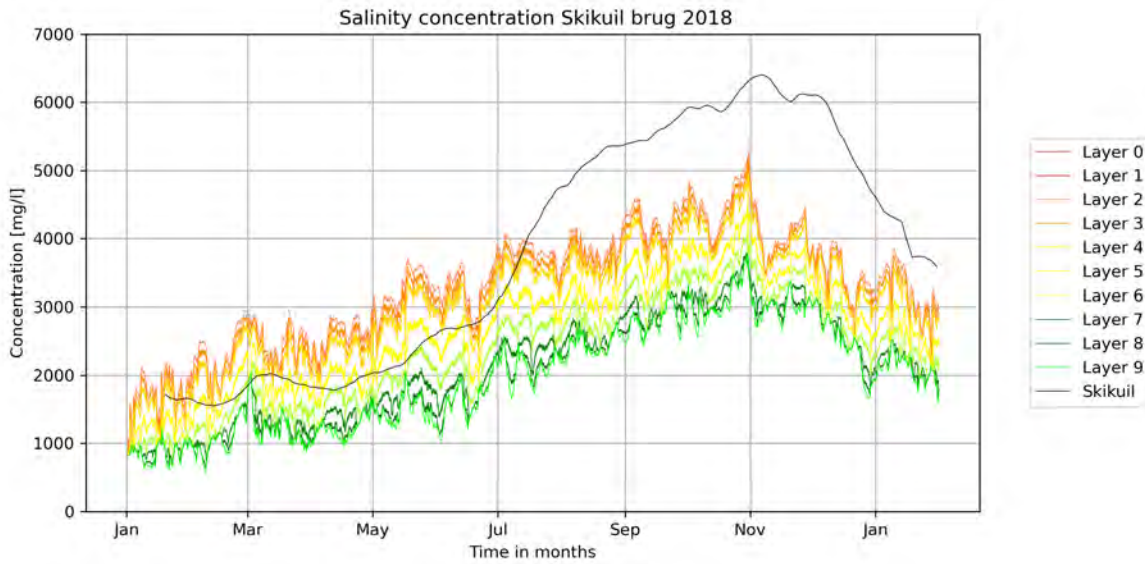


Figure 4.2: Initial results for salinity values across vertical layers at location Skikuil brug

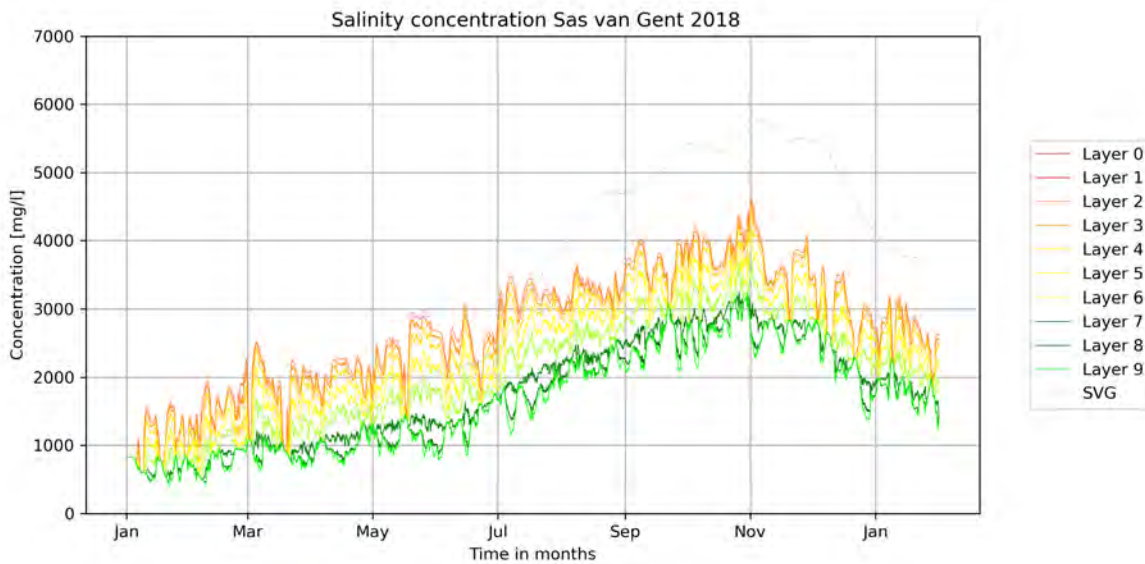


Figure 4.3: Initial results for salinity values across vertical layers at location Skikuil brug

### 4.3 Statistical performance of a model

Before elaborating on the analysis it's crucial to understand the significance of comparing numerical models effectively. When using numerical models, the ability to compare and analyze different models is essential for making informed decisions. Evaluating the statistical performance of a model is crucial in order to identify trends, patterns, and potential areas of improvement. To achieve this, a range of statistical performance parameters are employed to provide meaningful insights into the model's effectiveness. The used statistical performance parameters are the Root Mean Square Error (RMSE), Normalized Root Mean Square Error (NRMSE) and the BIAS indicator. The parameters will be explained below.

The Root Mean Square Error (RMSE) is employed as the statistical metric for evaluation. RMSE is chosen as a widely accepted measure for assessing the accuracy of predictive models. It calculates the average deviation between the model’s predicted values and the actual observed values in the same unit (mg/l). So, the lower the RMSE the better the fit of modelled output. In this case, RMSE has been selected due to its common usage and robustness, even when dealing with large datasets.

In addition to the RMSE, the Normalized Root Mean Square Error (NRMSE) is employed as a statistical metric to assess the accuracy of the model. The NRMSE considers the scale of the observed values and provides a relative measure of the model’s performance. By normalizing the RMSE using the range of the observed values, the NRMSE enables meaningful comparisons across different datasets and variables. When interpreting the NRMSE, it’s important to note that a lower value indicates a better fit of the model to the observed data, implying a higher level of accuracy in capturing the variability in salinity. Therefore, a smaller NRMSE suggests that the model closely replicates the observed salinity patterns, enhancing our understanding of its performance and suitability for predicting salinity variations in the study area. The NRMSE has a value ranging from 0 to 1, with 0 indicating a perfect fit between the model and the observed data, and 1 indicating a complete mismatch. By employing the NRMSE, we can quantitatively evaluate the model’s performance and make informed decisions based on its ability to accurately represent the salinity variations in the study area.

Additionally, the BIAS Indicator was utilized to assess the presence of systematic bias in the model’s predictions. The BIAS Indicator measures the model’s tendency to consistently overestimate or underestimate the observed values and is expressed in the calculated unit, ensuring that lower values are indicative of better performance. Ideally, a bias close to zero signifies that the model predictions are unbiased, accurately capturing the average behavior of the observed data. Positive bias values suggest a consistent overestimation of the observed values, while negative bias values indicate a consistent underestimation. It is important to consider the magnitude of the bias relative to the variability of the observed data to determine the significance of the bias. The BIAS Indicator provides valuable information regarding the model’s systematic deviation from the observed values, aiding in the evaluation of its performance and reliability.

All formulas are shown below, in which:

- $\text{obs}_i$ : Observed salinity concentration
- $\text{sim}_i$ : Simulated salinity concentration
- $\text{obs}_{(i,\text{mean})}$ : Mean observed salinity concentration
- $n$ : Number of values

$$\text{RMSE} = \sqrt{\frac{\sum_{i=1}^n (\text{obs}_i - \text{sim}_i)^2}{n}}$$

$$\text{NRMSE} = \sqrt{\frac{\text{RMSE}}{\text{obs}_{(i,\text{mean})}}}$$

$$\text{BIAS} = \text{mean}(\text{sim}_i - \text{obs}_i)$$

## 4.4 Sensitivity analysis

Accurately simulating physical processes in a specific study area requires the selection of suitable parameter values, making sensitivity analysis a critical step in the calibration process of a numerical model. This analysis evaluates the impact of parameter variations, in this specific case on the salinity model output, and identifies the optimal parameter values that best represent the physical processes in the study area based on their statistical performance. It is important to note that the appropriate parameter values depend on the specific conditions of the study area and the physical processes that

need to be represented. The initial model is set with default parameter values, and a range of values is selected based on initial test runs, literature, and existing models from Deltares. The process of selecting parameters and their corresponding value ranges will be explained in the following sections. Ultimately, the results of the sensitivity analysis will be presented in appendix B.

#### 4.4.1 Parameter selection

Within the Delft3D framework, there are numerous parameters that influence the model output, and each of these variables affects different aspects. For modelling saltwater intrusion, literature suggests calibrating on bottom roughness (Manning), bathymetry, and flow parameters such as water level, discharge, and waves (Prandle, 2004; Williams & Esteves, 2017; Baracchini et al., 2002). However, for this thesis, it was chosen to keep these external factors as close to reality as possible, without making any adjustments to bottom roughness or bathymetry, to ensure the most accurate representation of reality. This approach ensures a comprehensive and faithful depiction of the physical processes without introducing artificial adjustments that could compromise the integrity of the model. The same applies to the flow parameters, which are fixed, and any adjustments made to them could lead to less reliable results.

Parameters which are frequently used for the calibration process of saltwater intrusion are: horizontal/vertical eddy diffusivity/viscosity (Hasan et al., 2012; Verbruggen & Van Der Baan, 2022; Bushman et al., 2015). These parameters represent the horizontal and vertical mixing of water.

- *Horizontal Eddy Diffusivity / Viscosity (HED/HEV)*

Horizontal Eddy Viscosity (HEV) and Horizontal Eddy Diffusivity (HED) are key factors influencing the horizontal movement of flow and the transport of salt. These parameters play crucial roles in understanding the movement, mixing, and dispersion of saltwater in the horizontal plane. Horizontal Eddy Diffusivity quantifies the horizontal dispersion and diffusion of substances, while Horizontal Eddy Viscosity represents the resistance to shear and energy dissipation in horizontal fluid motion. When the diffusivity is increased, it indicates a higher rate of mixing due to eddies, resulting in more effective dispersion and diffusion of substances. Consequently, saltwater intrusion is expected to occur less rapidly due to the enhanced mixing of water. Consequently, when the viscosity is increased, it leads to higher salt concentration upstream.

- *Vertical Eddy Diffusivity / Viscosity (VED/VEV)*

Vertical Eddy Diffusivity (VED) and Vertical Eddy Viscosity (VEV) are crucial for comprehending the vertical movement, mixing, and dispersion of saltwater within the water column. These parameters capture the nonlinear turbulent advection of momentum. Vertical Eddy Diffusivity characterizes the vertical dispersion and diffusion, while Vertical Eddy Viscosity reflects the resistance to shear and energy dissipation in vertical fluid motion. Unlike the horizontal scenario, vertical eddy diffusivity tends to decrease with increasing stratification, accompanied by a decrease in vertical eddy viscosity. For vertical mixing, if the Vertical Eddy Diffusivity is increased, it implies intensified vertical mixing processes. This enhanced mixing leads to a more efficient vertical dispersion and diffusion of substances, including saltwater. Consequently, the vertical intrusion of saltwater is expected to occur at a faster rate and potentially penetrate to greater depths within the water column. Conversely, decreasing Vertical Eddy Diffusivity would result in reduced vertical mixing, limiting the vertical dispersion and diffusion of substances. In such cases, the vertical intrusion of saltwater may proceed at a slower pace and may not penetrate as deeply into the water column due to reduced mixing processes.

It is important to note that the selected parameters primarily influence the horizontal and vertical mixing of incoming saltwater within the system, without affecting the overall amount of incoming saltwater. Through a sensitivity analysis, it is expected that the adjustment of these parameters will allow for proper tuning of the constant inflow of saltwater component.

Moreover, the number of vertical grid layers can also be used to calibrate the model, where it can affect the vertical resolution of the model and its accuracy in representing the vertical mixing and stratification of water masses (Bushman et al., 2015).

- *Vertical grid layers (kmx)*

While a higher number of vertical grid layers can provide a more accurate representation of the vertical structure of the water column and can better capture the dynamics of salinity intrusion and mixing, too many layers can increase computational costs, while too few layers may result in inadequate vertical resolution and inaccurate representation of vertical mixing and stratification. However, the number of vertical grid layers should not significantly influence the results as it does not change the physics, but it mostly provides a better representation of the stratification. Therefore, the most significant difference will be in the level of stratification in the canal, as more layers can represent more salinity levels, and no averaging is needed.

#### 4.4.2 Parameter value selection

Prior to conducting the sensitivity analysis, preliminary test runs were carried out to assess the model’s sensitivity to variations in horizontal and Vertical Eddy Diffusivity and viscosity and also the vertical grid layers, which exhibit significant variations in the literature. Therefore a variety of values per parameters have to be analyzed during the sensitivity analysis. These parameters originate from literature and are shown below in table 4.1. In the following subsections the decision will be substantiated. The final selection of values is 19.

Table 4.1: Parameter value range for calibration indicated by lower end to higher end values

Parameter	Parameter code	Lower end	Default value	Higher end	Reference
Horizontal Eddy Diffusivity	HED	0.01	<b>0.1</b>	1	Verbruggen & Van Der Baan, 2022; Buschman et al., 2015
Horizontal Eddy Viscosity	HEV	0.01	<b>0.1</b>	1	Verbruggen & Van Der Baan, 2022; Buschman et al., 2015
Vertical Eddy Diffusivity	VED	1E-7	<b>1E-6</b>	5E-5	Buschman et al., 2015
Vertical Eddy Viscosity	VED	1E-7	<b>1E-6</b>	5E-5	Buschman et al., 2015
Vertical layer offset	kmx	10	<b>15</b>	20	Verbruggen & Van Der Baan, 2022

#### Horizontal Eddy Diffusion and Viscosity [HED & HEV]

The HED and HEV parameters are responsible for horizontal salt transport and the hydrodynamic. The default value for HED and HEV is 0.1 (Deltares, 2023). Actual models from Deltares for the North Sea Canal (Amsterdam-Rijnkanaal) have values ranging between 0.01 and 1 (Verbruggen & Van Der Baan, 2022). Therefore, it is chosen to analyze the default value by a factor of 10, both smaller and larger, in order to account for a wider range of possible values.

#### Vertical Eddy Diffusion and Viscosity [VED & VEV]

Vertical Eddy Diffusion (VED) and Vertical Eddy Viscosity (VEV) are important parameters that affect the vertical mixing of salt in water. The default value for VED and VEV is 1E-6 (Deltares, 2023). The recommended range for VED in small-scale simulations like the GTC system lays between 0 and 1E-7 m<sup>2</sup>/s, according to Deltares (2023). For the vertical exchange of momentum, it is suggested to apply Vertical Eddy Viscosity values in the order of 1E-5 m<sup>2</sup>/s for highly stratified flows. This value can help to simulate the turbulent mixing processes in the vertical direction more accurately (Deltares,

2023). To ensure that a wide range of values is considered for the sensitivity analysis of VED and VEV, the default values in Delft3D ( $1E-6$ ) are adjusted by multiplying and dividing by 10, resulting in values from  $1E-7$  to  $1E-5$  for VED and VEV. Additionally, values commonly used in model runs from Deltares, around  $5E-5$ , are taken into account as well. Therefore, five values ranging from  $1E-7$  to  $1E-5$  are included in the sensitivity analysis for both VED and VEV.

### Vertical layer offset (kmx)

The number of vertical grid layers has no direct influence on the actual physics of the model. However, it is important to choose the right number of vertical layers to accurately represent the physical aspects of the system. More layers can better represent the stratification as the values for each layer are better resolved. Deltares often employs a method where each vertical layer represents 1m, indicating that a range of 15-20 layers should be appropriate for the GTC (e.g. Verbruggen & Van Der Baan, 2022). For sensitivity analysis, the effects of 10, 15 and 20 vertical layers will be examined.

### 4.4.3 Evaluation of Sensitivity Analysis

The conducted sensitivity analysis involved 5 different parameters with a total of 19 different values. In this chapter, the sensitivity analysis will be evaluated based on the statistical performance.

It should be noted that for the analysis of HED, HEV, VED and VEV the most optimal vertical grid layer is used based on the statistical performance. The optimal vertical grid layer was layer 7, covering the depth of -5.1 mNAP to -6.3 mNAP, slightly deviating from the actual depth of -5 mNAP. As for the performance analysis of the vertical grid layer offset, the optimal layer is chosen and deviates as the number of vertical layers changes.

Table 4.2 below shows both the input values of the runs and their corresponding statistical performance. The associated graphs are presented in Appendix B. The color scale in table 4.2 indicates the favorability performance factor of each parameter, with green being more favorable and red less favorable.

Table 4.2: Overview of statistical performance indicators for the sensitivity analysis (19 runs). Green indicates the best performance indicator, while red indicates the worst performance indicator.

Parameter	Code	Run nr.	Value	RMSE	NRMSE	BIAS
Horizontal Eddy Diffusivity	HED	1	0.01	1310	0.33	-760
		2	0.1	1310	0.33	-760
		3	1	1318	0.34	-790
Horizontal Eddy Viscosity	HEV	4	0.01	1319	0.34	-787
		5	0.1	1310	0.33	-760
		6	1	1252	0.32	-580
Vertical Eddy Diffusivity	VED	7	1E-07	1302	0.33	-730
		8	1E-06	1310	0.33	-760
		9	5E-06	1337	0.34	-853
		10	1E-05	1365	0.35	-900
		11	5E-05	1500	0.38	-1120
Vertical Eddy Viscosity	VEV	12	1E-07	1311	0.33	-765
		13	1E-06	1310	0.33	-760
		14	5E-06	1306	0.33	-750
		15	1E-05	1300	0.33	-740
		16	5E-05	1282	0.32	-670
Vertical layer offset	kmx	17	10	2045	0.52	-850
		18	15	1310	0.33	-760
		19	20	1168	0.29	-250

### Evaluating HED and HEV

The assessment of Horizontal Eddy Diffusivity (HED) reveals a clear pattern in table 4.2, where higher values correspond to less favorable performance indicators, as indicated by the associated colors. Notably, the HED values of 0.01 and 0.1 exhibit similar results, suggesting that they have a comparable impact on the model's performance.

On the other hand, the assessment of Horizontal Eddy Viscosity (HEV) shows contrasting behavior. Increasing the HEV value leads to improved performance, with the HEV value of 1 demonstrating the best performance, implying a stronger resistance to shear forces and greater energy dissipation, which can result in better representation of the physical processes occurring in the system.

Figures B.1 and B.2 in Appendix B present the sensitivity analysis for Horizontal Eddy Diffusivity (HED), showcasing variations in salinity levels across different parameter values. Similarly, Figures B.3 and B.4 demonstrate the sensitivity analysis for Horizontal Eddy Viscosity (HEV). The salinity values for both HEV and HED exhibit variations, indicating the impact of different parameter values.

However, in the surface layer (layer 14), there are minimal discernible differences among the parameter values for both HEV and HED. This suggests that the surface layer is less sensitive to changes in these parameters, resulting in relatively stable salinity values in that layer.

Notably, higher HEV parameter values are associated with elevated salt peaks in the salinity values, indicating a stronger influence on the overall salinity distribution. In contrast, for HED, the observed variation between parameter values is relatively small, with lower values resulting in slightly higher salinity values. However, the magnitude of this difference is negligible.

Based on these observations, it can be inferred that Horizontal Eddy Viscosity (HEV) has a significantly greater influence on the salinity dynamics of the canal compared to Horizontal Eddy Diffusivity

(HED). The variations in HEV values lead to more noticeable changes in the salinity distribution, particularly in terms of elevated salt peaks.

### Evaluating VED and VEV

Table 4.2 provides clear results for the Vertical Eddy Diffusivity (VED) and Vertical Eddy Viscosity (VEV). The assessment reveals that the VED value of  $1\text{E-}7$  exhibits the best performance, while the VEV value of  $5\text{E-}5$  also demonstrates the best performance.

In contrast, the assessment of Vertical Eddy Viscosity (VEV) reveals contrasting behavior. Increasing the VEV value leads to improved performance, with the VEV value of  $5\text{E-}5$  demonstrating the best performance.

Figures B.5 & B.6 and B.7 in Appendix B illustrate the results for Vertical Eddy Diffusivity (VED) and Vertical Eddy Viscosity (VEV). Regarding VED, lower parameter values in the deeper layer (layer 4) correspond to higher salinity levels, indicating a greater influence of vertical mixing. However, in the surface layer (layer 14), there is minimal variability in salt values. This limited variability can be attributed to the restricted vertical mixing in the shallow top layer, resulting in relatively stable salt values with insignificant changes.

Similar patterns are observed for VEV in Figures B.7. The salt content displays slight variability in the deeper layer, while remaining relatively constant in the surface layer. However, contrary to VED, the highest salt content aligns with larger parameter values for VEV.

### Evaluating vertical layer offset

Table 4.2 clearly indicates that the model achieves the best performance when utilizing 20 vertical layers. Utilizing 15 vertical layers shows slightly less strong performance, but not drastically lower, compared to using 10 vertical layers. However, increasing the number of vertical layers from 15 to 20 significantly increases the computational time by 50 to 100% in comparison to using 15 layers. This substantial additional time necessitates a trade-off between accuracy and computational efficiency during the calibration phase.

Figures B.8, B.9, and B.10 in Appendix B demonstrate the impact of increasing the number of vertical layers from 10 to 20 on the salinity values. The transition from 10 to 15 layers results in a gradual increase in average salinity values, with higher peaks and an increased spread across the layers. This suggests that a higher number of layers provides better resolution for capturing the vertical variations in salinity, leading to a more accurate representation of saltwater intrusion dynamics. The transition from 15 to 20 layers shows less pronounced changes, although observable variation is still present. These observations indicate that using 10 layers may not be sufficient for the model, while increasing the number of layers improves the model's capability to accurately simulate saltwater intrusion dynamics. The increased spread and higher peaks in salinity demonstrate the improved resolution and accuracy of the model with a higher number of layers.

## 4.5 Calibration

As previously mentioned, the model calibration was performed for the year 2018. This year was interesting because a high salt peak was observed, and therefore, it was a relevant moment to investigate if the model could simulate this peak. If the model can simulate the high salinity peak, it is likely that it can also simulate other peak situations that are of interest for research purposes.

The model calibration was performed by combining various parameters based on the sensitivity analysis. It was decided to keep HED constant at 0.1 and HEV at 1 for all the runs. Thus, only different combinations of VED and VEV were executed. VED varied between  $1\text{E-}7$  and  $1\text{E-}6$  as they yielded similar results in the sensitivity analysis. VEV varied between  $5\text{E-}5$  and  $1\text{E-}5$ .

Table 4.3 below presents the four different combinations along with the corresponding statistical performance of the runs.

Table 4.3: Overview of statistical performance indicators for the 4 calibration runs. Green indicates the best performance indicator, while red indicates the worst performance indicator.

Run nr	HED	HEV	VED	VEV	RMSE	NRMSE	BIAS
1	0.1	1	1E-07	5E-05	1155	0.31	-241
2	0.1	1	1E-06	5E-05	1172	0.32	-375
3	0.1	1	1E-07	1E-05	1167	0.32	-340
4	0.1	1	1E-06	1E-05	1170	0.32	-386.5

After conducting the model calibration, during which careful consideration was given to all parameters, the final values for validation were determined as presented in table 4.4. The selection of these parameters was based on their statistical performance, as explained in Section 4.3 on statistical performance of a model. For the number of vertical ( $z$ ) layers, 15 layers were chosen due to their significantly advantageous computational time compared to 20 layers.

Table 4.4: Results of first calibration procedure

parameter	Description	Default value	Final value
HED	Horizontal Eddy Diffusivity	0,1	0.1
HEV	Horizontal Eddy Viscosity	0,1	1
VED	Vertical Eddy Diffusivity	1,0E-06	1,0E-07
VEV	Vertical Eddy Viscosity	1,0E-06	5,0E-05
kmx	Number of vertical layers	/	15

In addition to the parameter value selection from the sensitivity analysis, the model showed difficulties in accurately representing the peak salinity. Therefore, further adjustments were necessary. Upon evaluating the model, the assumption of a constant discharge at the Tollhuis weir in the inner city of Ghent was revised. The initial model setup assumed a constant discharge of  $4 \text{ m}^3/\text{s}$  throughout the year. However, this assumption is unrealistic as a noticeable decrease should be observed during the summer months. Consequently, the modification was made to reduce the summer discharge to  $1 \text{ m}^3/\text{s}$  from June 21st to September 21st. The adjustment made resulted in significant modifications to the model output, leading to a more accurate representation of the observed data. This adjustment increased the performance of the model as shown in in table 4.5. As a result of this adjustment, modifications were made to the model output, leading to a more accurate representation of the observed data. The performance of the model improved, as indicated by the decrease in the root mean square error (RMSE) and normalized root mean square error (NRMSE) by 5% and 10% respectively. However, despite the overall improvement in model performance, the BIAS indicator worsened. In this case, the modification made to the model has introduced a bias that led to a less accurate representation of the observed data, resulting in a higher BIAS indicator.

Table 4.5: Second calibration procedure; changing the assumption of constant upstream discharge at Tollhuis weir at the inner city of Ghent

	RMSE	NRMSE	BIAS
	[mg/l]	[-]	[mg/l]
Calibration 1; Based on Sensitivity Analysis	1155	0.31	-241
Calibration 2; Adjustment to upstream discharge	1095	0,28	-294
Improved performance	-5%	-10%	22%

The final calibration process resulted in calibration graphs for Skikuil brug (Calibration Point 1) and Sas van Gent (Calibration Point 2), as shown in Figures 4.4 and 4.5, respectively. The inclusion of discharge curves in these figures provides support for some of the observed salinity fluctuations.

The overall trend of the modelled salinity values aligns with the observations. However, the model tends to overestimate salinity concentrations (<5000 mg/l) while underestimating concentrations at higher levels (>5000 mg/l). Notably, the salinity peaks correspond well, including the three peaks observed between September and January, which are captured at both Skikuil brug and Sas van Gent. Comparatively, the fit to the observed data is better at the Sas van Gent location than at Skikuil brug.

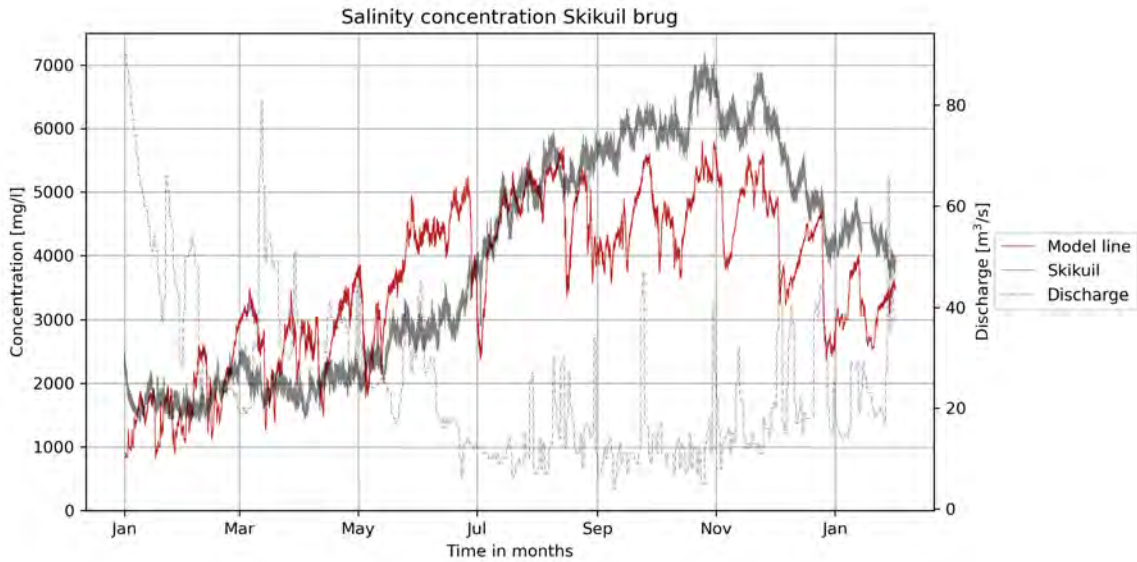


Figure 4.4: Calibration run at locatoin Skikuil brug (RMSE:1095, NRMSE:0.28, BIAS:-294)

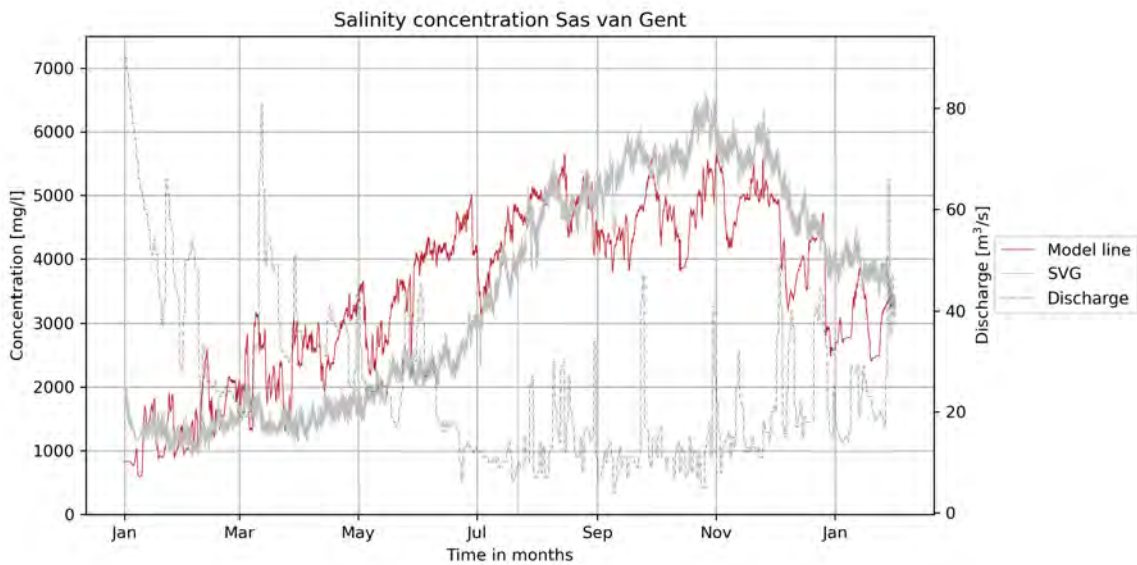


Figure 4.5: Calibration run at locatoin Sas van Gent (RMSE:985, NRMSE:0.26, BIAS:206)

## 4.6 Validation

To validate the 2018 calibrated model, the year 2020 was selected for validation. The input data related to upstream discharge, temperature, wind, and incoming salinity were adjusted to match the actual conditions and are obtained from the same sources as the calibration process. Figure 4.6 and Figure 4.7 illustrate the validation period both for Skikuil brug and Sas van Gent.

It is evident that the overall trend at both locations aligns with the observed values. However, the observed data at the Skikuil brug location contained a significant data gap, which was filled using the average difference between the Skikuil brug and Sas van Gent locations (factor 0.84). However, this data gap is not taken into account for calculating the statistical performance.

In addition to the coherent global trend, the model also captures the trend at smaller time scales. Local peaks and troughs are also reproduced by the model. However, the model tends to exhibit more extreme values, particularly in the case of local minima.

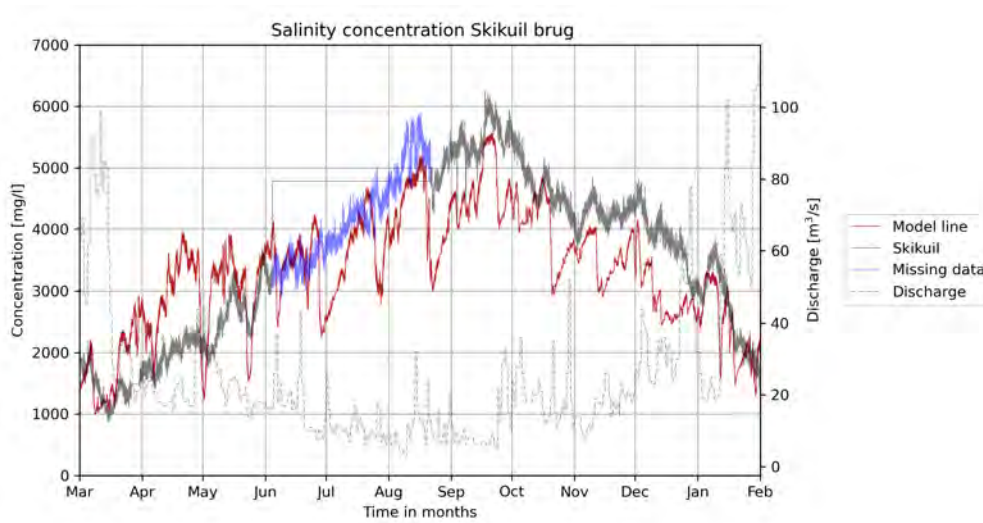


Figure 4.6: Validation run at locatoin Skikuil brug (RMSE:766, NRMSE:0.19, BIAS:-380)

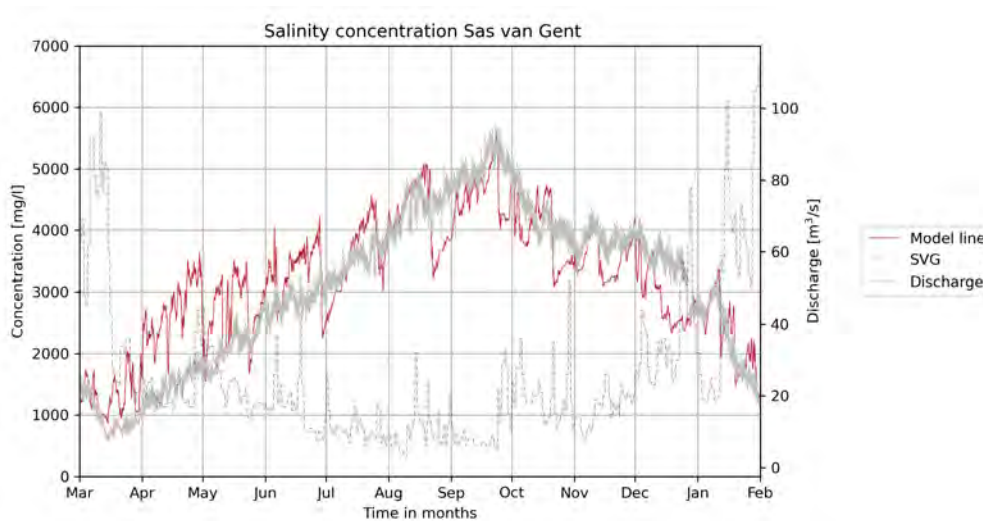


Figure 4.7: Validation run at locatoin Sas van Gent (RMSE:552, NRMSE:0.0.15, BIAS:199)

Below in table 4.6 the statistical performance of both the calibration and the validation phase are shown. Also the percentile improvement or worsening are shown. During the calibration phase, it became evident that accurately capturing the extremely high salinity peaks (with salt concentrations exceeding 6000 mg/l) poses challenges for the model. However, in the validation year, the model demonstrates a good overall fit to the observed values.

Table 4.6: Statistical performance for calibration and validation period

	<b>Skikuil</b>			<b>SVG</b>		
	Cal	Val	Improvement	Cal	Val	Improvement
RMSE [mg/l]	1095	766	-30%	985	552	-44%
NRMSE [-]	0,28	0,19	-32%	0,26	0,15	-42%
BIAS [mg/l]	-294	-380	29%	206	199	-3%

For the Skikuil brug location, during the calibration year, the RMSE value was 1095, indicating the average difference between observed and modelled values. The NRMSE value of 0.28 suggested a relatively good performance of the model compared to the observed data, while the Bias value of 294 indicated a slight underestimation of the modelled values.

During the validation year, the Skikuil brug location showed a notable improvement in performance. The RMSE value decreased to 766, indicating a significant 30% improvement in the average difference between observed and modelled values compared to the calibration year. This decrease signifies an enhancement in the accuracy of the model. The NRMSE value of 0.19 indicated a substantial improvement in performance by 32%. However, it's important to note that the Bias value of -380 suggested a consistent underestimation of the modelled values relative to the observed values during the validation year. This underestimation is a result of the modelled values consistently underestimating the observed values in the validation year, whereas in the calibration year, the model exhibited both overestimations and underestimations, resulting in a lower net Bias.

Similarly, for the Sas van Gent location, during the calibration year, the RMSE value was 985, slightly lower than the Skikuil location. The NRMSE value of 0.26 indicated a similar level of performance compared to the Skikuil brug location, while the Bias value of 206 suggested a slight overestimation of the modelled values.

In the validation year, the Sas van Gent location demonstrated further improvements. The RMSE value decreased to 552, indicating an improvement of agreement of between the observed and modelled values compared to both the calibration year and the Skikuil location in the validation year. The NRMSE value of 0.15 reflected a strong increase in performance by 42%. The Bias value of -199 suggested a slight underestimation of the modelled values compared to the observed values, but slightly improved compared to the calibration year.

These improvements in RMSE, NRMSE, and BIAS indicate the model's ability to enhance its accuracy and better simulate the observed data for both locations during the validation year. The lower RMSE values signify reduced differences between the modelled and observed values, while the decreasing NRMSE values indicate an increasingly better fit of the model to the observed data. The Bias values provide insights into the systematic errors, revealing the model's tendency to either overestimate or underestimate the observed values.

## 4.7 Understanding model discrepancies

To provide further justification, a brief analysis is conducted in this chapter to clarify the source of the (high) daily variability observed in the graphs for the modelled calibration and validation runs.

Figures 4.8 and 4.9 show the relationship of percentage increase in upstream discharge to the salinity concentration in the canal. The overall trend of the observed data is followed; however, the daily variability is excessively high to correspond with reality. These extreme peaks can be explained by the fact that the model is a simplified representation and reacts strongly to upstream discharge, which is also the most influential factor on saltwater intrusion (Vanderkimpen et al., 2012). In reality, factors such as shipping and surface water discharges exert control over the daily variability in channel mixing capacity.

In the graphs, the modelled salt concentration is plotted against the percentage increase or decrease in the daily average discharge. Logically, if there is a sudden large increase in upstream discharge, the salt concentration after a certain number of days should decrease.

The larger the relative increase, the more effectively the salt is flushed out as observed by the minimum value on July 1st. Other clear examples can be seen in the increase in discharge around October and November in 2018, which manages to flush out the salt with a short delay. In the year 2020, distinct examples can be observed in August and also October. In addition to these notable instances, the trend in both graphs is also evident during the months from January to May, even when there is higher discharge present.

Determining the cross-correlation for these graphs poses challenges due to the large datasets and significant noise. The primary interest lies in the local maxima and minima. As a result, the computed cross-correlation coefficients of -0.12 (2018) and -0.11 (2020) indicate a relatively weak correlation. However, the negative values of the cross-correlation suggest an inverse relationship between the datasets: an increase in discharge difference tends to correspond to a decrease in salt concentration.

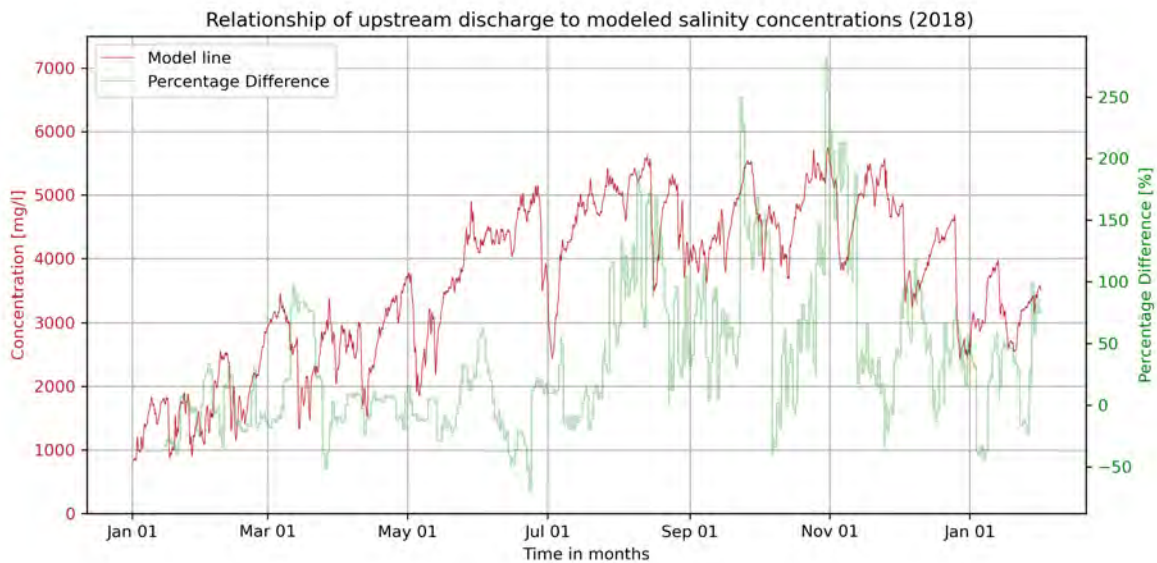


Figure 4.8: Relationship between percentage difference upstream discharge (green line) to salinity concentrations in the canal (red line) in 2020

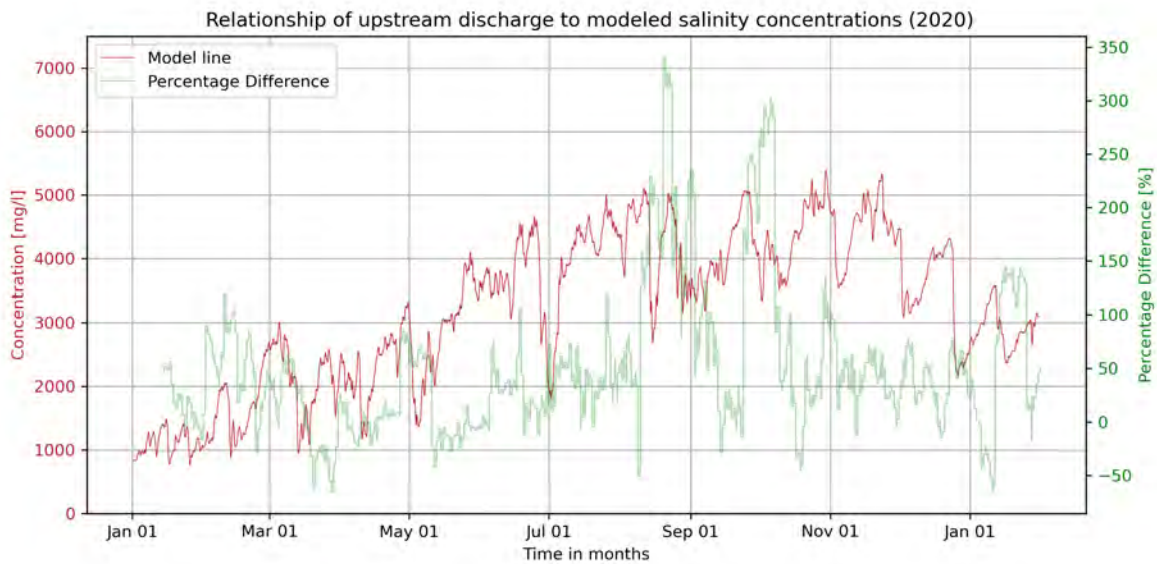


Figure 4.9: Relationship between percentage difference upstream discharge (green line) to salinity concentrations in the canal (red line) in 2020

Figure 4.10 depicts the average decrease in salt concentration based on varying discharge for both the modelled and observed values. It is immediately evident that the larger reductions in salt concentration occur during significant changes in discharge, while relatively smaller changes remain within certain limits. However, it does not imply that the greater the change in discharge, the greater the reduction in salt concentration. This is because the days between the discharge peak and the salt reduction still contain varying discharge, which influences the actual reduction. Nonetheless, the graphs provide a clear depiction. Figure 4.10 shows the graphs of the effect of abrupt percentage change in upstream discharge to salinity concentrations 2018 (left) and 2020 (right).

Depicting the 0 - 50% increase in discharge for both years, a consistent trend is observed where the modelled and observed salt concentrations exhibit similar patterns. This suggests that smaller increases in discharge lead to comparable reductions in salt concentration. However, it should be noted that the model tends to slightly underestimate the reduction in concentrations compared to the observed values.

Shifting focus to the 50 - 100% increase in discharge, significant discrepancies between the modelled and observed salt concentrations are evident. These discrepancies persist in both 2018 and 2020, with the model underestimating the reduction in salt concentration in 2018 and overestimating it in 2020. This observation indicates that the model may not accurately capture the dynamics of salt reduction during these increased discharge events. However, it is important to consider that the first 6 days of the observation period exhibit some coherence in the trend, potentially suggesting that the discharge during these initial days significantly influences the salinity. Therefore, caution should be exercised when drawing conclusions beyond this initial period.

Examining the 100 - 150% increase in discharge, a similar trend is observed between the modelled and observed salt concentrations. However, the reductions in salt concentration observed in the data are less pronounced compared to the values predicted by the model. This discrepancy highlights the model's sensitivity to these increased discharge scenarios and suggests the need for further refinement to improve its accuracy in capturing the dynamics of salt reduction.

The 150 - 200% increase in discharge, a consistent trend is observed between the modelled and observed salt concentrations. Despite the model underestimating the reduction in salt concentration in 2018 and overestimating it in 2020, both graphs display intersections, indicating a convergence of the salt concentrations. These intersections occur approximately 8 to 10 days after the onset of the discharge increase, suggesting a delayed response to the changes in discharge.

Comparing the 250 - 300% increase in 2018 to the >300% increase in 2020, it is important to note that these scenarios involve extreme magnitudes of discharge. In 2018, a strong coherence is observed between the modelled and observed behavior, with both showing the same reduction in salt concentration after 11 days. However, in 2020, where the discharge increase exceeds 300%, the model overestimates the reduction in salt concentration but still follows a similar trend line. An interesting observation is that the maximum reduction occurs one day earlier in the modelled data, suggesting the model's sensitivity to such high discharge scenarios. These findings highlight the complexity of capturing the dynamics of salt reduction during these extreme discharge events and emphasize the need for further investigation and model refinement.

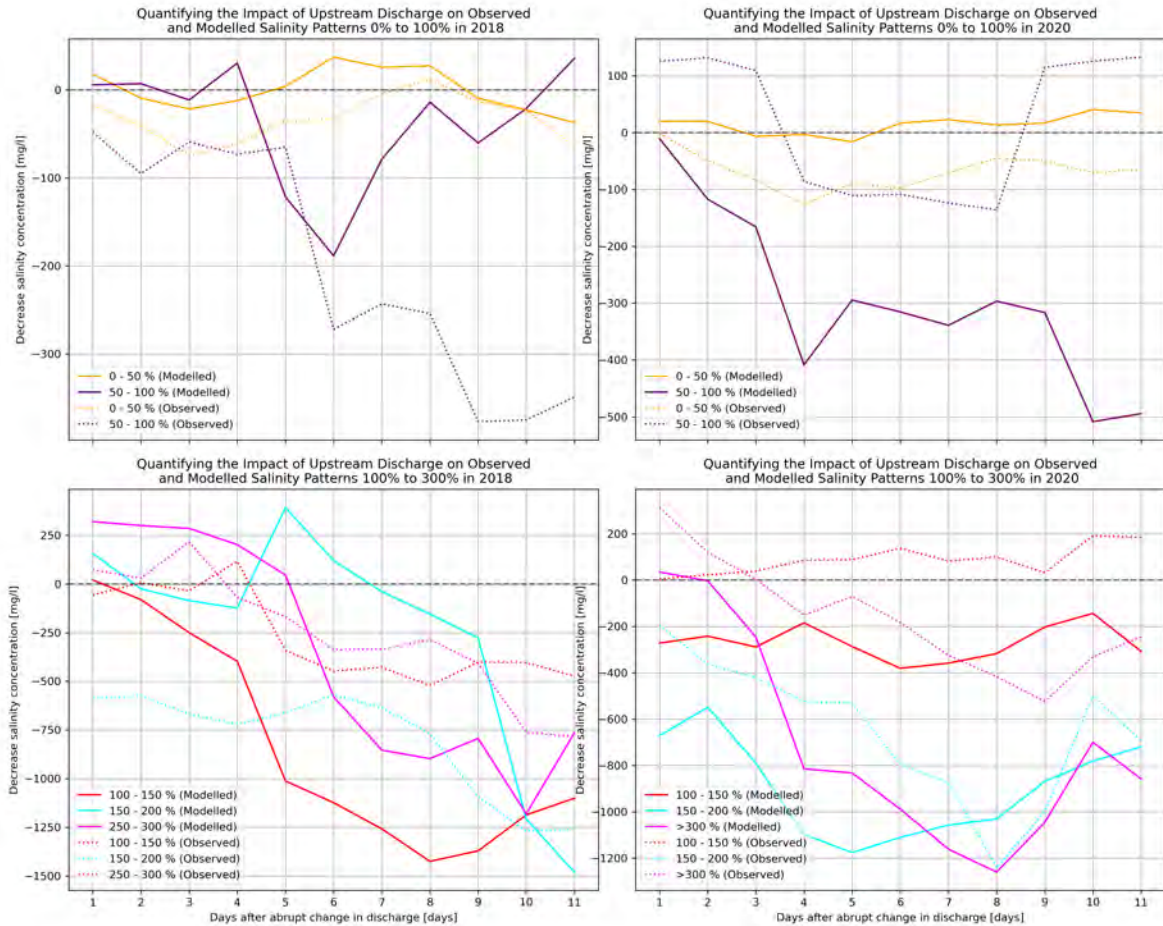


Figure 4.10: Effect of abrupt percentage change in upstream discharge to salinity concentrations 2018 (left) and 2020 (right)

## Chapter 5

# Results of mitigation measures New Lock Terneuzen

This chapter delves into the validation and assessment of measures implemented for mitigating saltwater intrusion at the New Lock Terneuzen. The previous validation phase confirmed the model's reliability by demonstrating a satisfactory fit to observed data. However, in order to proceed with the analysis, it is crucial to first incorporate the design changes into the Delft3D model by implementing the New Lock Terneuzen. These changes involve adjusting the computational grid, bathymetry, and downstream boundary conditions, including saltwater influx and lock passages per day.

The focus of this chapter is to present the results of the implemented measures outlined in chapter 3.6. Specifically, these measures aim to address the issue of saltwater intrusion for the year 2020 at the New Lock Complex of the GTC. The results will be presented individually for each measure, providing valuable insights into their effectiveness in combating saltwater intrusion.

### 5.1 Changed schematized domain

Below in figure 5.1, a visual comparison is presented between the previous computational grid configuration and the updated version. This comparative assessment aims to examine the modifications made to the grid structure while ensuring the preservation of the same resolution, specifically in terms of the number of grid cells across the canal. In the new schematization, the orthogonality in the main channel also has been maintained below 1%.

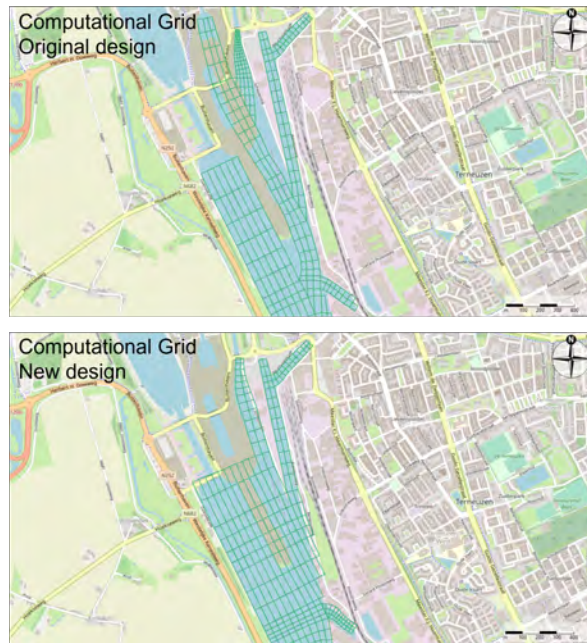


Figure 5.1: Visual comparison grid schematization new design Lock Terneuzen

Figure 5.2 below illustrates the existing and proposed bathymetry conditions near the lock complex. The bathymetric data for the original situation has been obtained from measurements, as previously mentioned. However, for the proposed scenario, no measurements, data, or information are available, necessitating the use of assumptions. The depths of the bottom near the New lock are based on the new design (see figure 3.12). The area between the West lock and the New lock has been kept constant. The connection of the East lock has been interpolated, resulting in a distinct transition. Additionally, the depth further into the canal has been interpolated based on the existing depth measurements.

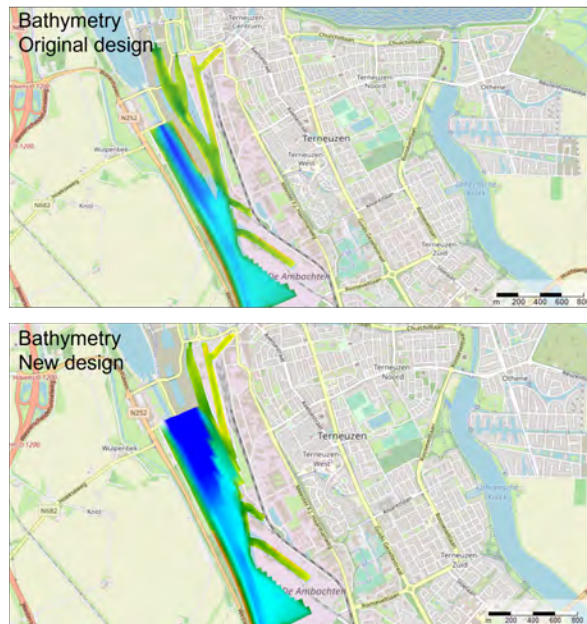


Figure 5.2: Visual comparison bathymetry new design Lock Terneuzen

### 5.1.1 Comparison to validated model

In order to examine the impact of the new designed system, a simulation is conducted using the updated model, incorporating increased salt exchange volumes and a higher frequency of lock passages based on research by Svasek, (2010) and presented in table 2.1 and 2.2. This simulation aims to assess the hydrodynamic and salinity-related aspects of the new design. The resulting model configuration serves as the reference for subsequent analyses and evaluations. Establishing the updated design as the benchmark allows for the comparison of alternative scenarios or operational strategies against the reference model. This comparative analysis enables the assessment of their potential impact and effectiveness. By using the reference model as a reliable foundation for decision-making, informed choices can be made regarding the management and optimization of the system.

Figure 5.3 displays the new reference model, allowing for visual comparison. The graph also includes the representation of the old situation for comparative purposes. Additionally, a simulation is presented where the old design is simulated using the new specifications of the sluice, including increased saltwater intrusion and a higher frequency of lock passages. This simulation aims to determine if the new design alone affects saltwater intrusion.

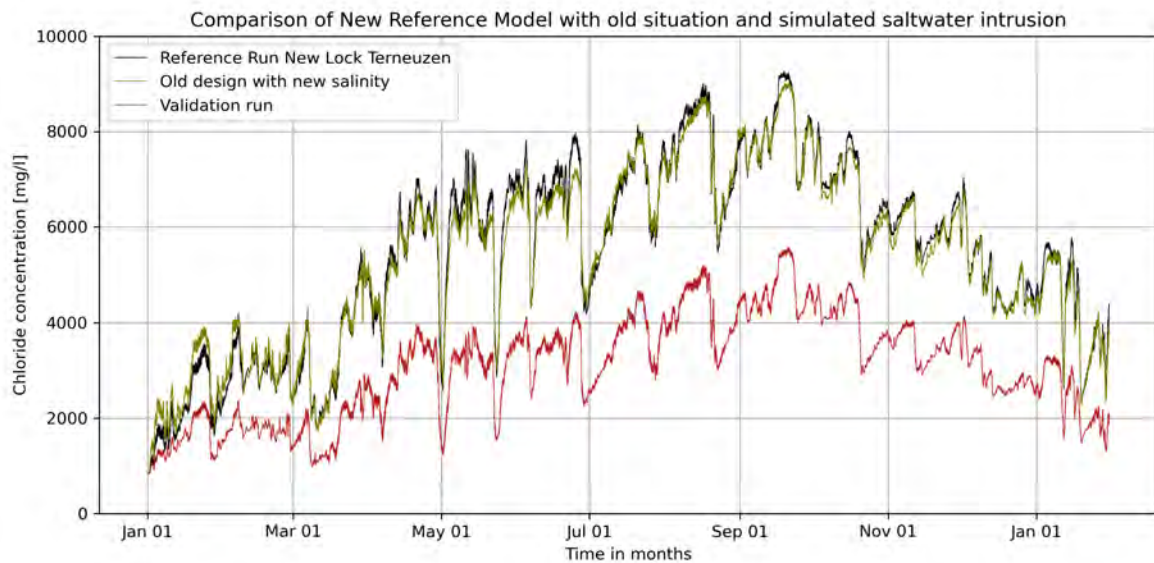


Figure 5.3: Comparison of New Lock Terneuzen (black) to old situation (red) and to old situation with new salt exchange volumes and door open times (green)

## 5.2 General overview of the effectiveness of implemented mitigation measures

Prior to analyzing each individual measure, a comprehensive overview is provided to demonstrate the effect of all tested measures. Table 5.1 presents this overview for measures related to physical structures, while table 5.2 displays the results for management-oriented measures. The impact of salt reduction is presented for each measure, both for the entire simulation period (i.e., the full year) and for the specific period where it has the most significant effect, and the remaining impact, particularly for management-oriented measures that vary in implementation duration and period.

It is evident that measures 1, 2, and 4 contribute to the highest reduction in salt concentration. On the other hand, management-oriented measures yield relatively less salt reduction. Additionally, the amount of reduction varies based on the analyzed period. For instance, winter flushing proves highly effective during the implementation period but demonstrates a smaller residual effect.

Table 5.1: Overview of the effectiveness of physical structure measures to reduce saltwater intrusion

nr	Measure	Avg. difference [mg/l]	Most effective in
1a	Submerged threshold (10m <sup>3</sup> /s)	-1200	May - July
1b	Submerged threshold (20m <sup>3</sup> /s)	-1750	May - July
2a	Elevated threshold (10m <sup>3</sup> /s)	-1100	May - July
2b	Elevated threshold (20m <sup>3</sup> /s)	-1660	May - July
3a	Canal constriction 170m	-7	March
3b	Canal constriction 400m	-1	March
4	Selective withdrawal	-1560	May - July

Table 5.2: Overview of the effectiveness of management-oriented measures to reduce saltwater intrusion

nr	Measure	Avg. difference [mg/l]	Implemented	During implementation [mg/l]	After implementation [mg/l]
5	Summer discharge spreading	-5	June 21 - September 21	45	-45
6a	Freshwater pulse 25m <sup>3</sup> /s	-12	June 21 - September 21	38	-61
6b	Freshwater pulse 50m <sup>3</sup> /s	-23	June 21 - September 21	25	-86
7	Winter flushing	-200	January 1 - April 1	-500	-50
8	Rainfall pulse	-42	August 1 & 2	-150	-90

### 5.3 Mitigation measure 1; Submerged threshold with additional discharge

Mitigation measure 1 involves the implementation of a submerged bed level threshold combined with an additional continuous discharge through the New Lock Terneuzen. This measure is implemented for the entire simulation period and aims to reduce salt concentration in the system. Two scenarios were considered, one with a discharge rate of 10 m<sup>3</sup>/s and another with a discharge rate of 20 m<sup>3</sup>/s. The details of this measure can be found in section 3.6.1.

Figure 5.4 illustrates the outcomes for both scenarios and highlights the difference compared to the reference scenario. It is evident that the implemented measures result in a reduction in salt concentration. The average reduction in salinity over the entire simulation period is 1200 mg/l for the scenario with 10 m<sup>3</sup>/s additional discharge and 1750 mg/l for the scenario with 20 m<sup>3</sup>/s additional discharge. It is noteworthy to mention that a discharge rate of 10 m<sup>3</sup>/s represents a realistic value, aligning with the capacity of the culverts, while 20 m<sup>3</sup>/s slightly exceeds this threshold.

The effectiveness of the implemented measures is particularly pronounced during the period from May to July. This is because during this time, the additional discharge is strongly coordinated with the available upstream discharge. However, after July, there are periods of time where the upstream discharge drops below 10 m<sup>3</sup>/s, which limits the ability to continue the additional discharge resulting in less saltwater reduction.

The submerged threshold plays a crucial role in capturing the heavier saltwater and preventing its upstream movement. The continuous discharge of saltwater from the system, contributes to the maintenance of a lower salt concentration. The combined effect of the submerged threshold and additional discharge enhances the efficiency of saltwater trapping resulting in reduced salinity throughout the simulation period. The reduction in salinity is observed throughout the entire domain, including locations upstream such as Evergem, as well as locations downstream like Skikuil Brug and Sas van Gent. This indicates that the implementation of the submerged threshold with additional discharge effectively reduces the incoming salt, as the inflow remains unchanged.

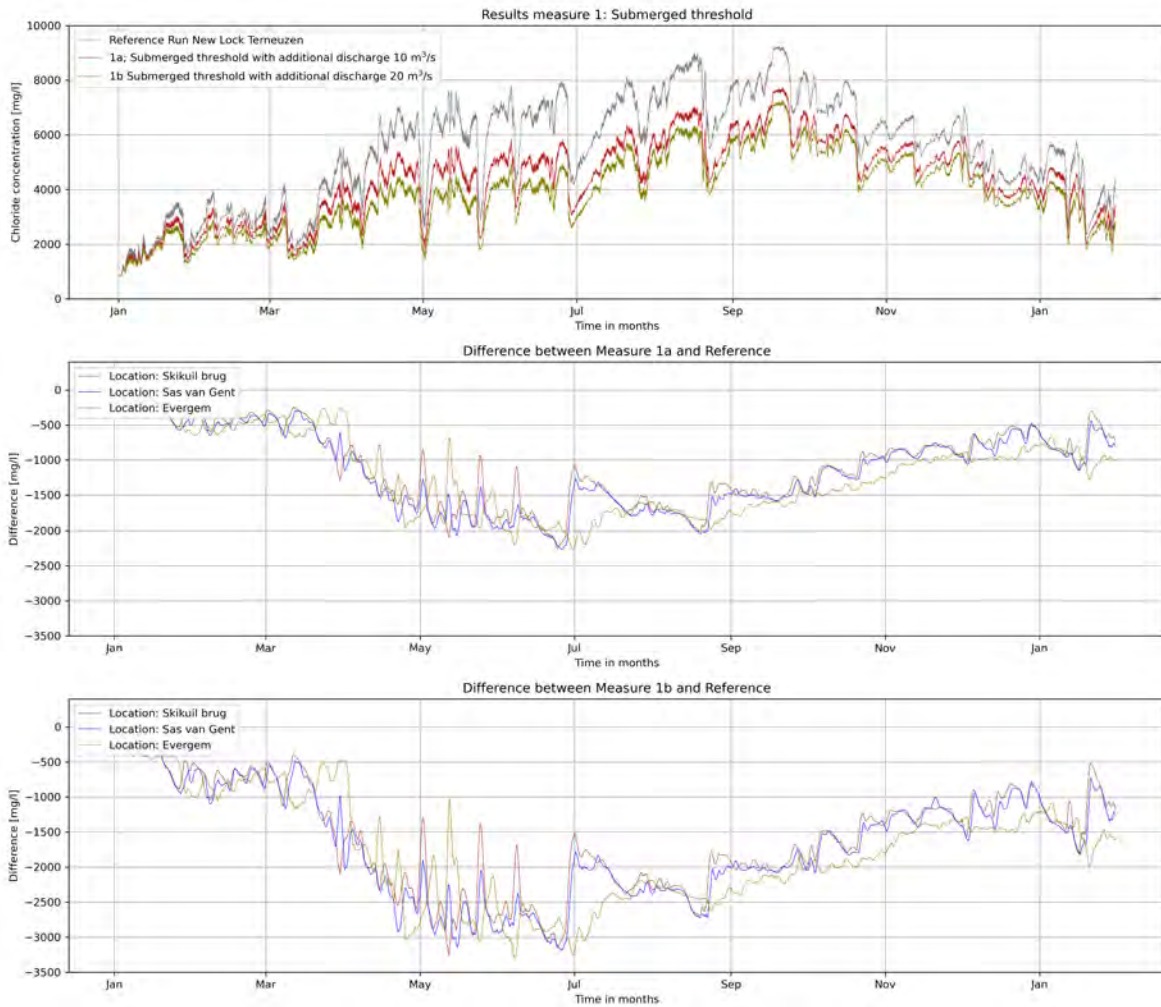


Figure 5.4: Results mitigation measure 1; Submerged threshold with additional discharge. Top figure: Comparison of reference scenario to mitigation measure 1a and 1b. Middle figure: Difference measure 1a compared to reference scenario. Lower figure: Difference measure 1b compared to reference scenario.

## 5.4 Mitigation measure 2; Elevated threshold with additional discharge

Mitigation measure 2 involves the implementation of an elevated threshold in combination with an additional continuous discharge through the New Lock Terneuzen. This measure, similar to the submerged threshold, is implemented for the entire simulation period and aims to reduce salt concentration in the system. Two scenarios were considered, one with a discharge rate of  $10 \text{ m}^3/\text{s}$  and another with a discharge rate of  $20 \text{ m}^3/\text{s}$ . The details of this measure can be found in section 3.6.2.

Figure 5.5 illustrates the outcomes for both scenarios and highlights the difference compared to the reference scenario. The trend of the salt concentration is accurately followed, and it is evident that a reduction in salt concentration occurs.

When a discharge rate of  $10 \text{ m}^3/\text{s}$  is applied, the average reduction in salt concentration throughout the entire simulation period is  $1100 \text{ mg/l}$ . This difference increases to  $1660 \text{ mg/l}$  when the discharge rate is set to  $20 \text{ m}^3/\text{s}$ . The effectiveness of the implemented measures is particularly pronounced during the period from May to July. This is because during this time, the additional discharge is strongly

coordinated with the upstream discharge. However, after July, there are periods of time where the upstream discharge drops below  $10 \text{ m}^3/\text{s}$ , which limits the ability to continue the additional discharge.

Although the implementation of an elevated threshold is slightly less effective than using a submerged threshold, the combination of the elevated threshold and the additional discharge still leads to a significant decrease in salt concentration within the system. The reduction in salinity is observed throughout the entire domain, including locations upstream such as Evergem, as well as locations downstream like Skikuil Brug and Sas van Gent. This indicates that the implementation of the elevated threshold and additional discharge effectively reduces the incoming salt, as the inflow remains unchanged.

The continuous additional discharge plays a crucial role in reducing salt concentration. By providing a continuous flow of water, it helps flush out the saline water and prevents its buildup within the system. This continuous flushing mechanism maintains a lower salt concentration, contributing to the overall reduction observed in the simulation.

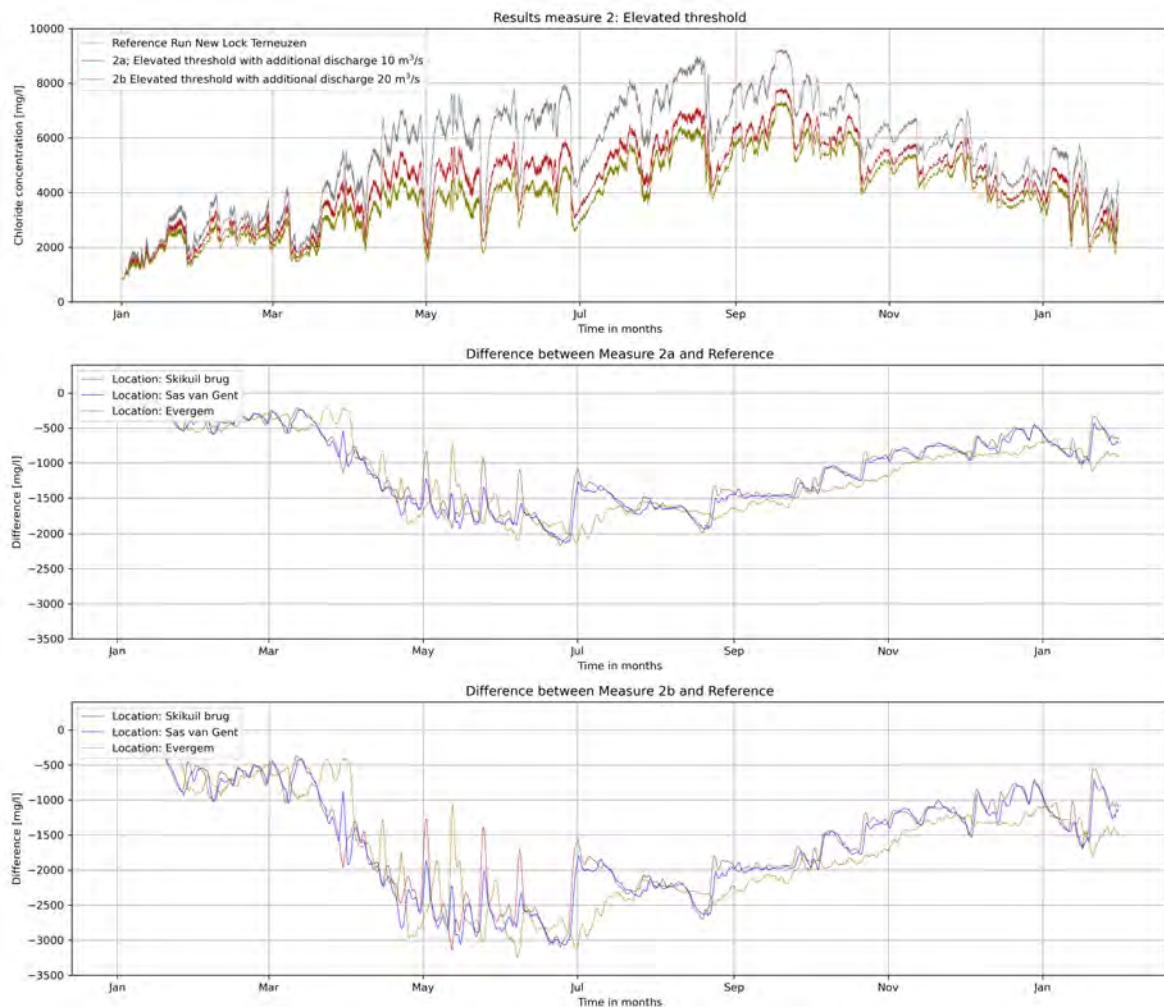


Figure 5.5: Results mitigation measure 2; Elevated threshold with additional discharge. Top figure: Comparison of reference scenario to mitigation measure 2a and 2b. Middle figure: Difference measure 2a compared to reference scenario. Lower figure: Difference measure 2b compared to reference scenario.

## 5.5 Mitigation measure 3; Canal constriction

Mitigation measure 3 involves the implementation of a canal constriction of 140 meters and 400 meters long near the location of Skikuil brug (approximately 2,5 km from the new lock), as described in section 3.6.3.

Figure 5.6 provides a visual representation of the outcomes for both scenarios compared to the reference scenario. However, the reduction in salt concentration for the whole simulation period is 7 and 1 mg/l for 140 m and 400 m long constriction respectively, indicating that this measure has neglectable effect on the salt load in the canal.

However, the findings presented in the bar plots of figures 5.7a and 5.7b reveal interesting patterns regarding the effectiveness of the canal constriction measure in reducing the salt load. The constriction point is situated 2,5 to 3 kilometers from the new lock. Prior to this location, a slight accumulation of salt is observed, indicating limited mixing and dispersion. After the constriction, a small reduction in salt concentration is observed in both cases.

When the width of the canal is reduced, it creates a constriction point where the flow becomes more restricted. As the flow approaches the constriction, the narrower channel leads to an increase in flow velocity, resulting in higher shear stresses and turbulence. This intensified mixing and dispersion of saltwater with freshwater downstream of the constriction cause an increase in salt concentration, as seen in figures 5.7a and 5.7b. The saltwater is more effectively distributed and mixed throughout the water column, leading to higher overall salinity levels.

On the other hand, the reduced width of the canal leads to a decrease in salt concentration upstream of the constriction as the local flow acceleration builds some kind of resistance to salt intrusion further upstream.

It is worth noting that the effectiveness of the canal constriction measure is influenced by the flow regime and discharge conditions. The (middle and lower) graphs in figure 5.6, which indicate the difference to the reference scenario in demonstrate that the measure is most effective during periods of high discharge, such as in March and January, when greater resistance and shear stress are present. Conversely, the measure exhibits limited effectiveness during the summer months when extremely low discharges are observed.

The observed small reductions in salt concentration indicate that the canal constriction measure alone is insufficient to effectively mitigate the negative impacts of saltwater intrusion in the Ghent-Terneuzen canal. The specific properties and flow dynamics of the canal limit the effectiveness of this measure.

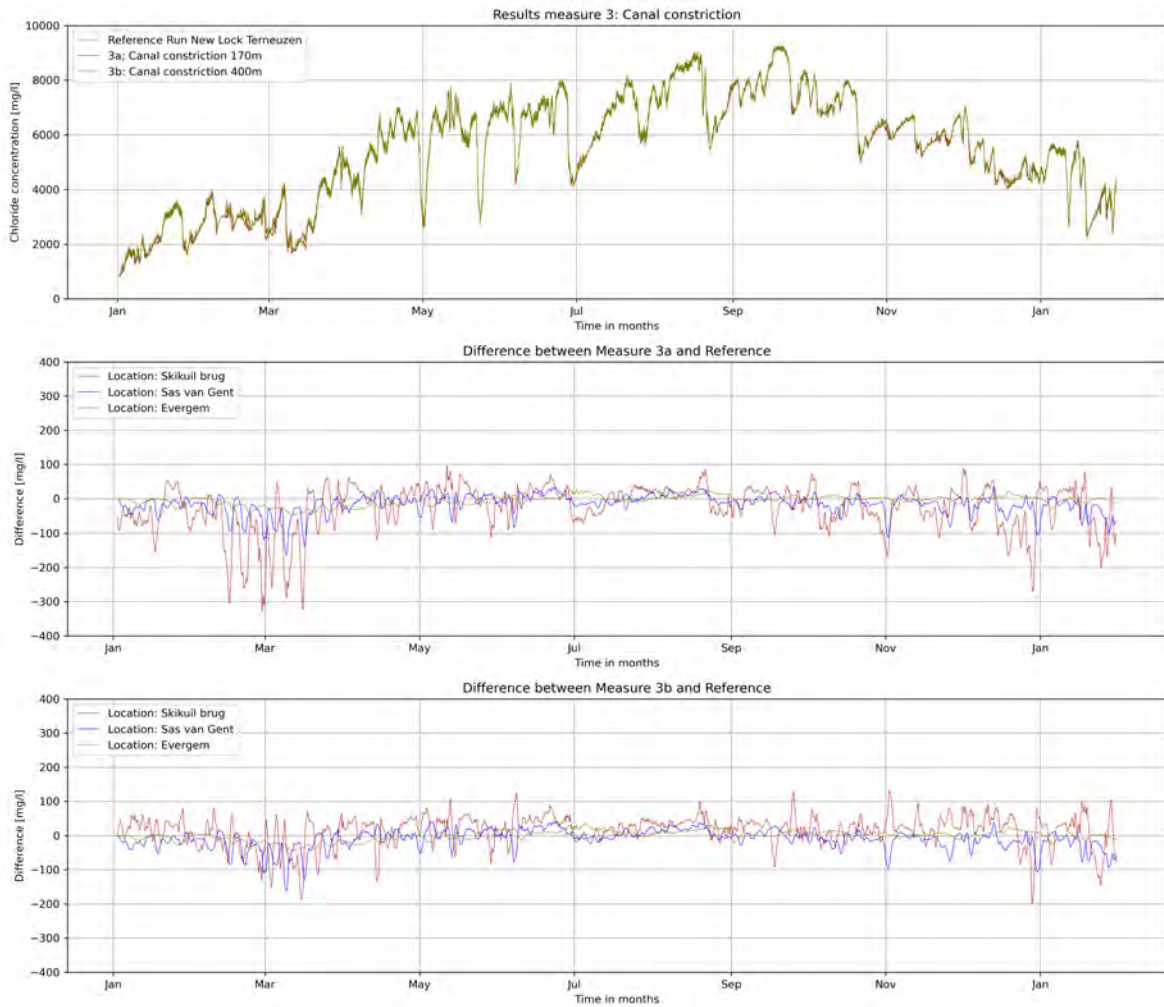
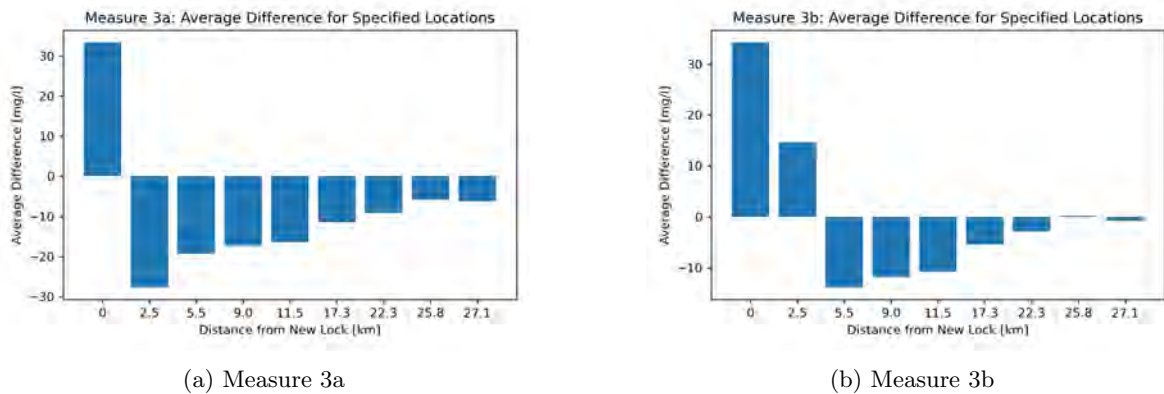


Figure 5.6: Results mitigation measure 3; Canal constriction.  
 Top figure: Comparison of reference scenario to mitigation measure 3a and 3b.  
 Middle figure: Difference measure 3a compared to reference scenario.  
 Lower figure: Difference measure 3b compared to reference scenario.



(a) Measure 3a

(b) Measure 3b

Figure 5.7: Bar plot showing the chainage (distance along the canal) of the salinity levels for Measure 3 and the reference scenario, providing a spatial representation of the salinity distribution along the canal for both scenarios.

## 5.6 Mitigation measure 4; Selective withdrawal

Mitigation measure 4 involves the implementation of selective withdrawal. This measure using the same principle as the submerged and elevated threshold, is implemented for the entire simulation period and aims to reduce salt concentration in the system. This measure only uses one scenario where all available discharge is withdrawal due to limitations in the modelling software Delft3D. The details of this measure can be found in section 3.6.4.

Figure 5.8 illustrates the outcomes of this scenario and highlights and the difference compared to the reference scenario. The trend of the salt concentration is accurately followed, and it is evident that a reduction in salt concentration occurs. .

The average reduction in salt concentration throughout the entire simulation period is 1560 mg/l. The effectiveness of the implemented measures is particularly pronounced during the period from May to July. This is because during this time, the additional discharge is strongly coordinated with the upstream discharge. However, after July, there are periods of time where the upstream discharge drops below 10 m<sup>3</sup>/s, which limits the ability to continue the additional discharge.

Although the implementation of selective withdrawal is slightly less effective than using a submerged or elevated threshold, the measure still leads to a significant decrease in salt concentration within the system. The reduction in salinity is observed throughout the entire domain, including locations upstream such as Evergem, as well as locations downstream like Skikuil Brug and Sas van Gent. This indicates that the implementation of the elevated threshold and additional discharge effectively reduces the incoming salt, as the inflow remains unchanged.

The continuous additional discharge plays a crucial role in reducing salt concentration. By providing a continuous flow of water, it helps flush out the saline water and prevents its buildup within the system. This continuous flushing mechanism maintains a lower salt concentration, contributing to the overall reduction observed in the simulation.

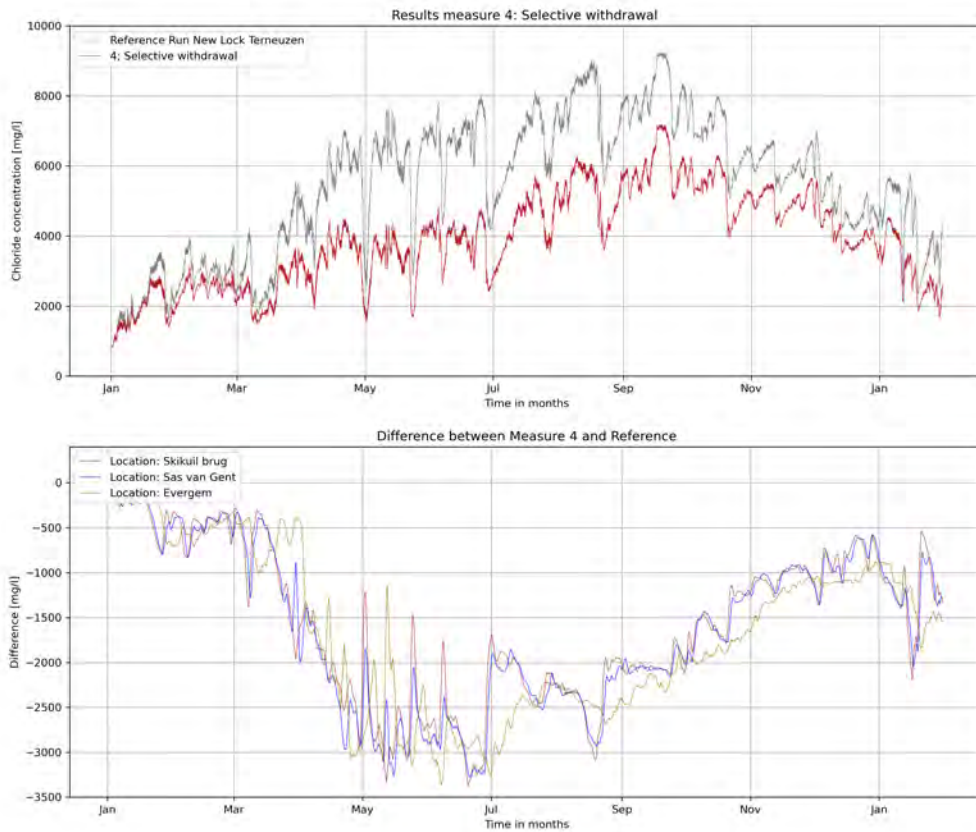


Figure 5.8: Results mitigation measure 4; Selective withdrawal.  
 Top figure: Comparison of reference scenario to mitigation measure 4.  
 Lower figure: Difference measure 4 compared to reference scenario.

## 5.7 Mitigation measure 5; Summer discharge spreading

The measure of spreading the discharge evenly over the summer period aims to investigate if a more evenly distributed discharge can effectively mitigate saltwater intrusion in the canal. However, the constant discharge is not strong enough to mitigate saltwater intrusion, revealing some limitations in achieving significant reductions in salt concentration. It is noteworthy that a significant buffer volume is needed to be able to perform this scenario. The details of this measure can be found in section 3.6.5.

Figure 5.9 illustrates the outcomes of this scenario and highlights and the difference compared to the reference scenario. Before analyzing the period of interest, some noise is observed from the period of January to June. Especially for the Evergem location. This noise is directly attributed of combining the upstream discharge locations of Evergem and Tolhuis weir which has been carried out for assessment of upstream discharge as mitigation measure.

During the implementation of this measure, an increase in salt concentration of 45 mg/l can be observed, attributed to the lowered discharge. With a reduced discharge, the flow velocity decreases, resulting in reduced shear stresses and mixing processes. As a result, the saltwater is less effectively distributed and mixed with the freshwater, leading to higher localized salt concentrations.

After the spreading period ends and the discharge returns to normal, a subsequent decrease in salt concentration is observed for locations skikuil and sas van gent. This decrease is a result of the sudden increase in discharge, which enhances flow velocities and mixing processes. The increased freshwater input promotes the dispersion of the saltwater, leading to a reduction in salt concentration downstream.

The observed increase in salinity more upstream at location Evergem can be attributed to the specific timing of the end of the summer discharge spreading. When the spreading period ends, there is a subsequent period of even lower discharge for two days. During this period, the reduced flow velocity and turbulence result in limited mixing and dispersion of saltwater with freshwater. As a result, the water becomes more concentrated, leading to an increase in salinity at Evergem. The short duration of this peak in salinity and the short distance between upstream discharge and the Evergem location explains why only Evergem encounters this increase in salinity. Locations further upstream experience a delay of several days before they are influenced by the changes in discharge. The time it takes for the altered discharge conditions to propagate upstream results in a temporal lag in the response of salinity at these locations.

It is noteworthy that the implemented measure of spreading the discharge over the summer period does not result in significant changes to the overall balance between freshwater and saltwater in the canal. The limited effectiveness of this measure can be attributed to several factors. Firstly, the constant discharge spread over the summer period is not sufficiently strong to induce significant dilution of the propagating saltwater. While the spreading of the discharge aims to distribute the saltwater more evenly, the continuous influx of saltwater, combined with the limited freshwater input, prevents significant dilution from occurring. As a result, the reduction in salt concentration is relatively small, with an average reduction of only 5 mg/l over the entire simulation period. Additionally, the dynamics of saltwater intrusion in canal systems are influenced by other river inflows as the Moervaart and Zuidlede and other local flow conditions. The spreading of the discharge alone may not be able to counteract the natural processes driving saltwater intrusion. The magnitude and timing of the inflows, along with the hydraulic properties of the canal, play significant roles in determining the effectiveness of mitigation measures. The small observed reductions may also be influenced by the specific characteristics of the Ghent-Terneuzen canal. Factors such as its length, width or shape can be of influence.

Overall, the summer discharge spreading was observed to be ineffective in mitigating saltwater intrusion. These results differ slightly from the findings reported in (Vuik & Lambrechts, 2023), where a lowering effect on salt concentrations was observed when a drier period followed a wetter period. However, the differences in salt concentrations were found to be limited, with a maximum restriction of 250mg/l.

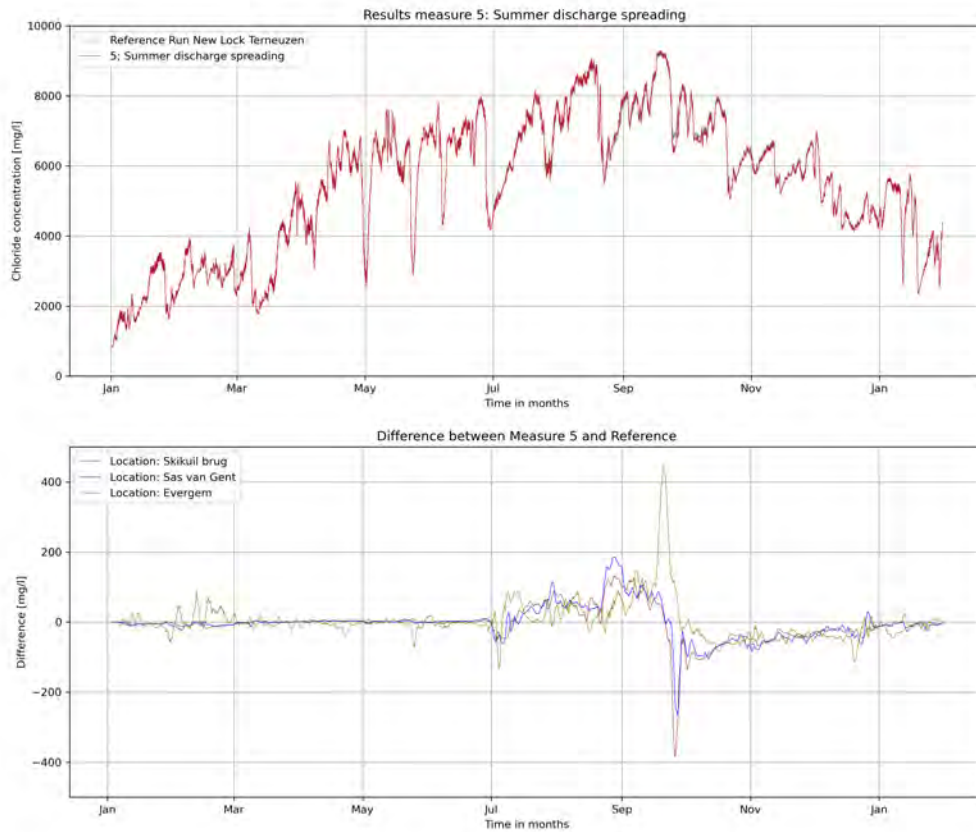


Figure 5.9: Results mitigation measure 5; Summer discharge spreading.  
 Top figure: Comparison of reference scenario to mitigation measure 5.  
 Lower figure: Difference measure 5 compared to reference scenario.

## 5.8 Mitigation measure 6; Freshwater pulse

The implementation of mitigation measure 6 involves the introduction of freshwater pulses during the summer period while maintaining the cumulative upstream discharge. The details of this measure can be found in section 3.6.6. Two scenarios were considered: one with freshwater pulses of  $25 \text{ m}^3/\text{s}$  and another with pulses of  $50 \text{ m}^3/\text{s}$ .

Before analyzing the period of interest, some noise is observed from the period of January to June. Especially for the Evergem location. This noise is directly attributed to combining the upstream discharge locations of Evergem and Tolhuis weir which has been carried out for assessment of upstream discharge.

Figure 5.10 presents a comprehensive visual depiction of the outcomes for both scenarios, allowing for a direct comparison with the reference. However, in the top figure, there is little observable difference between the scenarios, even though changes occur in reality. To further explore the variations between the scenarios, the middle and lower graphs in figure 5.10 provides a detailed illustration of the discrepancies between the reference model and the implemented measure. When freshwater pulses of  $25 \text{ m}^3/\text{s}$  are introduced, the upstream discharge is not strong enough to counteract the intrusion

of saltwater. As a result, it is evident that more salt enters the entire channel during this period. When the measure is discontinued, a similar trend is observed as with the spreading of summer discharge, characterized by a small peak and subsequent decline, depending on the location in the channel.

On the other hand, when the pulses are initiated with a flow rate of 50 m<sup>3</sup>/s, a different trend becomes apparent. The pulses seem to have some degree of force in partially flushing out the salt, but the extremely low discharge for the rest of the week results in significant salt intrusion into the channel resulting in a graphs which shows disturbance.

It is noteworthy that despite the fluctuations and noise observed in the graphs, the overall trend remains similar to previous measures. The limited effectiveness of these freshwater pulses in significantly reducing salt concentration can be attributed to several factors. Firstly, the pulses are of short duration and followed by extended periods of low discharge, which allows for saltwater intrusion to occur. Secondly, the magnitude of the freshwater pulses may not be sufficient to counteract the natural processes driving saltwater intrusion.

Overall, the freshwater pulses are not effective in mitigating saltwater intrusion. These findings align with the observations reported in (Vuik & Lambrechts, 2023), where the same measure was analyzed using a 2DV model.

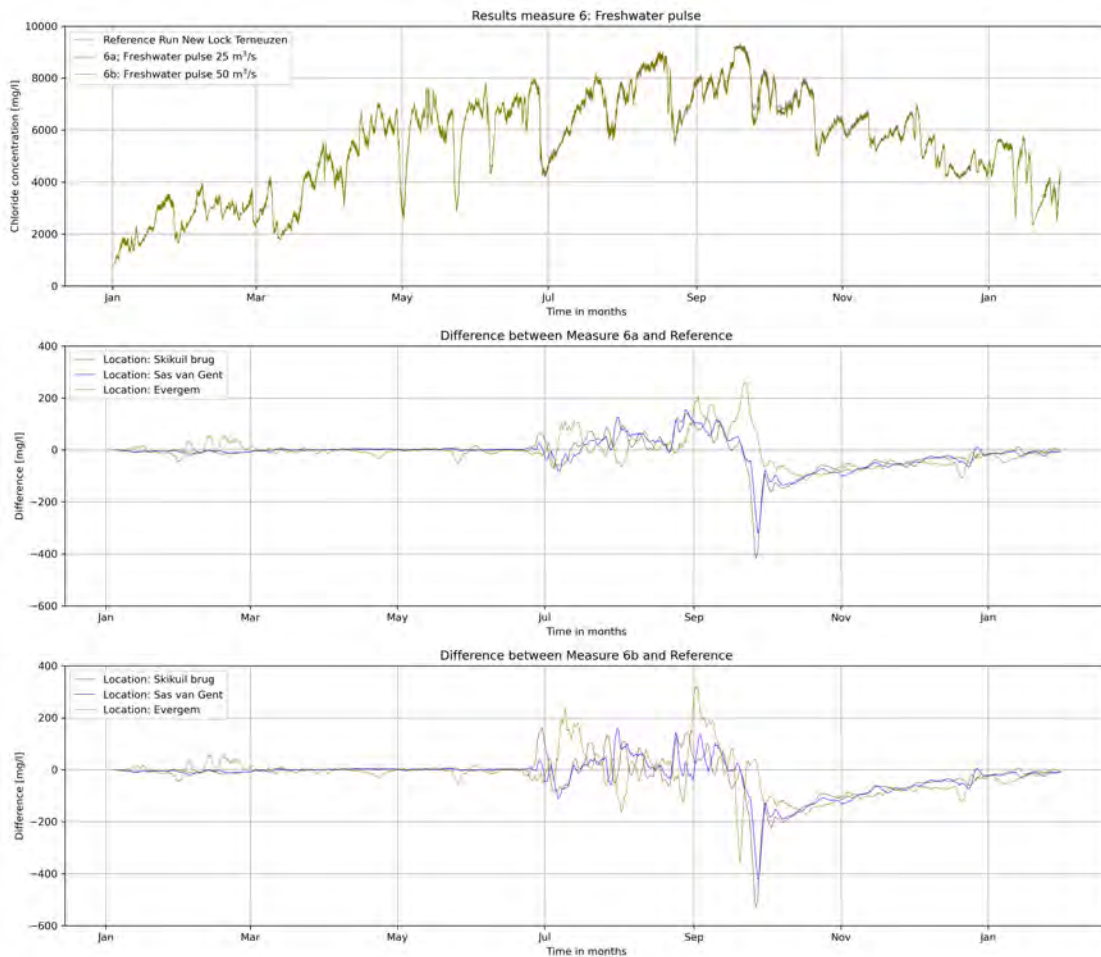


Figure 5.10: Results mitigation measure 6; Summer pulses.

Top figure: Comparison of reference scenario to mitigation measure 6a and 6b.

Middle figure: Difference measure 6a compared to reference scenario.

Lower figure: Difference measure 6b compared to reference scenario.

## 5.9 Mitigation measure 7; Winter Flushing

Mitigation measure7 involves the implementation of winter flushing, where the discharge from January to April is doubled compared to the reference scenario. The details of this measure can be found in section 3.6.7.

Figure 5.11 provides a visual representation of the scenario compared to the reference scenario, showing a clear reduction in salt concentration in the canal. The difference between the reference scenario and this measure demonstrates a significant maximum reduction around late February/early March. This reduction indicates the effectiveness of the winter flushing measure in mitigating saltwater intrusion. However, it is noteworthy that the maximum reduction occurs during the winter period when the upstream discharge is higher and the salt concentration is typically lower.

Subsequently, as the discharge returns to normal levels, the salt concentration in the canal gradually reaches a recovery point around August. This observation suggests that the winter flushing measure does have an effect, but it is not primarily targeted during the desired period of summer when the upstream discharge is low, and the salt concentration is high. The average decrease in salt concentration resulting from the winter flushing measure throughout the entire simulation period is 200 mg/l, indicating a notable reduction in salinity.

These results align with the findings reported in (Vuik & Lambrechts, 2023), where the same measure was analyzed using a 2DV model. The winter flushing measure demonstrates its potential in mitigating saltwater intrusion by reducing salt concentrations in the canal, particularly during the winter period, but the equilibrium in the 2DV model is established more quickly (around June).

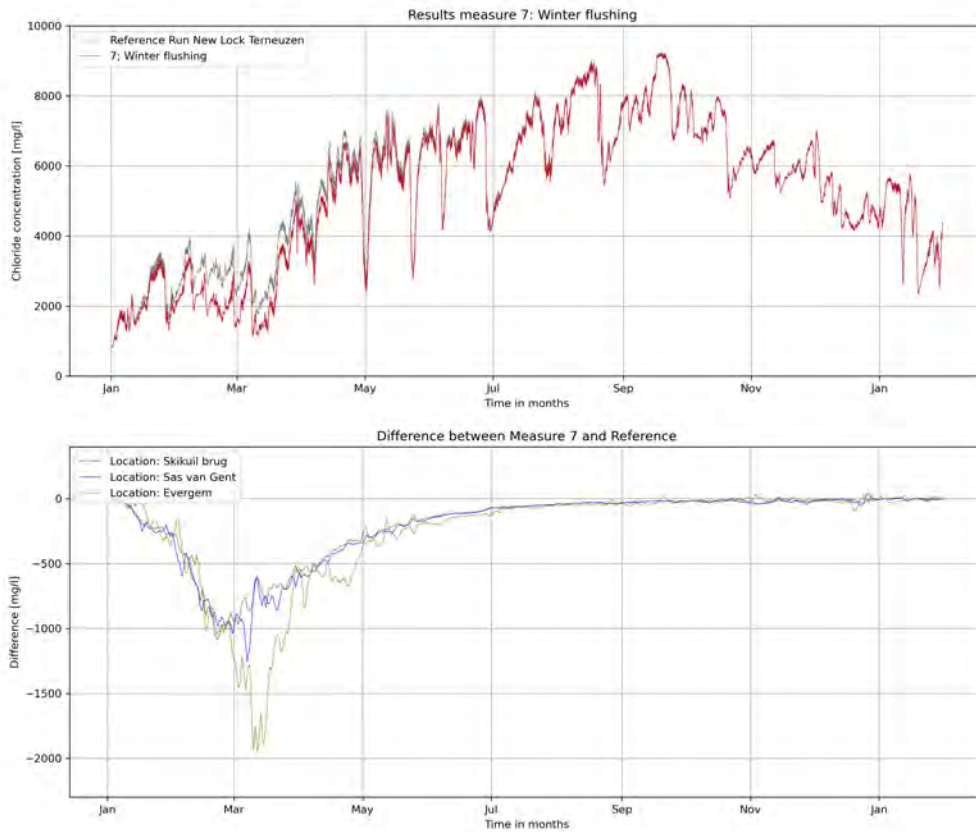


Figure 5.11: Results mitigation measure 7; Winter flushing.  
 Top figure: Comparison of reference scenario to mitigation measure 7.  
 Lower figure: Difference measure 7 compared to reference scenario.

## 5.10 Mitigation measure 8; Rainfall pulse

Mitigation measure 8 involves the implementation of a short-term freshwater pulse on August 1st and 2nd, representing a short period of intense rainfall. The details of this measure can be found in section 3.6.8.

Before analyzing the period of interest, some noise is observed from the period of January to June, particularly for the Evergem location. This noise is directly attributed to the combination of the upstream discharge locations of Evergem and Tolhuis weir, which was carried out for the assessment of upstream discharge.

Figure 5.12 provides a graph comparing the scenario to the reference scenario. Initially, there appears to be little difference, but the difference graph shows a disturbance a few days after August 1st, indicating the impact of the rainfall pulse. The average difference in salt concentration values for the entire simulation period is 40 mg/l, while the effect residual effect after implementation is a reduction of 90 mg/l.

When comparing the results to the research conducted by Vuik & Lambrechts (2023), which tested

a similar measure with an increased discharge of  $75 \text{ m}^3/\text{s}$  for two full days resulting in a temporary decrease of 500 to 1000 mg/l, it is evident that this measure shows less significant effectiveness. Additionally, in this simulation, it takes a longer period of time to reach its equilibrium again compared to the research conducted by Vuik & Lambrechts. This indicates the sensitivity of discharge variability on saltwater intrusion.

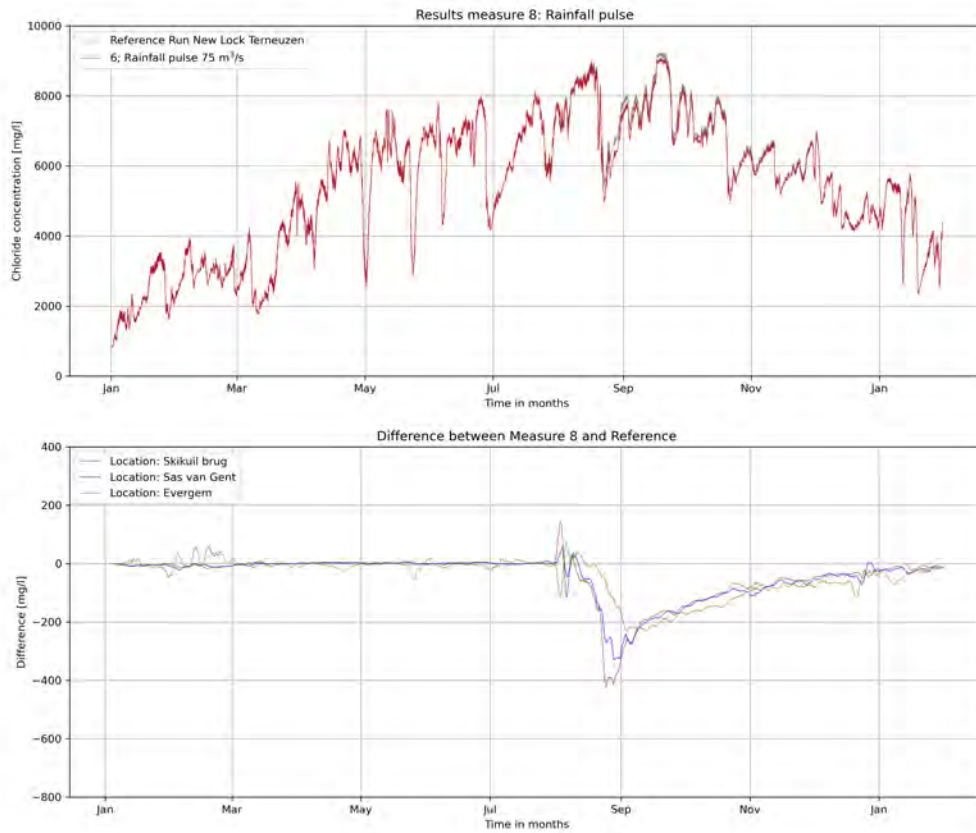


Figure 5.12: Results mitigation measure 8; Rainfall pulse.  
 Top figure: Comparison of reference scenario to mitigation measure 8.  
 Lower figure: Difference measure 8 compared to reference scenario.

# Chapter 6

## Discussion

This chapter delves into the model setup, interpretation of the obtained results, the main assumptions and simplification of the research. The trustworthiness of the model will be carefully examined, along with the implications of this study for canal management.

### 6.1 Model set up

The simulation of saltwater intrusion in the Ghent-Terneuzen canal was conducted using a comprehensive Delft3D model, a key feature of which is its 3D nature, allowing for the representation of dynamic saltwater intrusion processes.

The model was carefully constructed, considering the trade-off between accuracy and computational efficiency. Data-driven approaches were employed whenever possible to ensure a realistic representation of real-world conditions. The model includes essential processes and aspects such as the computational grid, bathymetry, wind, temperature, clouds, humidity, as well as the critical components of saltwater intrusion and upstream discharge. In this chapter, the most significant aspects related to the model's establishment will be discussed.

The model setup for simulating saltwater intrusion dynamics in the Ghent-Terneuzen canal was a critical aspect of this study. Given the constraints of limited data and time, certain simplifications were necessary. Notably, downstream boundary conditions posed a challenge due to data availability. To address this, daily averages of lock passages were used throughout the computational period. Although the duration of lock door openings was unknown, it was assumed that each lock passage resulted in a complete saltwater exchange. Saltwater exchange volumes from previous research by Svasek (2015) were employed to quantify the exchange during lock passages. These averaged values represented the mean saltwater exchange through the locks, considering one inflow and one outflow as a complete lock cycle in a cyclic representation. While in reality, each lock passage may involve varying volumes of water entering the canal, which deviates from the uniform assumption made in the model, this led to a consistent incoming salinity for each day in the simulation period. These assumptions thus do not account for phased closures during periods of low water levels, such as in the summer. Based on these cumulative assumptions, the model adapted a methodology that was primarily focused on the dispersion of saltwater within the canal system. It is therefore important to recognize that the model may not fully capture the complex dynamics and real-world intricacies of the canal. Factors such as temporal variations in upstream discharge, the number and duration of lock operations, and the effects of changing water levels and flow rates could influence the actual saltwater exchange and dispersion patterns within the canal.

## 6.2 Depth dependent Calibration and validation on a stratified system

The calibration and validation of the model was conducted using observational data from Rijkswaterstaat (n.d.), collected at relatively higher positions in the water column, where lower salt concentrations were expected compared to the bottom. The measurement heights concern +0.25 mNAP and -5 mNAP, while the canal's water depth at both observation locations is approximately 12 meters. As certain processes such as ship traffic and water extraction, which contribute to additional mixing in the upper water layer, were not accounted for in the model, relatively significant stratification was observed in the modelled upper layers compared to the observations. To improve the model's representation, incorporating ship traffic could involve adjustments to the horizontal and/or vertical mixing components. However, due to limited time availability and the need to maintain realistic parameter values, it is chosen to not implement this refinement and is therefore discussed here.

Figure 6.1 presents a compelling comparison between the observed depth-dependent values (illustrated in green) and the corresponding modelled layers (depicted in blue). The model layers 8 and 12 are shown which cover the depth range of -0.3mNAP to -5mNAP, showing a slight deviation from the observed depths.. The figure clearly highlights the distinctive stratification patterns exhibited by the model within these layers. For the assessment of mitigation measures layer 7 has been selected from the model, which is one layer deeper than the corresponding layer to the observations. Figure 6.2 illustrates the difference in salt concentration between the layers and displays a clear halocline-like structure (Georgiou & McCorquodale, 2000; Zhang et al., 2021; Valle-Levinson, 2009). Layer 7 is situated at the steepest gradient, and during the calibration and validation process, it likely demonstrated the best fit, as the layers above were too strongly stratified, hindering an accurate reproduction of the salt concentration. A different value for the Vertical Eddy Diffusivity (VED) and/or Vertical Eddy Viscosity (VEV) could be necessary.

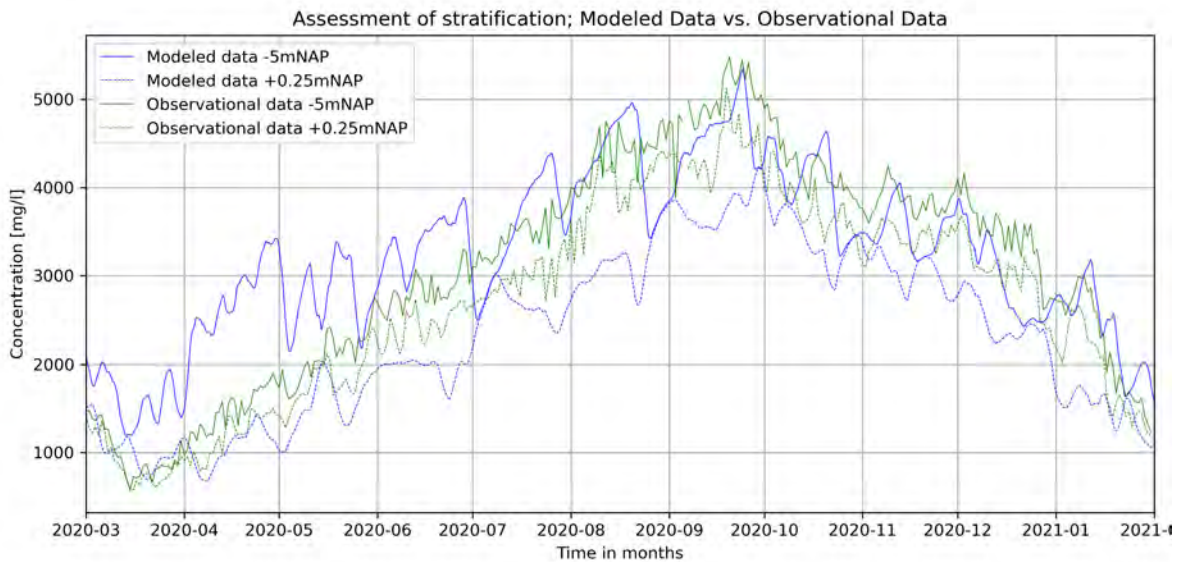


Figure 6.1: Stratification observed +0.25mNAP and -5mNAP and modelled, layer 8 and 12 at location Sas van Gent

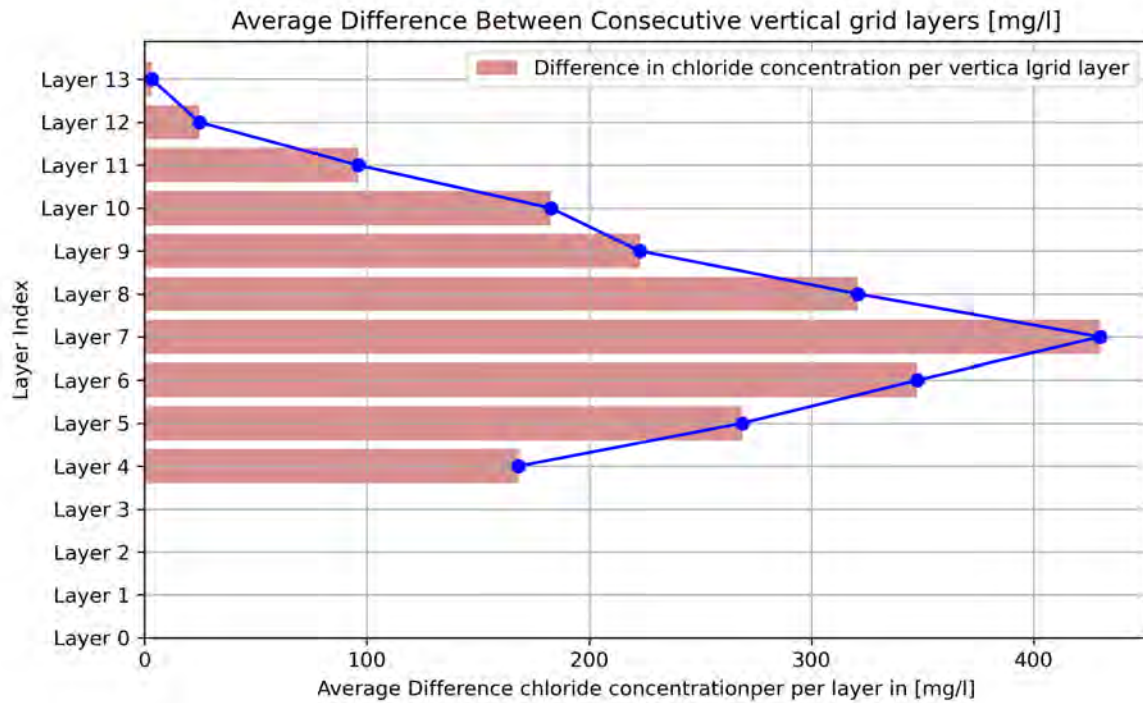


Figure 6.2: Difference in salt concentration per layer

The stratified nature of the model allows for insights into its response to upstream discharge and its recovery to this, for example in the form of a freshwater pulse. The increased stratification in the model can lead to various effects on the behavior to this freshwater pulse compared to less stratification. One significant aspect is that stronger stratification restricts vertical mixing between water layers. Consequently, the freshwater pulse will penetrate less rapidly and to a shallower depth in the water column due to the stratification hindering its vertical displacement. As a result, the impact of the freshwater pulse on saltwater intrusion and the salt concentration in the canal system may be less pronounced (both in distance and intensity), as described by Biemond et al. (2022). Moreover, the stronger stratification causes the freshwater to spread more slowly throughout the canal system. This gradual decrease in salt concentration over space is also observed during the simulations.

Additionally, the stronger stratification can lead to the formation of more complex flow patterns. The interaction between layers and the surrounding water movement becomes more complicated, influencing the dispersion and distribution of the freshwater pulse, which in turn can affect the results of the pulse. This information will be further addressed in the subsequent chapter during the analysis of the measures.

The model calibration process faced inherent challenges due to the lack of 100% accurate downstream boundary conditions, making it difficult to attain perfect calibration. As evident from the results, the model struggled to precisely reproduce salt peaks exceeding 5500mg/l, despite assuming that the calibration parameters fell within realistic ranges (Verbruggen & Van Der Baan, 2022; Buschman et al., 2015). Nonetheless, noteworthy advancements were achieved through the calibration procedures. The initial calibration step involved adjusting the parameters for horizontal and vertical mixing, resulting in reasonable accuracy when evaluating statistical performance. Subsequently, the second calibration step entailed modifying the assumption of a constant upstream discharge, leading to improvements in the (N)RMSE. However, it is crucial to recognize that this adjustment also heavily relies on assumptions influenced by data limitations.

The validated model employed for the design of Lock Complex Terneuzen demonstrated satisfactory statistical performance, with Root Mean Square Error (RMSE) values falling within an acceptable

range when compared to values reported by Akter et al. (2019). Additionally, the Normalized Root Mean Square Error (NRMSE) values for both measurement locations, SKikuil brug and Sas van Gent, were below 0.2, indicating a good predictive model according to Williams and Esteves (2017). Moreover, the BIAS indicator for both locations remained within the limits set by Williams and Esteves (2017), with an acceptable range of 1ppt (+/- 550 mg/l) of bias.

Despite the well-performing model based on the observation data, deviations remained visible between modelled and observational data across the water column. Subsequently, the availability of TSO (Temperature, Salinity, Oxygen) measurements, encompassing a greater number of calibration points and depth coverage, was realized later during the thesis. A comparison between these TSO measurements and the initial calibration data revealed higher values in the TSO measurements. This discrepancy can be attributed to the fact that TSO measurements were obtained across the entire water column, whereas the initial calibration data from RWS was limited to specific depths.

While the model showed a good fit with the observations in layer 7, caution should be exercised when generalizing the results to other layers in the water column. The model's performance in other layers may vary depending on the degree of stratification and the interaction between different processes.

### 6.3 Interpretation of the effectiveness of implemented measures to reduce saltwater intrusion

In this study, eight measures, including both physical and management-related were examined to mitigate saltwater intrusion in the Ghent-Terneuzen canal. The validated model used for the new design of the complex demonstrated satisfactory statistical performance, categorizing it as a well-working model for the year 2020.

The first two physical measures involved submerged and elevated thresholds with additional discharge. These measures were chosen due to their known effectiveness in reducing saltwater intrusion, as found by Vijverberg et al. (2010), Nieuwe Sluis Terneuzen (n.d.), and Friocourt et al. (2014). The submerged threshold exhibited slightly better performance than the elevated threshold, which can be attributed to its larger volume for capturing saltwater. However, it is important to note that the continuous flushing of saltwater from the bottom may have influenced the results, contrasting the reference run where an external correction factor was applied in the top layer to maintain the target water level. The continuous flushing was idealized in this study, and in reality, it may not be possible to continuously flush the saltwater. Nonetheless, both measures showed high potential for effectively managing saltwater intrusion in the Ghent-Terneuzen canal.

The canal narrowing measure was considered for its potential in open systems like estuaries, as indicated by Veerapaga et al. (2020). However, the actual implementation of this measure did not yield the desired effect. A slight reduction in salt was observed upstream of the constriction due to its impact on local hydrodynamics. The reduction is mainly attributed to the increase in flow velocity, resulting in higher shear stresses and turbulence as the flow approaches the constriction. This intensified mixing and dispersion of saltwater with freshwater downstream of the constriction led to an increase in salt concentration. On the other hand, Veerapaga et al. suggest that the narrowing reduces salt by promoting stratification, which subsequently results in lower salt content. Nevertheless, since the canal is already stratified, the additional stratification caused by this measure is less pronounced than it could be in reality, resulting in a minimal reduction of salt.

The selective withdrawal of saltwater was explored as last physical measure. While this measure has shown potential in the Amsterdam-Rijnkanaal at Zeesluis IJmuiden, its actual implementation is cost-intensive compared to the other measures. Due to limitations in the modeling capabilities of Delft3D, an alternative implementation using thin dams and source/sinks was employed. However, this alternative method closely resembled the elevated and submerged thresholds, as it involved re-

moving saltwater from the bottom at a different location. This deviation from reality may influence the effectiveness of the measure, considering the continuous withdrawal of water in order to maintain the water level.

The management-oriented measures examined variations in upstream discharge to analyze their impact on saltwater intrusion. Simulations were conducted for comparison to the 2DV model described in Vuik & Lambrechts (2023).

The first measure involved spreading the summer discharge to gradually reduce saltwater intrusion. However, practical constraints in water management and the need for a large buffer volume make real-life implementation challenging. While the constant discharge of  $7.5 \text{ m}^3/\text{s}$  during the implementation period was insufficient to effectively reduce saltwater intrusion, a small positive effect was observed afterward. The model's slow recovery to equilibrium may be attributed to the strong stratification in the upper layer of the canal, leading to a slower spread of freshwater and a gradual decrease in salt concentration.

The second measure explored the use of freshwater pulses to counteract saltwater intrusion. Real-life implementation of this measure is also hindered by practical constraints. In this analysis simulations with pulses of  $25$  and  $50 \text{ m}^3/\text{s}$  were examined while the cumulative discharge remains the same. Pulses with a discharge of  $25 \text{ m}^3/\text{s}$  proved insufficient to reduce saltwater intrusion, along with the averaged discharge between these pulses. The  $50 \text{ m}^3/\text{s}$  pulses showed some positive effect, but the low discharge between pulses limited its effectiveness. Similar to Kranenburg et al. (2023), the results indicated that large quantities of discharge pulses are required to effectively flush channels and reduce saltwater intrusion. This observation could potentially indicate the limited effectiveness of short-term pulses, likely attributed to the stratification present in the canal system.

The third measure involved a winter flushing, doubling the upstream discharge from January to April. This measure relied on a strong assumption of water availability in the catchment of the Ghent-Terneuzen canal. However, this discharge level is higher than realistic, making the measure dependent on external factors. Nevertheless, the model showed a reduction in saltwater intrusion, and the flushing effect extended until July, one month longer recovery than the 2DV model of Vuik & Lambrechts (2023). This discrepancy may be attributed to the stronger stratification in the canal's upper layer resulting in a longer recovery time. It is noteworthy that larger discharge scenarios exhibit less variability in the recovery time compared to shorter-duration discharge scenarios.

Lastly, a simulation of a short-duration summer rainstorm with increased discharge for two days was performed. While the model demonstrated a reduction in saltwater intrusion, the amount of reduction and the model's recovery raised questions. The extended recovery period may be attributed to the model's sensitivity to upstream discharge, suggesting potential limitations in using the model for assessments of short duration discharge scenarios.

## 6.4 Assumptions and simplifications throughout the research

The process of assessing the saltwater intrusion dynamics in the Ghent-Terneuzen canal involved making several critical assumptions and simplifications. These decisions were necessary due to data limitations, computational constraints and time, understanding these assumptions is essential for a comprehensive interpretation of the model's capabilities and limitations.

As already highlighted, the downstream boundary conditions have contain the most assumptions and simplifications. The duration of lock door openings was assumed to be 10 minutes for each lock passage. To quantify saltwater exchange during lock passages, averaged values from previous research were utilized. Additionally, the model assumed that lock passages occurred uniformly for each day throughout the simulation period. Cyclic representation accounted for water losses during lock operations. These assumptions may not fully capture the variability of saltwater (exchange) that can occur in the variable real-world lock operations.

At the upstream boundary, a uniform daily discharge was assumed, and the salinity concentration was set to 0.5 ppt (250 mg/l). Assumption of the upstream discharge was needed for the Zuidlede and Tollhuis weir as no data was present. Furthermore, the bathymetry data for the New Lock Terneuzen is not present, so assumptions are needed. However, some side branches, such as Moervaart, Zuidlede, Evergem, and the branch to Gent, lacked measured bathymetry data and were assigned fixed values.

Continuous (additional) discharges were considered for certain measures 1, 2, and 4. It was assumed that upstream discharge could be controlled and that the required buffer volume for measures 5,6 and 7 could be provided. Moreover, to maintain the target water level of 2.13mNAP in the canal, an external correction factor was applied in the upper layer of the canal to account freshwater losses during lock passages. This correction factor played a critical role in balancing the water levels and allowed for a feasible and validated model setup, facilitating the assessment of saltwater intrusion dynamics in the Ghent-Terneuzen canal.

However, it is crucial to acknowledge that these assumptions introduce uncertainties and may impact the accuracy of the results. The cyclic representation of lock operations and uniform up- and downstream discharge assumption might limit the model's ability to capture dynamic variations in water levels and salinity concentrations accurately. Furthermore, assigning fixed values to side branches may not fully represent their actual behavior, leading to potential discrepancies in the model's performance.

## 6.5 Trustworthiness of the model and its applicability

As previously mentioned, the validated model can be categorized as a well-performing model based on the NRMSE findings of Williams and Esteves (2017). However, the validation of the new design incorporating New Lock Terneuzen can only be achieved once the actual construction is completed and data becomes available.

The majority of assumptions and simplifications were made concerning the downstream boundary conditions. To ensure that errors do not compound, no measures were tested that directly influenced these the boundary conditions. This approach allows for the testing of measures relative to the same model, thereby providing reliable results.

Consequently, the model is reliable for testing measures that are independent of the downstream boundary conditions. However, predicting future scenarios for examination of the saltwater intrusion is not possible with this model. During the calibration phase, the model exhibited resistance to salt peaks exceeding 5500 - 6000 mg/l, which limits its predictive capabilities for extreme salt concentrations.

Additionally, when discussing the model's applicability for testing the effects of upstream discharge on the canal's salt concentration, there are some considerations. Despite the model's good fit during validation, it demonstrated sensitivity to variations in changing upstream discharges during the simulations. The reproduction of the years 2018 and 2020 showed coherent behavior compared to observations but with increased fluctuations. However, the measures related to changing upstream discharge yielded different results compared to Vuik & Lambrechts' findings. The model required a prolonged recovery time to return to equilibrium after applying these measures. Although the 2DV model was not used in the same year, it can be concluded that the model in this study requires an extended recovery time from individual events, possibly indicating it is not suitable for these kind of assessments.

## 6.6 Research's implication on management of the Ghent-Terneuzen canal

The implications of this research have significant implications for managing saltwater intrusion in the Ghent-Terneuzen canal. While it cannot be 100% validated at this stage, there is an expectation that the new design of Lock Complex Terneuzen, without additional measures, will lead to a considerable increase in salt concentration in the canal. The current design minimally accounts for salt reduction. Statements such as "possible use of bell screen" and "foundation for possible elevated threshold" do not instill much confidence in mitigating saltwater intrusion. However, it becomes essential to address and mitigate saltwater intrusion in this scenario.

Three dominant factors necessitate action. Firstly, the Environmental Impact Assessment (MER) predicts no breach of the 3000 mg/L chloride limit even after the realization of the New Sluice Terneuzen (NST). This limit is mandated by the Water Framework Directive (2018) and established agreements between the Netherlands and Belgium in the Amendment Treaty 1985. Secondly, industries along the canal utilize surface water for cooling purposes, but these installations are not equipped to handle saltwater (Maas & Oorthuijsen, 2012). Consequently, the increased salt concentration in the canal can lead to the salinization of groundwater, affecting local farmers reliant on this water source.

# Chapter 7

## Conclusion

This study aimed to investigate saltwater intrusion dynamics in man-made canals, with specific focus on the Ghent-Terneuzen canal and evaluate measures to mitigate its impacts. Despite limitations in data availability and computational efficiency, the model setup successfully simulated saltwater intrusion within the canal. This research contributes to the understanding of saltwater intrusion dynamics and provides valuable information for decision-making processes related to the management and protection of canal systems. This chapter effectively addresses the research questions outlined in section 1.3 through the knowledge acquired from the simulations conducted in this thesis.

- **What mitigation measures can be identified to effectively reduce saltwater intrusion, and which among them appears to be the most promising in terms of mitigating saltwater intrusion, feasibility and practicality?**

Scientific literature provides substantial information on measures to reduce saltwater intrusion, mainly focusing on open systems like estuaries. However, valuable insights can also be derived specifically for closed systems. This research investigates two types of measures: physical structures and management-related measures.

Widely known and applied method are the use of an elevated or submerged thresholds, temporarily trapping heavier salt, which can then be efficiently removed. Considering the inclusion of a foundation for a future threshold in the new design of the Terneuzen Lock Complex makes the assessment essential. A similar method is selective withdrawal, already implemented in the Amsterdam-Rijnkanaal, where freshwater in the upper layer is restricted, allowing controlled intake of saltwater, which is subsequently removed. Additionally, insights from open systems primarily contribute to measures related to geometry. As the height or shape of a canal cannot be adjusted, narrowing the canal remains the only viable measure to be tested, as it has shown effectiveness in reducing saltwater intrusion in estuaries according to existing literature.

The management-related measures in this study explore the use of upstream discharge to effectively mitigate saltwater intrusion, given its significant influence on the amount and extend of saltwater intrusion. Four distinct measures related to upstream discharge were thoroughly examined: the spread of summer discharge, freshwater pulses, winter flushing, and simulation of an intense summer rainstorm. The selection of these measures was based on their relevance and previous investigations using a 2DV model, enabling a comprehensive comparison with the outcomes derived from the 3D model in this research.

- **Can a Delft3D model be established to accurately simulate observed salinity levels in the Ghent-Terneuzen canal?**

Based on thorough calibration and validation, this research confirms the established Delft3D model has the capability in accurately simulating observed salinity levels in the Ghent-Terneuzen canal. While the model encountered challenges in capturing salinity peaks exceeding 5500 mg/l during calibration, its robust performance during validation, indicated by strong statistical performance at both measurement locations demonstrates its reliability in replicating real-world salinity conditions for values below 5500 mg/l. These findings firmly support the model's suitability for assessing mitigation measures, providing invaluable insights for effective salinity management strategies in the canal. However, for projecting salinity values beyond 5500 mg/l, further refinements and data assimilation may be required to enhance the model's predictive capacity.

- **What effect do the (identified) mitigation measures have on saltwater intrusion, as determined by in-depth analysis using Delft3D, and what are the additional insights for these measure(s)?**

In conclusion, the research using the Delft3D model provides valuable insights into the impact of various mitigation measures on saltwater intrusion in the Ghent-Terneuzen canal. Both physical and management oriented measures are assessed.

Among the physical measures tested, the submerged and elevated thresholds with additional discharge prove highly effective in reducing saltwater intrusion, while the canal narrowing measure shows limited success. The study also highlights the potential of the selective withdrawal of saltwater, although its implementation may present cost and technical challenges. These findings offer crucial guidance for water management authorities, informing them about effective solutions to address saltwater intrusion in the canal and paving the way for sustainable water management practices.

The analysis of management-oriented measures using the Delft3D model involved four scenarios. The spread summer discharge demonstrated limited effectiveness in gradually reducing salt intrusion. This measure also posed practical challenges due to the buffer volume requirements. The implementation of freshwater pulses to counteract salt intrusion encountered practical constraints, with low pulses being ineffective and high pulses leading to low discharge between the pulses, limiting the effectiveness. This highlights the importance of using large discharges to effectively flush channels, as supported by Kranenburg et al.'s research (2023). Winter flushing showcased promising results in reducing saltwater intrusion, but its feasibility depended on external factors as the availability of upstream discharge. The model revealed a prolonged effect of winter flushing until July, differing from previous studies, possibly due to stratification in the canal's upper layer. Finally, a simulation of a short-lived summer rainstorm with increased discharge for two days revealed reduced saltwater intrusion. However, the model's prolonged recovery period of approximately four months, compared to one month in Vuik & Lambrecht's model, highlights the model's sensitivity to upstream discharge, potentially limiting its suitability for assessment of upstream discharge.

# Bibliography

- [1] Akter, R., Asik, T. Z., Sakib, M., Akter, M., Sakib, M. N., Azad, A. S. M. a. A., Maruf, M., Haque, A., & Rahman, M. (2019). *The Dominant Climate Change Event for Salinity Intrusion in the GBM Delta*. *Climate*, 7(5), 69. <https://doi.org/10.3390/cli7050069>
- [2] Baracchini, T., Hummel, S., Verlaan, M., Cimadoribus, A., Wüest, A., & Bouffard, D. (2020). *An automated calibration framework and open source tools for 3D lake hydrodynamic models*. *Environmental Modelling and Software*, 134, 104787. <https://doi.org/10.1016/j.envsoft.2020.104787>
- [3] Bathymetrische databank. (n.d.). *www.vlaanderen.be*. <https://www.vlaanderen.be/geopunt/kaarttoepassingen/bathymetrische-databank>
- [4] Biemond, B., De Swart, H., Dijkstra, H. A., & Díez-Minguito, M. (2022). *Estuarine Salinity Response to Freshwater Pulses*. *Journal of Geophysical Research: Oceans*, 127(11). <https://doi.org/10.1029/2022jc018669>
- [5] Buschman, Schueder, R., Apecechea, M. I., & Van Der Kaaij, T. (2015). *Ontwikkeling van een Delft3D model voor het Noordzeekanaal en Amsterdam-Rijnkanaal*. *Deltares*, 1220072–012.
- [6] Chen, W., Liu, W., & Hsu, M. (2015). *Modeling assessment of a saltwater intrusion and a transport time scale response to sea-level rise in a tidal estuary*. *Environmental Fluid Mechanics*, 15(3), 491–514. <https://doi.org/10.1007/s10652-014-9367-y>
- [7] Costa, Y., Martins, I., de Carvalho, G. C., & Barros, F. (2023). *Trends of sea-level rise effects on estuaries and estimates of future saline intrusion*. *Ocean & Coastal Management*, 236, 106490. <https://doi.org/10.1016/j.ocecoaman.2023.106490>
- [8] Dataregister Rijkswaterstaat. (n.d.). <https://maps.rijkswaterstaat.nl/dataregister/srv/dut/catalog.search/metadata/1ab66022-066a-4cd5-9a8e-720eb8490ed5?tab=relations>
- [9] de la Reguera, E., Veatch, J., Gedan, K., & Tully, K. L. (2020). *The effects of saltwater intrusion on germination success of standard and alternative crops*. *Environmental and Experimental Botany*, 180, 104254. <https://doi.org/10.1016/j.envexpbot.2020.104254>
- [10] Deltares. (2023). *Delft3D-FLOW, User Manual (Version: 4.05)*. [https://content.oss.deltares.nl/delft3d4/Delft3D-FLOW\\_User\\_Manual.pdf](https://content.oss.deltares.nl/delft3d4/Delft3D-FLOW_User_Manual.pdf)
- [11] Deltares. (2023b). *Delft3D FM Suite*. <https://www.deltares.nl/en/software/delft3d-flexible-mesh-suite/>
- [12] DINoloket. (n.d.). <https://dinoloket.nl/>
- [13] Flemisch government. (1960). *Verdrag verbetering kanaal Gent-Terneuzen*. In *Juridische Codex Kustzone (Artikel 32)*. <https://www.kustcodex.be/kustcodex-consult/plainWettekstServlet?wettekstId=56579&lang=nl>
- [14] Friedrichs, C. T., & Aubrey, D. G. (1988). *Non-linear tidal distortion in shallow well-mixed estuaries: a synthesis*. *Estuarine Coastal and Shelf Science*, 27(5), 521–545. [https://doi.org/10.1016/0272-7714\(88\)90082-0](https://doi.org/10.1016/0272-7714(88)90082-0)

- [15] Friocourt, Y., Kuijper, N., & Leung, N. (2014). *Salt intrusion*. STOWA. <https://www.stowa.nl/deltafacts/zoetwatervoorziening/delta-facts-english-versions/salt-intrusion>
- [16] Georgiou, & McCorquodale. (2000). *Salinity Stratification from a Navigation Canal into a Shallow Lake*. Researchgate.
- [17] Hasan, G. M. J., Maren, D. S., & Fatt, C. (2012). *Numerical Study on Mixing and Stratification in the Ebb-Dominant Johor Estuary*.
- [18] iv-groep. (n.d.). *Het ontwerp van de basculebruggen over de Nieuwe Sluis bij Terneuzen*. <https://iv-groep.nl/nl/blog/overzicht/het-ontwerp-van-de-basculebruggen-over-de-nieuwe-s>
- [19] KNMI - Daggegevens van het weer in Nederland. (n.d.). <https://www.knmi.nl/nederland-nu/klimatologie/daggegevens>
- [20] Kranenburg, W., Tiessen, M. C., Blaas, M., & Van Veen, N. P. (2023). *Circulation, stratification and salt dispersion in a former estuary after reintroducing seawater inflow*. *Estuarine, Coastal and Shelf Science*, 282, 108221. <https://doi.org/10.1016/j.ecss.2023.108221>
- [21] Lievense CSO. (2015). *Nieuwe Sluis Terneuzen; Deelrapport MER Water*. Rapport Vlaams Nederlandse Scheldec commissie VNZT-R-127-7, 23 maart 2015.
- [22] Liu, B., Peng, S., Liao, Y., & Wang, H. (2019). *The characteristics and causes of increasingly severe saltwater intrusion in Pearl River Estuary*. *Estuarine, Coastal and Shelf Science*, 220, 54–63. <https://doi.org/10.1016/j.ecss.2019.02.041>
- [23] Maas & Oorthuijsen. (2012). *Brondocument Waterlichaam Kanaal Gent-Terneuzen: Doelen en maatregelen rijkswateren Ministerie van IenM*. Rijkswaterstaat, 2009. <https://www.commissiener.nl/docs/mer/p28/p2875/2875-012brondocument-waterlichaam.pdf>
- [24] Mendelsohn, D., Peene, S., Yassuda, E., & Davie, S. (2000). *Hydrodynamic model calibration study of the Savannah River Estuary with an examination of factors affecting salinity intrusion*.
- [25] Ministerie van Infrastructuur en Waterstaat. (2023). *Sluizencomplex Terneuzen*. Rijkswaterstaat. <https://www.rijkswaterstaat.nl/water/waterbeheer/bescherming-tegen-het-water/waterkeringen/dammen-sluizen-en-stuwen/sluizencomplex-terneuzen#:~:text=Het%20sluizencomplex%20van%20Terneuzen%20bestaat,buiten%20bedrijf%20en%20wordt%20gesloopt.>
- [26] Nieuwe Sluis Terneuzen — Nieuwe Sluis Terneuzen. (n.d.). <https://nieuwesluisterneuzen.eu/over-de-nieuwe-sluis>
- [27] Nieuwe Sluis Terneuzen. (n.d.). — *Zoutdrempel tegen verzilting* <https://nieuwesluisterneuzen.eu/nieuws/2021-06/zoutdrempel-tegen-verzilting>
- [28] R1860/Q281. WL-rapport C6201, H.W.R. Perdijk, maart 1988.
- [29] Prandle, D. (2004). *Saline intrusion in partially mixed estuaries*. *Estuarine Coastal and Shelf Science*, 59(3), 385–397. <https://doi.org/10.1016/j.ecss.2003.10.001>
- [30] Ralston, D. K., Geyer, W. R., & Warner, J. C. (2012). Bathymetric controls on sediment transport in the Hudson River estuary: Lateral asymmetry and frontal trapping. *Journal of Geophysical Research: Oceans*, 117(C10), n/a-n/a. <https://doi.org/10.1029/2012jc008124>
- [31] Rijkswaterstaat (1984). Chlorideconcentratie op het kanaal van Gent naar Terneuzen. Periode 1975-1981. Directie Waterhuishouding en waterbeweging, distrikt Zuidwest. Notanummer 71.013.01, Dordrecht, mei 1984.
- [32] Rijkswaterstaat. (2017). Richtlijnen Vaarwegen: Kader verkeerskundig vaarwegontwerp Rijkswaterstaat. <https://waterrecreatienederland.nl/content/uploads/2018/04/richtlijnen-vaarwegen-2017.pdf>

- [33] Rijkswaterstaat. (2020). Operationeel Watermanagement Kanaal Gent-Terneuzen. In Rijkswaterstaat (wv10820zb47f). <https://www.rijkswaterstaat.nl/water/waterbeheer/watermanagementcentrum-nederland>
- [34] Rijkswaterstaat. (n.d.). Waterinfo [Dataset]. <https://waterinfo.rws.nl/#!/nav/index/>
- [35] Scroccaro, I., Spitz, Y. H., & Seaton, C. M. (2023). Effect of Local Winds on Salinity Intrusion in the Columbia River Estuary. *Water*, 15(2), 326. <https://doi.org/10.3390/w15020326>
- [36] Sistermans, P., & Nieuwenhuis, O. (2003). WESTERN SCHELDT ESTUARY (THE NETHERLANDS). In EUROSION Case Study. DHV group. [http://copranet.projects.eucc-d.de/files/000142\\_EUROSION\\_Western\\_Scheldt.pdf](http://copranet.projects.eucc-d.de/files/000142_EUROSION_Western_Scheldt.pdf)
- [37] Standardisation of inland waterways. (2020). [Slide show]. PROPOSAL FOR THE REVISION OF THE ECMT 1992 CLASSIFICATION. incomnews. <http://incomnews.org/WGs/WG%20179%20-%20New%20Ships%20in%20the%20CEMT%2092%20Classification/ATTACHEMENTS/Presentatie%20rapport%20WG%20179%20tbv%20Pianc%20website%2021092020.pdf>
- [38] Svašek. (2010). Invloed nieuwe voorkeursvariant op chloride concentratie in het kanaal Gent-Terneuzen. Available at: [https://nieuwesluisterneuzen.eu/sites/default/files/downloads/MER-deelrapport%20Water-%20Bijlage%2010-%201724U15001BLdW\\_Invloed\\_chloride\\_nieuweVKV.pdf](https://nieuwesluisterneuzen.eu/sites/default/files/downloads/MER-deelrapport%20Water-%20Bijlage%2010-%201724U15001BLdW_Invloed_chloride_nieuweVKV.pdf)
- [39] Svasek. (2015). Memo: invloed nieuwe voorkeursvariant op chloride concentratie in kanaal Gent - Terneuzen. Available at: [https://nieuwesluisterneuzen.eu/sites/default/files/downloads/MER-deelrapport%20Water-%20Bijlage%2010-%201724U15001BLdW\\_Invloed\\_chloride\\_nieuweVKV.pdf](https://nieuwesluisterneuzen.eu/sites/default/files/downloads/MER-deelrapport%20Water-%20Bijlage%2010-%201724U15001BLdW_Invloed_chloride_nieuweVKV.pdf)
- [40] Tully, K., Gedan, K., Epanchin-Niell, R., Strong, A., Bernhardt, E. S., BenDor, T., Mitchell, M., Kominoski, J., Jordan, T. E., Neubauer, S. C., & Weston, N. B. (2019). The Invisible Flood: The Chemistry, Ecology, and Social Implications of Coastal Saltwater Intrusion. *BioScience*, 69(5), 368–378. <https://doi.org/10.1093/biosci/biz027>
- [41] Valle-Levinson. (2009). *Contemporary issues in estuarine physics*. Cambridge University Press, 978-0-521-89967-3.
- [42] Van Den Bergh, Van Damme, Graveland. (2021). Ecological Rehabilitation of the Schelde Estuary (The Netherlands–Belgium; Northwest Europe): Linking Ecology, Safety against Floods, and Accessibility for Port Development. *Purews*. <https://purews.inbo.be/ws/portalfiles/portal/29362711/174185.pdf>
- [43] Vanderkimpen, P., & Pereira, F. (2012). Opmaak van modellen voor onderzoek naar waterbeschikbaarheid en -allocatiestrategieën in het scheldestroomgebied. In Mobiliteit En Openbare Werken. *Flemish government*. <https://publicaties.vlaanderen.be/view-file/10533>
- [44] Vanoutrive, P. (2020, January 29). De Nieuwe Sluis Terneuzen wordt één van de grootste ter wereld. *EOS Wetenschap*. <https://www.eoswetenschap.eu/nieuwe-sluis>
- [45] Veerapaga, N., Shintani, T., Azhikodan, G., Yokoyama, K. (2020). Study on salinity intrusion and mixing types in a conceptual estuary using 3-D hydrodynamic simulation: Effects of length, width, depth, and bathymetry. *Part of the Springer Water book series (SPWA)* [https://doi.org/10.1007/978-981-15-2081-5\\_2](https://doi.org/10.1007/978-981-15-2081-5_2)
- [46] Veerapaga, N., Azhikodan, G., Shintani, T., & Yokoyama, K. (2019). Numerical Study on Effect of Topography, Shape, and Multi-branch on Saltwater Intrusion in a Conceptual Estuary. *Journal of Japan Society of Civil Engineers, Ser. B2 (Coastal Engineering)*, 75(2), L19-L24. [https://doi.org/10.2208/kaigan.75.i\\_19](https://doi.org/10.2208/kaigan.75.i_19)
- [47] Verbruggen, W., & Van Der Baan. (2022). Ontwikkeling zesde-generatie 3D Noordzeekanaal Amsterdam-Rijnkanaal model. *Deltares*. [https://publications.deltares.nl/11208053\\_009\\_0005.pdf](https://publications.deltares.nl/11208053_009_0005.pdf)

- [48] Vijverberg, T., Folmer, I., Carron, T., Talstra, H., Blik, B., & Svasek. (2010). Verkenning maritieme toegankelijkheid Kanaal Gent-Terneuzen: Aanvullend oppervlaktewateronderzoek (Eindrapport 9V4098.A0). <https://nieuwesluisterneuzen.eu/sites/default/files/downloads/3.2.1%20No-Regret%20Milieu%20en%20Veiligheid%20Aanvullend%20Oppervlaktewateronderzoek.pdf>
- [49] VNSC (2015) Aanvulling deelrapport MER Water. Rapport Vlaams Nederlandse Scheldecommissie, uitgevoerd door Svasek Hydraulics, Rapportnummer VNZT-R-404-3, 22 september 2015.
- [50] Vuik, V., Lambregts, P., & HKV. (2023). Verzilting Kanaal Gent-Terneuzen: Internal document.
- [51] Vreeken, T., & Weiler, O. (2022). ZSF documentation — libzsf documentation. Retrieved from <https://libzsf.readthedocs.io/en/latest/>
- [52] Water Framework Directive. (2018). <https://water.europa.eu/freshwater/europe-freshwater/water-framework-directive>
- [53] Welcome to Waterinfo. (n.d.). <https://www.waterinfo.be/>
- [54] Waterloopkundig Laboratium (1988)
- [55] Williams, J. J., & Esteves, L. S. (2017). Guidance on Setup, Calibration, and Validation of Hydrodynamic, Wave, and Sediment Models for Shelf Seas and Estuaries. *Advances in Civil Engineering*, 2017, 1–25. <https://doi.org/10.1155/2017/5251902>
- [56] Zhang, Y., Ren, J., Zhang, W., Wu, J. (2021). Importance of salinity-induced stratification on flocculation in tidal estuaries. *Journal of Hydrology*, 596, 126063. <https://doi.org/10.1016/j.jhydrol.2021.126063>
- [57] Zhang, E., Gao, S., Savenije, H. H. G., Si, C., & Song, W. (2019). Saline water intrusion in relation to strong winds during winter cold outbreaks: North Branch of the Yangtze Estuary. *Journal of Hydrology*, 574, 1099–1109. <https://doi.org/10.1016/j.jhydrol.2019.04.096>

# Appendix A

## Management practices and additional information for the Ghent-Terneuzen canal

### A.1 Management and Development Plan of National Waters

Rijkswaterstaat Zeeland has defined the primary functions for Lock Terneuzen in the Management and Development Plan of National Waters (Vanderkimpen et al., 2012), listed in order of priority as follows:

1. Flood protection and drainage of the Ghent-Terneuzen canal;
2. Traffic management;
3. Mitigating saltwater intrusion.

#### A.1.1 Flood protection and drainage of the Ghent-Terneuzen canal

One of the functions of the lock complex is to serve as a flood protection measure by protecting the hinterland against the sea. With the construction of the New Lock Terneuzen the flood protection function will be situated at a height of 9.5 mNAP. As a result, the flood protection measure will be resilient for a sea level rise of approximately one meter over the course of the next 100 years.

Besides flood protection, the lock complex also serves to control the water level for the canal, both during high canal discharges and high water levels in the Western Scheldt. As the GTC is a closed system where water can only be discharged at the lock complex, it is essential to have a clear objective regarding water level management, as water cannot be discharged in any other way than through the locks. If the water level in the GTC is equal to or higher than that in the Western Scheldt, water cannot be discharged from the canal, and shipping is temporarily halted in all locks. This happens because the freshwater from the canal is used to level the lock chambers. Regular coordination is necessary between the upstream inflow and outflow via the Terneuzen locks to prevent significant water level fluctuations.

In order to avoid large water level fluctuations, water is discharged, the lock culverts in the Middle Lock are first utilized, with the option of partially opening the lock doors if needed. This process begins as soon as the water level in the canal surpasses the target level of 2.13 m + NAP and can reach a maximum of 2.23 m + NAP. If this method is not enough, the Eastern Lock is used next. Discharging water through the levelling valves in the Eastern Lock starts at a level of 2.23 m + NAP and can reach a maximum level of 2.33 m + NAP. During flood situations, the Western Lock is utilized as a last resort. To alleviate flooding, water is drained through the lock culverts in the Western Lock starting at a level of 2.33 m + NAP and reaching a maximum level of 2.43 m + NAP.

### A.1.2 Traffic management

Lock Complex Terneuzen relies on commercial shipping and requires operational locks. Shipping moves in both directions towards the GTC and Western Scheldt. To balance water levels differences, the lock chambers are adjusted during each cycle using fresh or low brackish water from the channel. This results in a significant loss of relatively fresh water, limiting the available water or flow rate through the locks in the summer.

Water is discharged through the Middle and Western locks to maintain a constant water level in the GTC when there is sufficient inflow from Flanders. The East Lock serves inland navigation and recreational boating. The West Lock is the largest and accommodates ocean-going vessels (CEMT III-IV) with a carrying capacity of 83,000 tons. It has five roller gates, including two outer gates facing the Westerschelde, two inner gates facing the canal, and one central gate for partial use of the lock chamber. The northern outer gate protects the lock during storms.

### A.1.3 Mitigating saltwater intrusion

The current design of the lock complex incorporates measures to mitigate saltwater intrusion, with variations in the specific measures implemented for each lock. Also, the design of the new lock includes provisions to address saltwater intrusion.

In the current situation, without any reducing measures, the West lock accounts for 80% of the total salt exchange in the complex. In the situation with the New Sea Lock, 60% of the salt exchange occurs through the New Lock, 35% through the West lock, and 5% through the East lock.

The East lock and previous middle lock have/had no measures against saltwater intrusion. To prevent saltwater intrusion, a saltwater trap has been constructed at the West lock (see Figure A.1). Saltwater that enters via the West lock first accumulates in this trap. The inlet of the culverts of the West lock is located at the bottom of the saltwater trap (see Figure A.2). When water is discharged through the culverts, the relatively salty water from the saltwater trap is the first to be removed. This mitigating measure limits the net salt intrusion through the West lock.

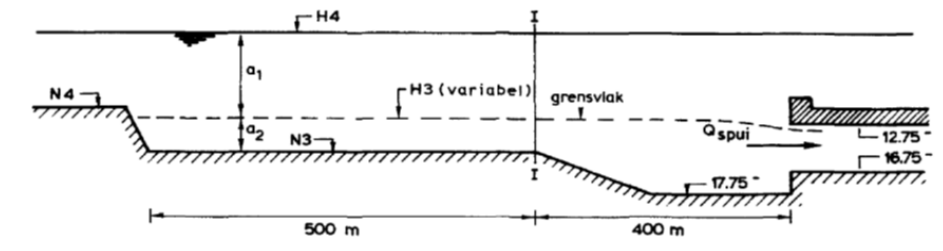


Figure A.1: The cross-sectional area of the salt trap at the Westsluis (Waterloopkundig Laboratorium, 1988).

Discharging through the West lock can be done in three ways: exchange flushing, continuous flushing, or surface water flushing. The principles of exchange flushing and continuous flushing are collectively known as the "Terneuzen system" (Rijkswaterstaat, 1984).

Exchange flushing and continuous flushing aim to achieve the desired chloride concentration principles on the GTC. originating from (Lievense CSO, 2015):

- The objective of the Water Framework Directive (2018) for the GTC is to maintain the chloride concentration between 300 and 3000 mg/l, the range associated with Good Ecological Potential (GEP). The objective applies to the summer average chloride concentration, averaged over multiple summers (April 1 to October 1), at a depth of 1.8 meters below the water surface at the Sas van Gent measurement point (GTC) (Ministerie van Verkeer en Waterstaat, Rijkswaterstaat,

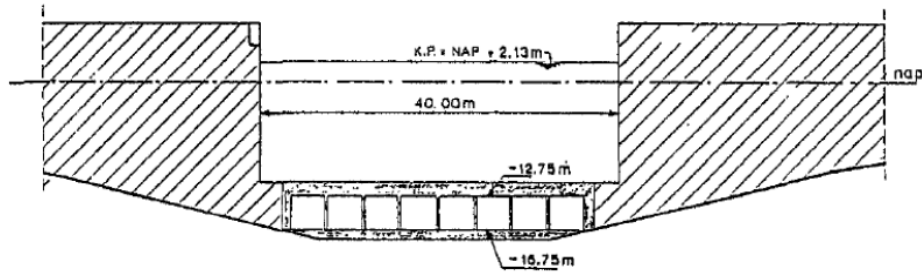


Figure A.2: Interior view of the West Lock with the entrance of the bypass sewer (Waterloopkundig Laboratorium, 1988).

2012). The objective is also enshrined in the Decision on the New Lock, which gives it extra value.

- Amendment Treaty 1985, Article 32 (Wijzigingsverdrag). The two governments shall take the necessary measures in their respective territories to ensure that the salt load remains limited.

## A.2 Upstream discharge

The discharge through the canal is largely originating from the lock complex at Evergrem, where a weir and two lock chambers are present. After the discharge at Evergrem, the Moervaart contributes the largest share to the total flow through the canal. Water also flows into the canal from Ghent, partly via the Tolhuis weir.

The Amendment Treaty of 1985 (wijzigingsverdrag 1985) stipulates that the minimum supply of fresh water to the KGT should be  $13 \text{ m}^3/\text{s}$ , averaged over two months, or alternative measures should be taken that provide equivalent relief from saltwater intrusion. In practice, achieving this water supply is not always possible. The agreed maximum discharge is  $100 \text{ m}^3/\text{s}$ . This agreement will ensure the freshwater supply and a controllable water level.

The upstream water supply to the GTC is a distribution of the available water from the Upper Scheldt and Leie (Figure A.3). However, this water has to be distributed over multiple water bodies (Vuik & Lambrechts, 2023).

## A.3 Water level management

In addition to the Amendment Treaty on chloride concentrations and upstream discharge, there are several agreements on water level management in the Ghent-Terneuzen Canal. Three treaties (1843, 1969, and 1985) have established the following agreements (Rijkswaterstaat, 2020):

- No drainage of polder water takes place in the Netherlands;
- The canal has a target water level of 2,10 mNAP (TAW+4.45 m) with margins of +/- 25 cm;
- The Netherlands ensures that saltwater intrusion in Terneuzen remains limited;
- Belgium ceases supply when the water level exceeds 2,35 mNAP;
- Belgium ensures a minimum flow of  $13 \text{ m}^3/\text{s}$  averaged over 2 months (or implements alternative measures that achieve an equivalent reduction in saltwater intrusion).

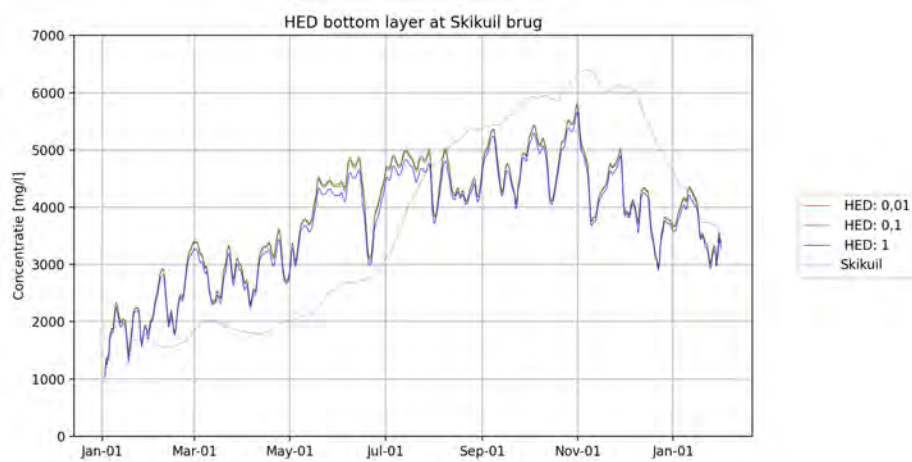
The net water transfer at the lock complex occurs in the direction from the Ghent-Terneuzen Canal towards the Westerschelde. For simplicity, the assumption is made that the water level of the Ghent-Terneuzen Canal remains constant during the computational period.



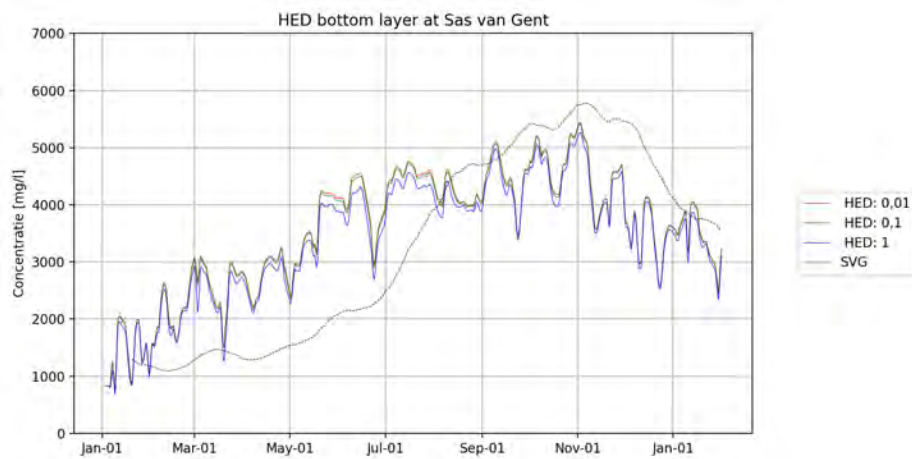
Figure A.3: Water distribution around Ghent (Rijkswaterstaat, 2020)

# Appendix B

## Sensitivity analysis

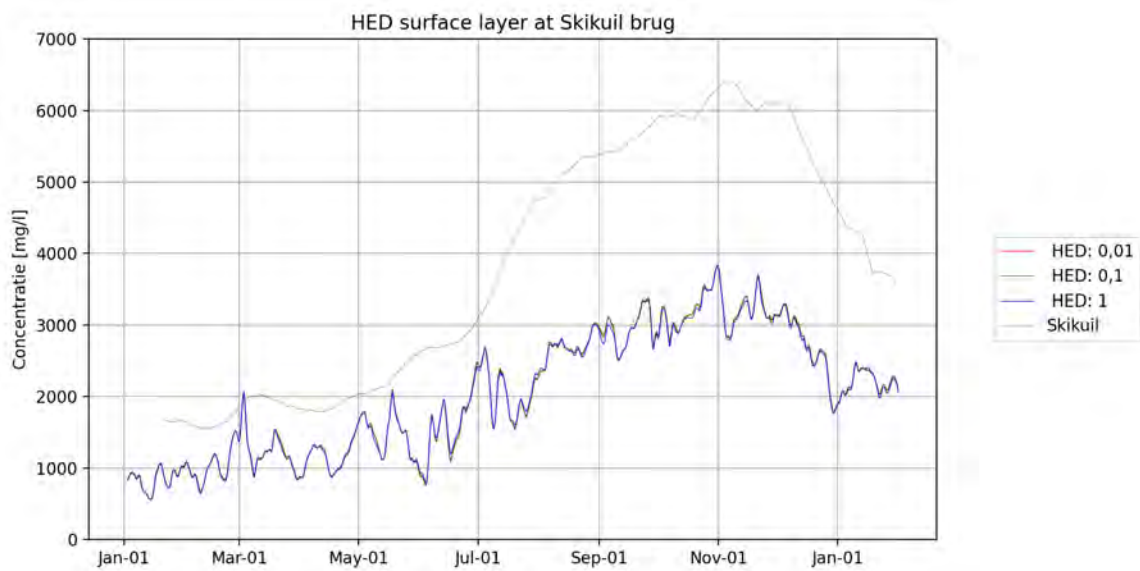


(a) Location Skikuil brug

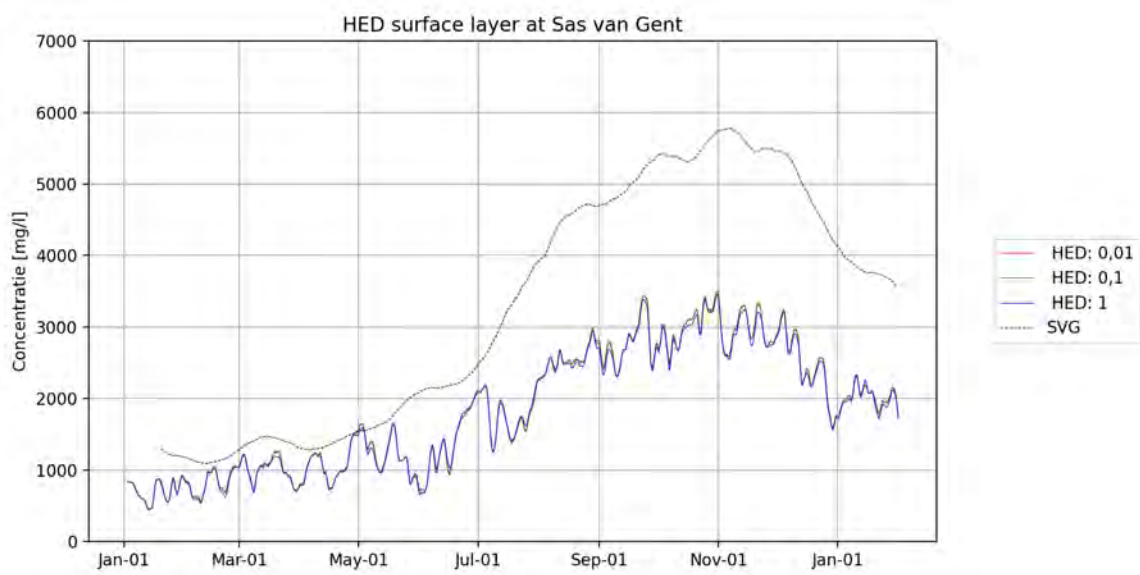


(b) Location Sas van Gent

Figure B.1: Horizontal Eddy Diffusivity bottom layer

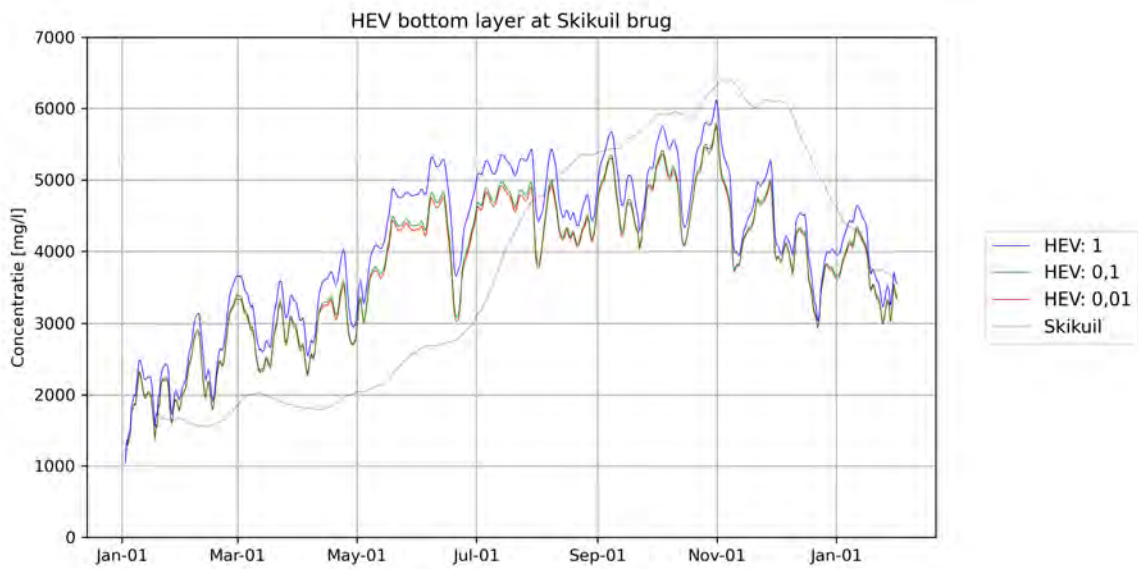


(a) Location Skikuil brug

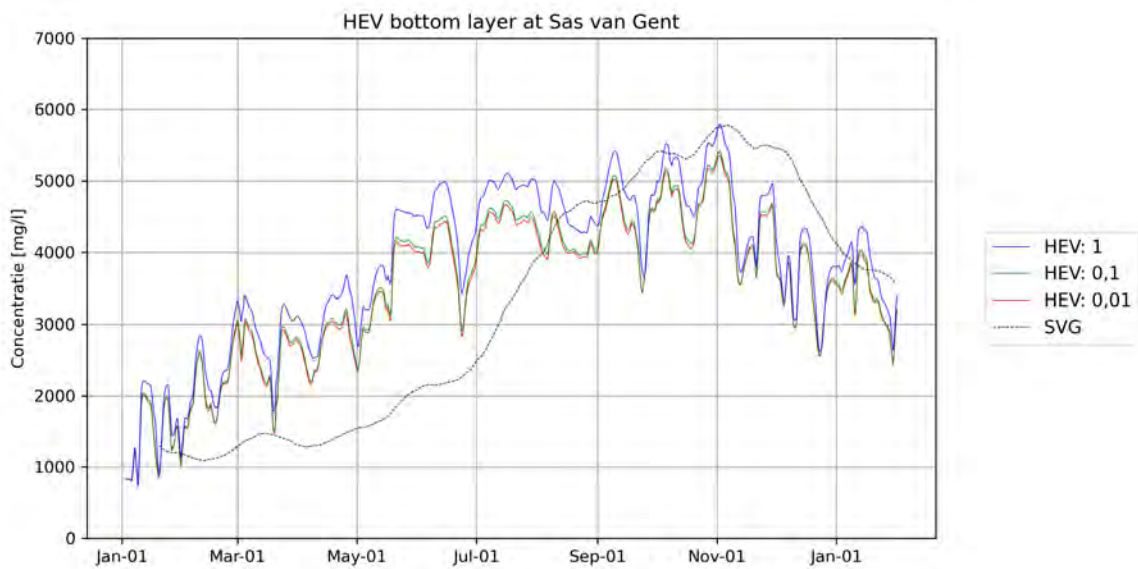


(b) Location Sas van Gent

Figure B.2: Horizontal Eddy Diffusivity surface layer

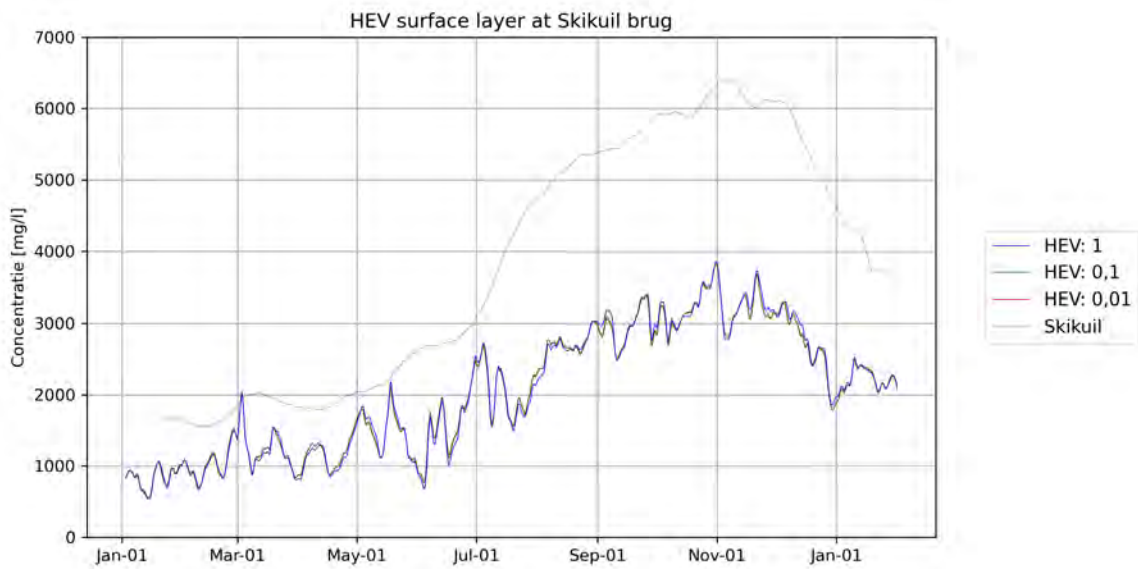


(a) Location Skikuil brug

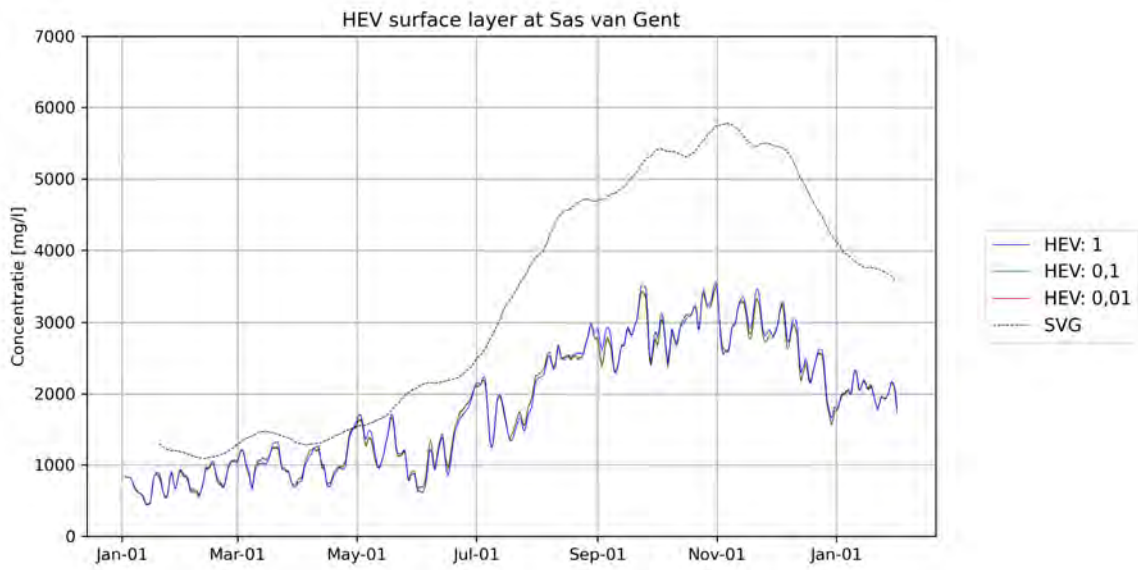


(b) Location Sas van Gent

Figure B.3: Horizontal Eddy Viscosity bottom layer

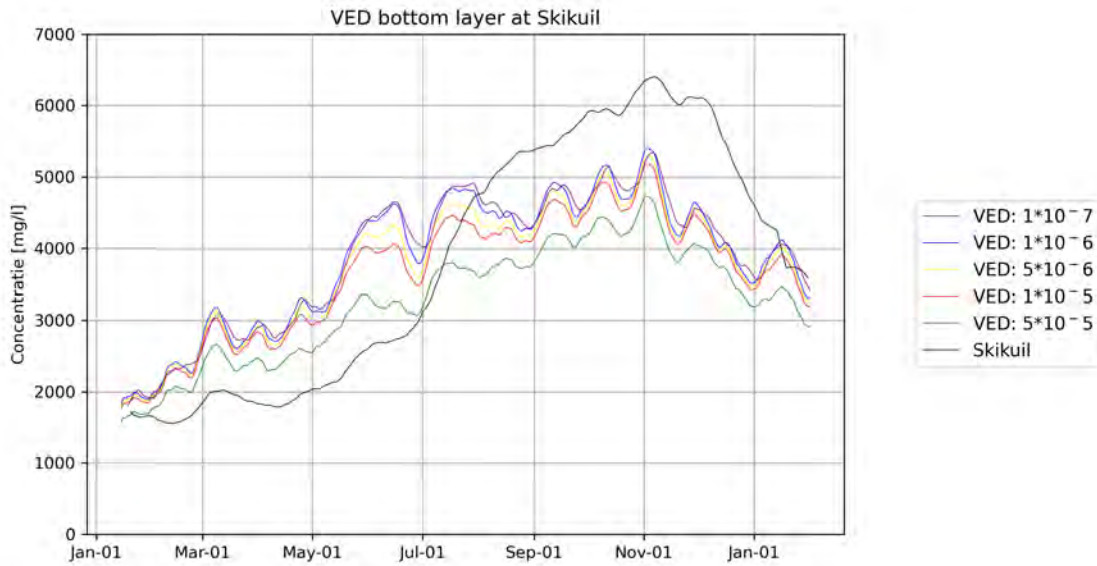


(a) Location Skikuil brug

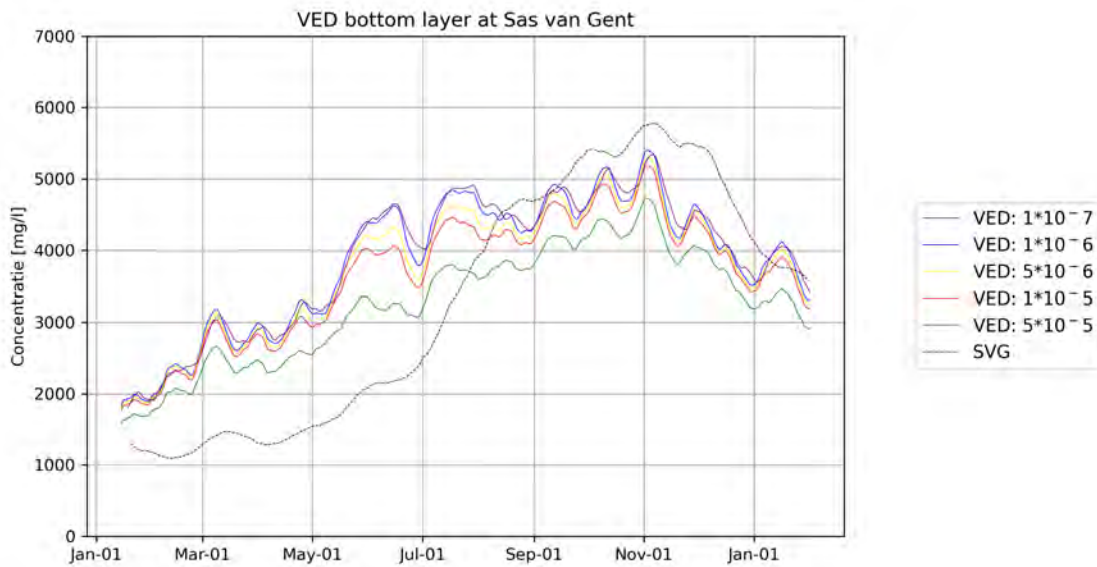


(b) Location Sas van Gent

Figure B.4: Horizontal Eddy Viscosity surface layer

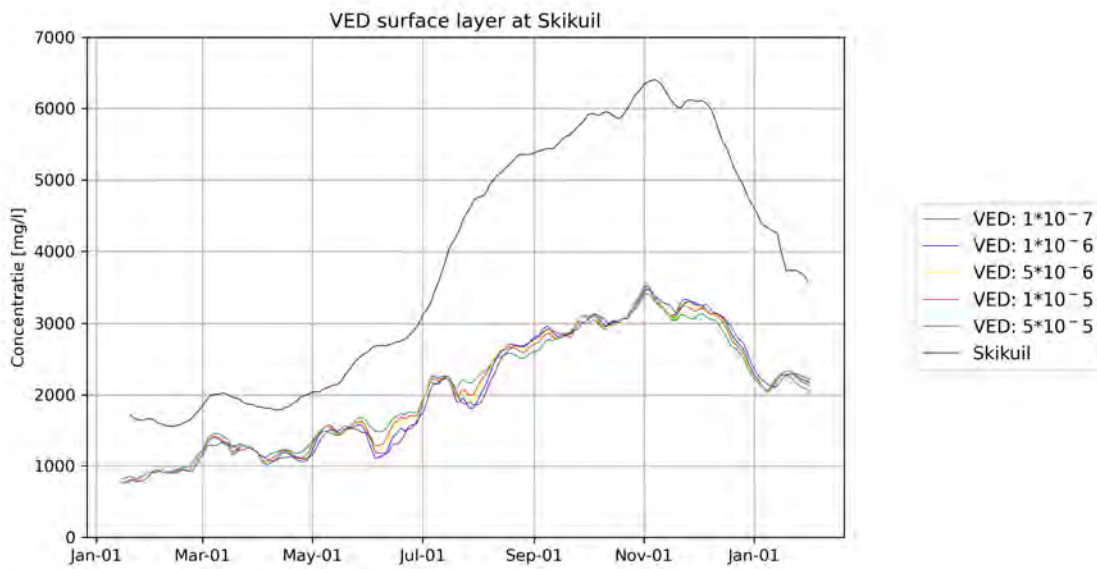


(a) Location Skikuil brug

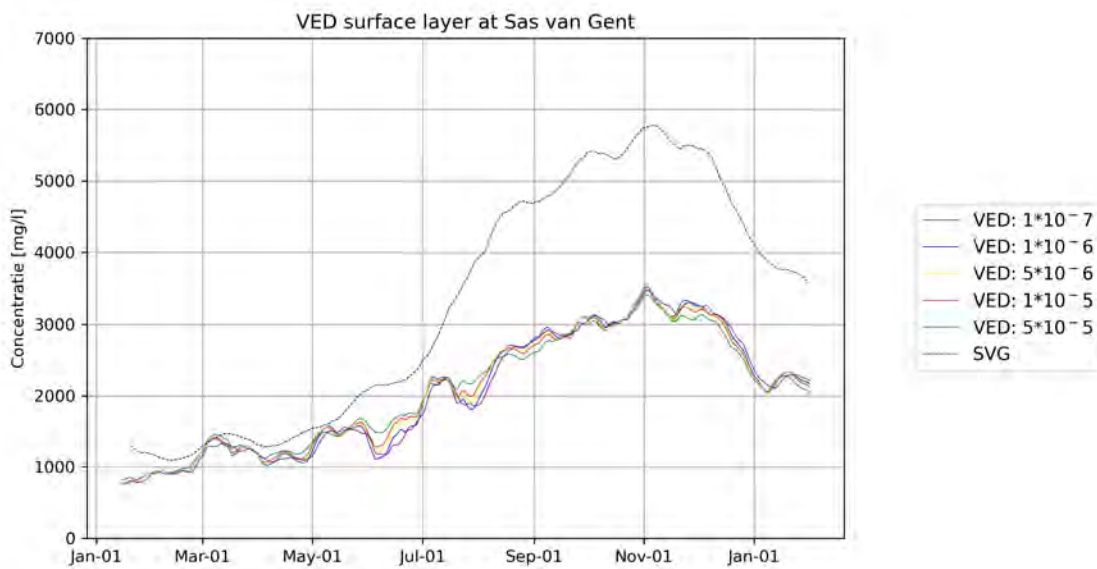


(b) Location Sas van Gent

Figure B.5: Vertical Eddy Diffusivity bottom layer

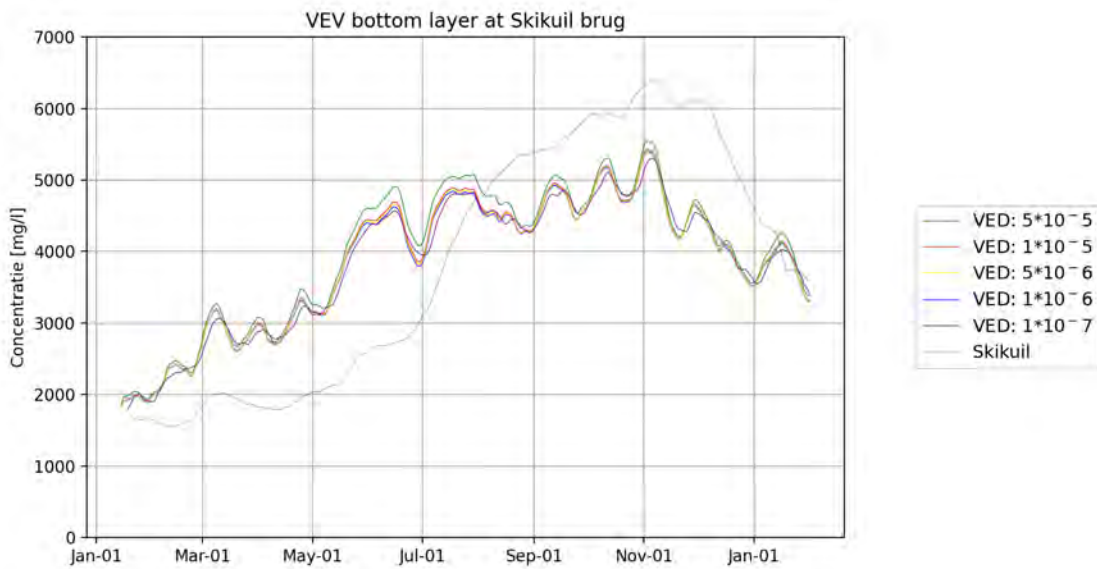


(a) Location Skikuil brug

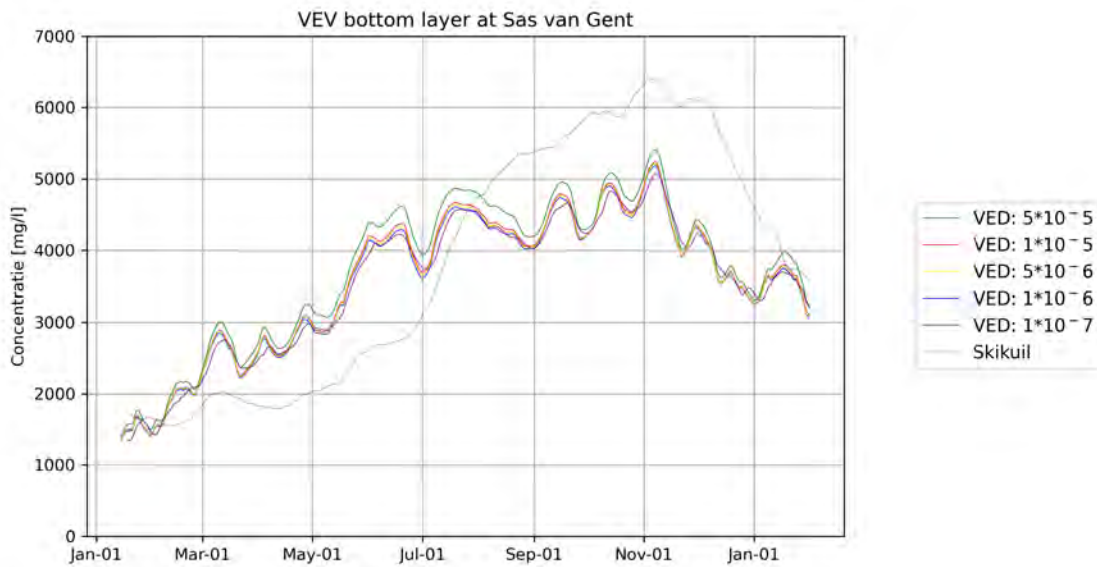


(b) Location Sas van Gent

Figure B.6: Vertical Eddy Diffusivity surface layer

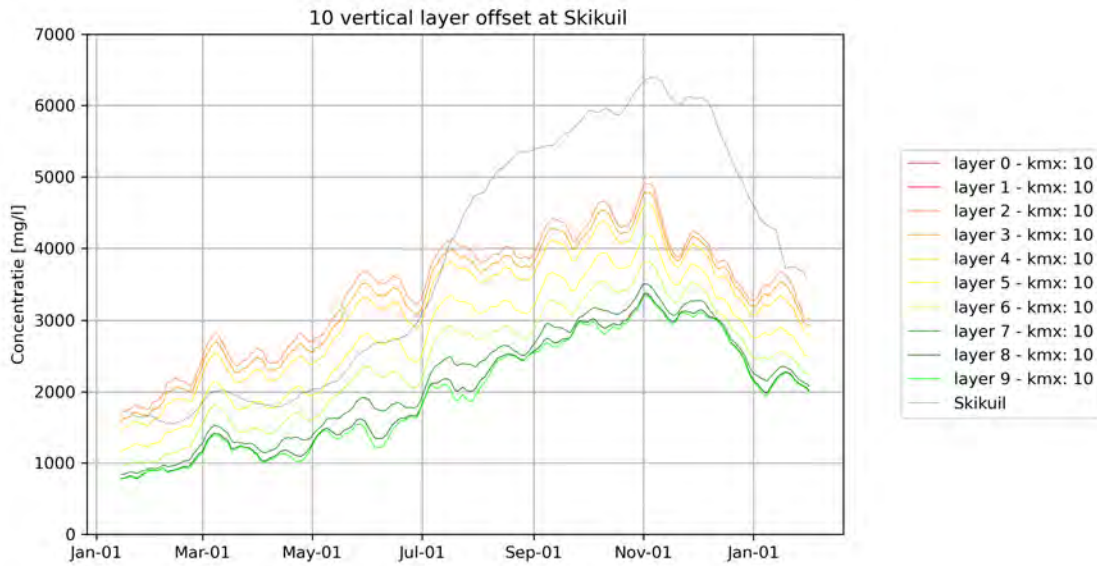


(a) Location Skikuil brug

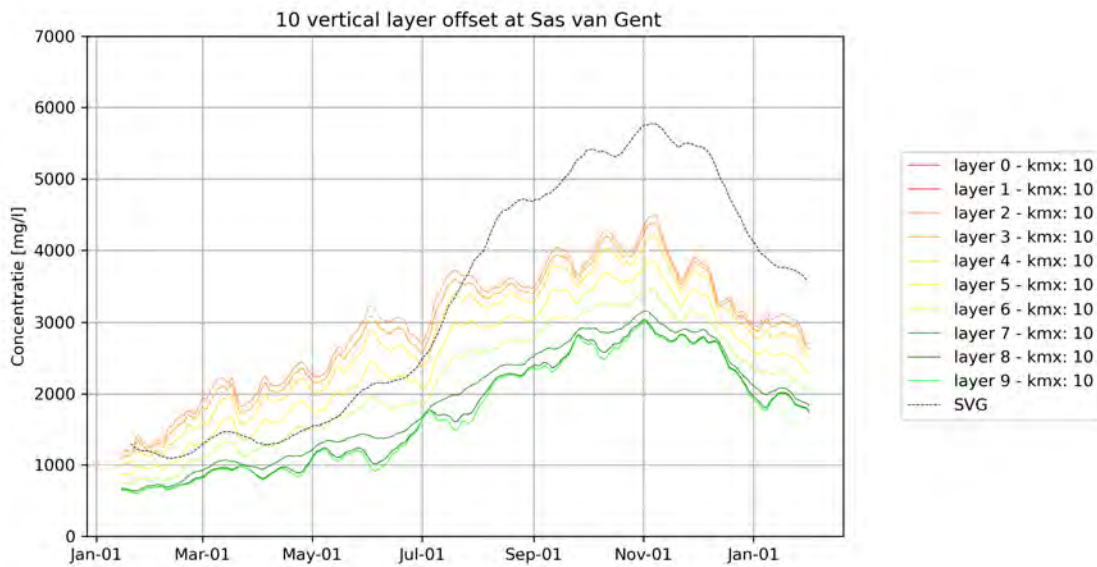


(b) Location Sas van Gent

Figure B.7: Vertical Eddy Viscosity bottom layer

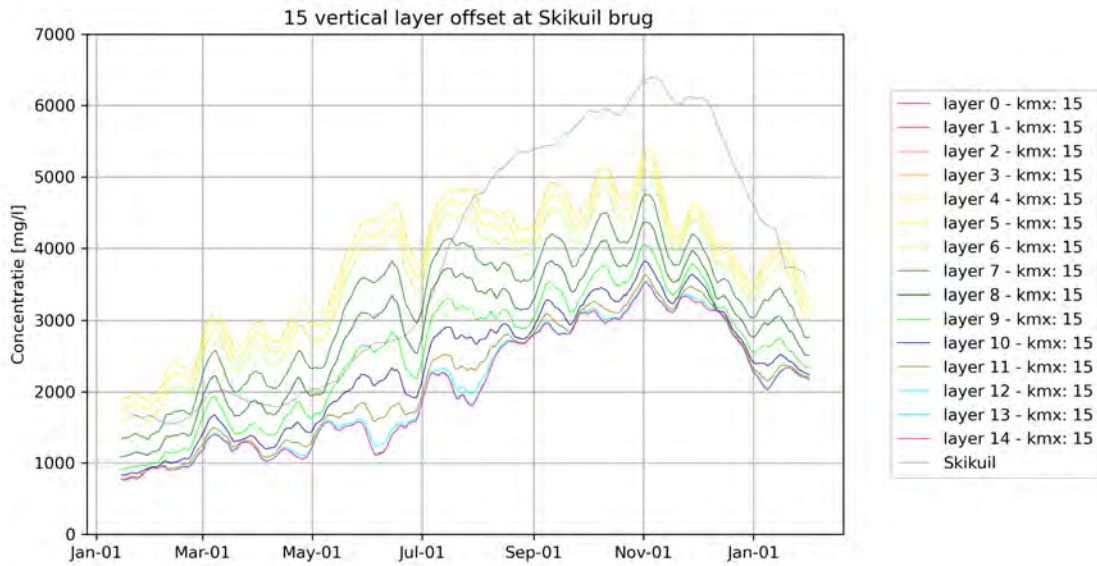


(a) Location Skikuil brug

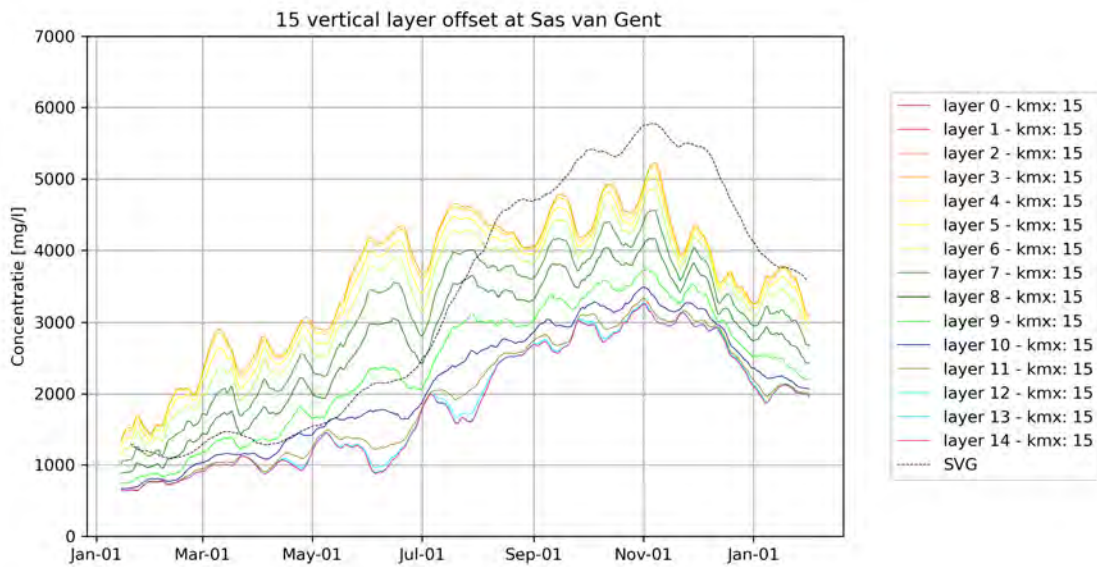


(b) Location Sas van Gent

Figure B.8: Vertical layer offset (kmx); 10

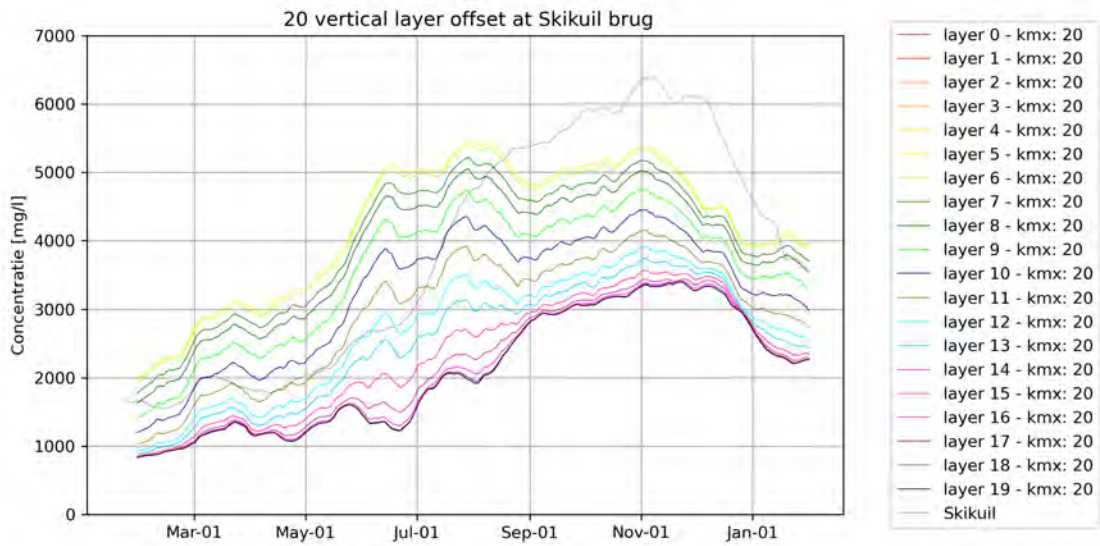


(a) Location Skikuil brug

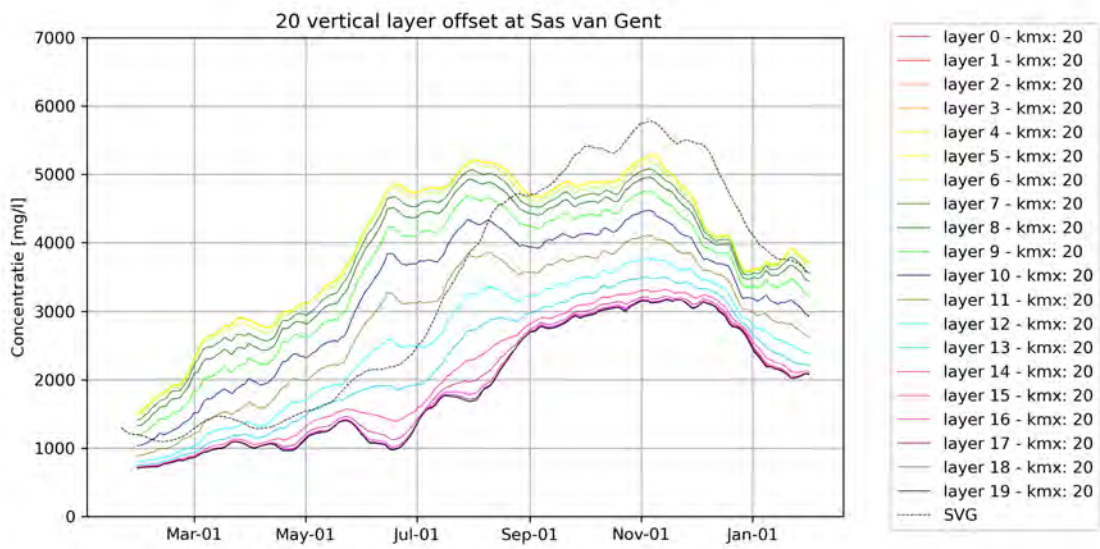


(b) Location Sas van Gent

Figure B.9: Vertical layer offset (kmx); 15



(a) Location Skikuil brug



(b) Location Sas van Gent

Figure B.10: Vertical layer offset (kmx); 20